

Elastic lepton–proton two-photon exchange scattering: An exact HB χ PT analysis including hadronic effects at NNLO

Rakshanda Goswami,^{1,*} Pulak Talukdar,^{2,†} Bhoomika Das,^{1,‡} Udit Raha,^{1,§} and Fred Myhrer^{3,¶}

¹*Department of Physics, Indian Institute of Technology Guwahati, Guwahati - 781039, Assam, India.*

²*Department of Physics, S. B. Deorah College, Guwahati - 781007, Assam, India.*

³*Department of Physics and Astronomy, University of South Carolina, Columbia, SC 29208, USA.*

We present an exact analytical evaluation of the two-photon exchange (TPE) correction to the elastic lepton–proton differential scattering cross section at low energies within the framework of heavy-baryon chiral perturbation theory. Our analysis focuses on the kinematic regime relevant to the ongoing MUSE experiment, and we therefore restrict the intermediate states to the dominant elastic channel. All loop integrals are evaluated analytically without approximations. Radiative and chiral recoil contributions of the proton are included, retaining kinematical and dynamical TPE corrections to the cross section through next-to-next-to-leading order [i.e., $\mathcal{O}(\alpha/M^2)$] accuracy in the recoil expansion where M is the proton mass. At this chiral order, pion-loop contributions demonstrate that structure-dependent TPE effects arise through the proton form factors. Our analytical results for the scattering cross section reveal non-vanishing residual proton structure effects of $\mathcal{O}(\alpha/M^2)$, despite substantial cancellations between TPE box and crossed-box contributions. Such effects were entirely absent at this accuracy in our earlier analysis based on the soft-photon approximation. Although the next-to-leading-order contributions are numerically sizable, the next-to-next-to-leading-order TPE corrections are found to be small, thereby indicating that the chiral expansion exhibits reasonably good perturbative convergence.

* r.goswami@iitg.ac.in

† pulaktalukdar45@gmail.com

‡ bhoomika.das@iitg.ac.in

§ udit.raha@iitg.ac.in

¶ myhrer@mailbox.sc.edu

I. INTRODUCTION

In recent years, the two-photon exchange (TPE) process in elastic (anti-)lepton-proton (ℓ^\pm -p) scatterings has garnered considerable interest in the high-energy physics community. This was primarily driven by several unexpected findings in precision experiments over the last two decades, which could be ostensibly resolved by including the TPE effects of the radiative corrections to the cross section. These observations include the discrepancies between polarized and unpolarized measurements of the proton's form factors, e.g., Refs. [1–15], and between scattering and atomic spectroscopy measurements of the proton charge-radius puzzle, e.g., Refs. [16–23]. It has been realized that the TPE radiative correction to the one-photon exchange (OPE) process plays a decisive role in the precise determination of the unpolarized elastic cross section, representing one of the dominant sources of systematic uncertainty that can no longer be neglected at the sub-percent level accuracy of current experiments. In particular, the interference between the OPE and TPE amplitudes modifies the elastic scattering cross section at the few-percent level, thereby affecting the extraction of fundamental proton properties. The most direct experimental access to the TPE contribution is provided by the measurement of the lepton–anti-lepton charge asymmetry (A_{ℓ^\pm}), defined as the relative difference between the elastic cross sections for oppositely charged leptons. Since, the interference term is *charge-odd*, namely, that it changes sign under lepton charge conjugation, this isolates the interference between the OPE (\mathcal{M}_γ) and TPE ($\mathcal{M}_{\gamma\gamma}$) amplitudes, thereby providing direct sensitivity to the real part of the TPE correction *via* the asymmetry observable, $A_{\ell^\pm} \propto \text{Re}(\mathcal{M}_\gamma^* \mathcal{M}_{\gamma\gamma})$. Experimental Collaborations, such as OLYMPUS (DESY) [24], VEPP-3 (Novosibirsk) [25], and CLAS (Jefferson Lab) [26] have previously measured the electron–proton charge asymmetry by alternately scattering electron and positron beams off protons under identical conditions. However, the data from these measurements suffer from limited statistics at very low-momentum transfers, below $|Q^2| \lesssim 0.1 \text{ GeV}^2/c^2$, precisely where the systematic uncertainties associated with the TPE are the most pronounced. In this context, the MUSE Collaboration [27] is soon poised to publish a simultaneous measurement of the charge asymmetry using both electron and muon beams, as well as their antiparticles, at unprecedentedly low-momentum transfers, $Q^2 < 0.1 \text{ GeV}^2/c^2$.

Since the TPE intermediate hadronic state can involve all possible excitations of the proton, its evaluation is theoretically challenging relying on a variety of complementary theoretical approaches have been developed over the past decades. The existing methods include hadronic models [11, 28–40], dispersion relations [35, 37, 40–48], and effective field theoretical analysis based on non-relativistic QED (NRQED) [49, 50] and chiral dynamics [45, 51–60]. Furthermore, recent lattice QCD simulations [61, 62], albeit computational challenges, have shown promising first-principle results for evaluating the TPE contribution. At low-energies heavy baryon chiral perturbation theory (HB χ PT) provides a convenient analytical tool for studying TPE effects of elastic lepton–proton scatterings (see e.g., Refs. [52, 56, 57, 59, 60]), due to its transparent and systematic diagrammatic formulation. This low-energy EFT offers a systematic, model-independent approach by exploiting the approximate chiral symmetry of QCD and its dynamical breakings. In HB χ PT observables are simultaneously expanded in powers of small external momenta compared to the chiral-symmetry breaking scale $\Lambda_\chi \simeq 1 \text{ GeV}/c$, or the inverse powers of the proton mass, $M \simeq 938 \text{ MeV}$. This allows the proton to be treated as a heavy, non-relativistic source where perturbative momentum-dependent corrections can be incorporated order-by-order. This allows a controlled organization of higher-order *radiative* and proton *recoil* effects, see, e.g., Refs. [63–70].

The evaluation of the TPE contributions to lepton-proton radiative corrections within HB χ PT, up-to-and-including next-to-leading order (NLO), was first undertaken by Talukdar *et al.* in Ref. [56]. Motivated by earlier studies of low- and intermediate-energy TPE effects, e.g., Refs. [32, 33, 38, 39], Talukdar *et al.* employed HB χ PT for the first time to provide a model-independent evaluation of TPE corrections in elastic lepton–proton scattering. Their first TPE analysis utilized SPA [71, 72] to simplify the 4-point loop-integrals arising in the evaluation of the box and crossed-box diagrams. Subsequently, the TPE contribution in HB χ PT at NLO accuracy was evaluated exactly by Choudhary *et al.* in Ref. [59]. Their study demonstrated that the inclusion of the full TPE loop kinematic region including configurations with two *hard photon* exchange, yields a significant contribution to the elastic cross section, which is missed in SPA. In addition, our exact TPE approach yielded a LO contribution akin to the McKinley and Feshbach [73]. In contrast, the SPA approach of Talukdar *et al.* yielded a vanishing LO contribution. Unfortunately, within the standard HB χ PT power-counting scheme the NLO corrections do not incorporate proton's internal hadronic structure within the radiative corrections, effectively treating the proton as a point-like particle. To account for the important finite-size effects arising from the proton's structure, which in HB χ PT is introduced *via* the pion-loop contributions and low-energy constants (LECs) such as the anomalous magnetic moment, $\kappa_p = 1.795$, the TPE must include the dominant part of the next-to-next-to-leading order (NNLO) modifications stemming from the γpp vertex corrections, *vis-a-vis* proton's electromagnetic form factors. In our recent SPA work by Goswami *et al.* [60], we improved the SPA analysis of Talukdar *et al.* by *partly*¹ including these NNLO effects and by employing a more rigorous treatment of

¹ A complete treatment of all NNLO contributions requires the evaluation of the full set of two-loop TPE diagrams in which pion exchange

the loop-integrals, while retaining the SPA used in Talukdar *et al.*'s original approach in Ref. [56]. Particularly in the analysis of Goswami *et al.* it was observed that at the intended $\mathcal{O}(\alpha^3/M^2)$ precision of the radiative corrected elastic cross section the NNLO TPE contributions, especially those stemming from the proton's internal structure, either *fortuitously* cancel at this order, or manifest themselves only at higher recoil order, namely, $\mathcal{O}(\alpha^3/M^3)$. In addition, $\mathcal{O}(\alpha^3/M^2)$ effects also arise from proton recoil correction terms present in the NNLO squared amplitudes as well as from the kinematically suppressed LO and NLO terms. The latter corrections are dependent on the outgoing lepton energy (E') and velocity (β'), which can also be expressed *via* the following recoil-expansions:

$$E' = E + \frac{Q^2}{2M} \quad \text{and} \quad \beta' = \beta + \frac{Q^2(1 - \beta^2)}{2ME\beta} - \frac{Q^4(2\beta^4 - 1 - \beta^2)}{8M^2E^2\beta^3} + \mathcal{O}\left(\frac{1}{M^3}\right), \quad (1)$$

respectively. Here E and β are the incident lepton beam variables. Consequently, the continued use of the SPA methodology, particularly in the low-energy MUSE kinematic region, is discouraged, as was already emphasized in Ref. [60]. In the present work, we therefore abandon the SPA framework and extend the NLO exact TPE analysis of Choudhary *et al.* [59] to include the dominant NNLO proton's finite-size contributions along with the other $\mathcal{O}(\alpha^3/M^2)$ terms mentioned above *via* the heavy baryon formalism.

This paper is organized as follows. In Sec. 2, we briefly outline the essential features of our EFT methodology, along with the kinematical setup required for our analytical evaluations. The analytical details are then presented in Sec. 3, where we extend the NLO TPE evaluations of Choudhary *et al.* [59] by including all possible kinematically suppressed NNLO [i.e., $\mathcal{O}(\alpha/M^2)$] corrections to the elastic cross section arising from the LO and NLO TPE diagrams of $\mathcal{O}(e^4)$ and $\mathcal{O}(e^4/M)$, respectively. In Sec. 4, we evaluate the genuine dynamical NNLO TPE corrections to the cross section including the pion-loop or hadronic structure contributions. Here we include the additional contribution from all possible NNLO TPE diagrams of $\mathcal{O}(e^4/M^2)$, retaining corrections terms up to $\mathcal{O}(\alpha/M^2)$ accuracy. We provide our numerical results in Sec. 5 and analyze them in the context of low-energy MUSE kinematics as specified in Ref. [27]. Section 6 contains our summary and conclusions. At the end, we include two appendices where we relegate the explicit analytical expressions for several modified loop-integrals that appeared in our past works in Refs. [59, 60], as well as several additional new ones appearing for the first time in the present analysis.

II. HB χ PT: GENERAL FORMALISM AND KINEMATICS

We briefly discuss the basic EFT methodology of the HB χ PT formalism whose details could be obtained, e.g., in Refs. [63–70]. HB χ PT emerges from a non-relativistic expansion of the relativistic pion-nucleon Lagrangian in inverse powers of M . The original relativistic χ PT Lagrangian, invariant under the action of the *chiral gauge group* $\mathcal{G} = \text{SU}(2)_L \otimes \text{SU}(2)_R$, is constructed such that the corresponding pions emerge as the Goldstone bosons associated with the spontaneous breaking of chiral symmetry. The pion reside in the coset space \mathcal{G}/\mathcal{H} , and are defined *via* the *non-linear realization*: $K = \sqrt{LU^\dagger R^\dagger}R\sqrt{U}$, where the elements $L \in \text{SU}(2)_L$, $R \in \text{SU}(2)_R$, and U is the non-linearly realized pion field $\vec{\pi}$. The so-called *compensator* element $K \in \mathcal{H} = \text{SU}(2)_{V=L+R} \subseteq \mathcal{G}$ belongs to the unbroken vector (flavor) subgroup \mathcal{H} of the chiral group \mathcal{G} . Likewise, the relativistic iso-spinor nucleon field $\Psi_N = (p \ n)^T$ can also be shown to transform non-linearly as $\Psi_N \rightarrow K(U, L, R)\Psi_N$, leading to the following representation of the covariant derivatives in this theory, namely,

$$D_\mu \Psi_N \equiv (\partial_\mu + \Gamma_\mu)\Psi_N, \quad \text{and} \quad \nabla_\mu U = \partial_\mu U - i(v_\mu + a_\mu)U + iU(v_\mu - a_\mu), \quad (2)$$

where the *chiral connection* Γ_μ and *chiral vielbein* u_μ enter as

$$\Gamma_\mu = \frac{1}{2}[u^\dagger, \partial_\mu u] - \frac{i}{2}u^\dagger(v_\mu + a_\mu)u - \frac{i}{2}u(v_\mu - a_\mu)u^\dagger; \quad u = \sqrt{U} \quad \text{and} \quad u_\mu = iu^\dagger \nabla_\mu U u^\dagger. \quad (3)$$

Here v_μ and a_μ are the external vector and axial fields, respectively. Furthermore, induced by the action of \mathcal{G} , the following transformations of the basic elements of the effective Lagrangian manifest:

$$D_\mu \rightarrow K D_\mu K^\dagger, \quad \Gamma_\mu \rightarrow K \Gamma_\mu K^\dagger + K \partial_\mu K^\dagger, \quad \text{and} \quad u_\mu \rightarrow K u_\mu K^\dagger, \quad (4)$$

occurs in one of the loops. In the recent SPA work of Goswami *et al.* [60], only the dominant “reducible” two-loop topologies were considered, in which the pion-loops factorize within the TPE box and crossed-box diagrams, effectively renormalizing and dressing the proton-photon vertices through form factors. At NNLO, however, there also exists several “non-form-factor” type (see Ref. [60]), involving non-factorizable pion-loops that do not contribute to vertex renormalization. These genuine two-loop TPE contributions are considerably more challenging to compute analytically, and are therefore omitted in the present work. Nevertheless, such diagrams are expected to yield contributions that are numerically suppressed relative to the typical NNLO corrections.

motivating the construction of the most general effective relativistic Lagrangian, allowed by all possible low-energy symmetries, such as invariance under P, C, T, cluster decomposition, Lorentz, and chiral transformations.

It is well known that a fully relativistic formulation of χ PT for the pion–nucleon system encounters severe practical difficulties in diagrammatic evaluations. In particular, the power-counting scheme fails to maintain a *one-to-one correspondence* between the expansion in pion-loops and the chiral expansion, thereby raising concerns about the efficacy of low-energy perturbative convergence. However, this issue was shown to be effectively circumvented by adopting a non-relativistic expansion [63–67], wherein one projects out from the relativistic nucleon spinor field Ψ_N only the “large” Dirac components $\mathcal{N}_v \sim \mathcal{O}(M)$, which depend on the four-velocity, we choose $v_\mu = (1, \mathbf{0})$ in the nucleon rest frame, using the velocity projector $\mathcal{P}_v^+ = (1 + \not{v})/2$, i.e.,

$$\Psi_N(x) = e^{-iMv \cdot x} [\mathcal{N}_v(x) + h_v(x)] , \quad \text{with} \quad (5)$$

$$\mathcal{N}_v(x) = e^{iMv \cdot x} \mathcal{P}_v^+ \Psi_N(x) , \quad \text{and} \quad \not{v} \mathcal{N}_v(x) = \mathcal{N}_v(x) \equiv \begin{pmatrix} \mathbf{p}_v \\ \mathbf{n}_v \end{pmatrix} . \quad (6)$$

Here the effects of the “small” Dirac components h_v are integrated out in the theory. For an early review, see Ref. [67] which also contains some early references. A pedagogical derivation of HB χ PT can be found in the book given by Ref. [74]. Nevertheless, an additional re-parametrization invariance allows us to express the proton’s four-momenta in an arbitrary boosted frame as $P^\mu = Mv^\mu + p_p^\mu$, where p_p^μ is the small nucleon, *residual* off-shell four-momentum with $v \cdot p_p \ll M$. The advantage of this formulation lies in the decoupling of the nucleon mass in the equation of motion up to corrections suppressed by powers of $1/M$, for example, $v \cdot \partial \mathcal{N}_v = \mathcal{O}(1/M)$. Consequently the M dependence of the heavy nucleon propagator is moved to the interaction vertices, which are ordered by a *1/M-recoil expansion*. Thus, up to chiral-order $\nu = 2$ [i.e., $\mathcal{O}(1/M^2)$], the proton propagator is represented as

$$iS_{\text{full}}^{(p)}(l) = \frac{i}{v \cdot l + i0} + \frac{i}{2M} \left[1 - \frac{l^2}{(v \cdot l + i0)^2} \right] + \frac{i}{4M^2} \left[\frac{(v \cdot l)^3 - l^2(v \cdot l)}{(v \cdot l + i0)^2} \right] + \mathcal{O}\left(\frac{1}{M^3}\right) , \quad (7)$$

where l^μ denotes the generic residual off-shell proton momentum. The simultaneous chiral and nucleon recoil expansion scheme restores the aforementioned one-to-one diagrammatic correspondence. An immediate practical benefit of the HB χ PT formalism is that the vital low-energy recoil effects of the heavy proton are naturally captured in a controlled manner. The SU(2) HB χ PT pion–nucleon Lagrangian is well established in the literature [66–69, 78, 79]. Given the lengthy sequence of operator structures and the phenomenologically determined LECs that parameterize the short ranged and unresolved ultraviolet (UV) physics, the explicit form of the effective Lagrangian will not be presented here, and instead we refer to the literature, see e.g., Ref. [67]. In fact, in our previous TPE analysis reported in Ref. [60], we employed the same relevant parts of the effective Lagrangian, to which we hereby refer the reader for the detailed expressions. It is important to emphasize that the heavy proton is treated within a manifestly non-relativistic framework, whereas the pions, and other light particles, such as leptons ($\ell^\pm \equiv e^\pm, \mu^\pm$) and photon are treated relativistically. We symbolically express the most general form of the HB χ PT Lagrangian as terms up to NNLO, i.e., with chiral dimension $\nu = 2$, at the intended level of accuracy in this work.

$$\begin{aligned} \mathcal{L}_{\ell\pi N\gamma} &= \mathcal{L}_\ell^{\text{QED}} + \mathcal{L}_{\pi N}^{\text{eff}} , \quad \text{where} \\ \mathcal{L}_{\pi N}^{\text{eff}} &= \mathcal{L}_\pi^{(2)} + \sum_{\nu=0}^2 \mathcal{L}_{\pi N}^{(\nu)} . \end{aligned} \quad (8)$$

In particular, the pion-loop corrections arising at NNLO generate UV divergences, which necessitate local counter terms for renormalization, see, e.g., Sec. I.

To facilitate a straightforward comparison, we have, for the most part, kept the notation and convention close to Ref [60]. The choice of a laboratory frame (lab-frame) where the target proton is at rest greatly simplifies our evaluations and kinematics, especially bearing in mind the low energy MUSE kinematic region of interest [27] (also see Table I in Ref. [56]). In this work we shall consider $Q_\mu = (p - p')_\mu = (p'_p - p_p)_\mu$ as the four-momentum transfer for the elastic scattering process, with $p(p')$ and $p_p(p'_p)$ as the incoming (outgoing) lepton four-momentum and the proton’s *residual* four-momentum, respectively, where in the lab. frame $p_p = (0, \mathbf{0})$. Furthermore, we wish to emphasize that terms like $v \cdot Q$ and $v \cdot p'_p$ are $\mathcal{O}(1/M)$, i.e., $v \cdot p'_p = v \cdot Q = E - E' = -Q^2/2M$.

In summary, a complete and exact analytical study of the TPE contribution up to NLO accuracy was already performed in Ref. [59]. The present work aims to extend that analysis by incorporating the NNLO corrections to assess the convergence behavior of HB χ PT and thereby obtain a more robust estimate of the higher order systematic uncertainties. In the following two sections we identify the relevant sources of these NNLO contributions.

III. KINEMATICAL NNLO RECOIL CORRECTIONS FROM LO AND NLO TPE DIAGRAMS

Here we shall extend the analysis of Choudhary *et al.* [59] of the fractional TPE corrections $\pm\delta_{\gamma\gamma}^{(\text{LO+NLO})}$ to the elastic (anti)lepton-proton (ℓ^\mp -p) differential cross section, namely,

$$\begin{aligned} \left[\frac{d\sigma_{el}(Q^2)}{d\Omega'_l} \right]_{\text{LO+NLO}}^{(\ell^\mp)} &= \left[\frac{d\sigma_{el}(Q^2)}{d\Omega'_l} \right]_0 \left[1 \pm \delta_{\gamma\gamma}^{(\text{LO+NLO})}(Q^2) \right], \quad \text{where} \\ \delta_{\gamma\gamma}^{(\text{LO+NLO})}(Q^2) &= \frac{2\mathcal{R}e \sum_{\text{spins}} \left[\mathcal{M}_\gamma^{(0)*} \left(\mathcal{M}_{\gamma\gamma}^{(\text{LO})} + \mathcal{M}_{\gamma\gamma}^{(\text{NLO})} \right) + \mathcal{M}_\gamma^{(1)*} \mathcal{M}_{\gamma\gamma}^{(\text{LO})} \right]}{\sum_{\text{spins}} \left| \mathcal{M}_\gamma^{(0)} \right|^2}. \end{aligned} \quad (9)$$

These terms were evaluated analytically up-to-and-including NLO [i.e., $\mathcal{O}(\alpha/M)$] where the LO OPE term [57] is

$$\left[\frac{d\sigma_{el}(Q^2)}{d\Omega'_l} \right]_0 = \frac{1}{64\pi^2 M^2} \left(\frac{E'\beta'}{E\beta} \right) \frac{1}{4} \sum_{\text{spins}} \left| \mathcal{M}_\gamma^{(0)} \right|^2 = \frac{\alpha^2 E'\beta'}{Q^2 E\beta} \left(1 - \frac{Q^2}{4M^2} \right) \left[\frac{Q^2 + 4EE'}{Q^2} \right]. \quad (10)$$

In Eq. (9) the expressions $\mathcal{M}_\gamma^{(0,1)}$ denote the (LO, NLO) OPE amplitudes whereas $\mathcal{M}_{\gamma\gamma}^{(\text{LO,NLO})}$ represent the sum of the (LO, NLO) TPE amplitudes shown in Fig. 1 for lepton-proton (ℓ^- -p) scattering. Their expressions are as follows:

$$\mathcal{M}_\gamma^{(0)} = -\frac{e^2}{Q^2} [\bar{u}(p')\gamma^\mu u(p)] [\chi^\dagger(p'_p)v_\mu\chi(p_p)], \quad (11)$$

$$\begin{aligned} \mathcal{M}_\gamma^{(1)} &= -\frac{e^2}{2MQ^2} [\bar{u}(p')\gamma^\mu u(p)] \left[\chi^\dagger(p'_p) \left\{ (p_p + p'_p)_\mu - v_\mu v \cdot (p_p + p'_p) \right. \right. \\ &\quad \left. \left. + (2 + \kappa_s + \kappa_v)[S_\mu, S \cdot Q] \right\} \chi(p_p) \right], \quad \text{where} \end{aligned} \quad (12)$$

$$\mathcal{M}_{\gamma\gamma}^{(\text{LO})} = \mathcal{M}_{\text{box}}^{(a)} + \mathcal{M}_{\text{xbox}}^{(b)}, \quad \text{and} \quad \mathcal{M}_{\gamma\gamma}^{(\text{NLO})} = \mathcal{M}_{\text{box}}^{(c)} + \cdots + \mathcal{M}_{\text{xbox}}^{(h)} + \mathcal{M}_{\text{seagull}}^{(i)}. \quad (13)$$

The general frame-independent integral representations of these individual TPE amplitudes are provided in Ref. [59, 60]. Specializing to the lab-frame and performing the shift $k \rightarrow -k + Q$ for each loop-integration four-momentum variable k in the NLO crossed-box amplitudes $\mathcal{M}_{\text{xbox}}^{(b)}$, $\mathcal{M}_{\text{xbox}}^{(d)}$, $\mathcal{M}_{\text{xbox}}^{(f)}$, and $\mathcal{M}_{\text{xbox}}^{(h)}$, and with further partial cancellation of the $v_\mu v_\nu$ terms among the amplitudes $\mathcal{M}_{\text{box}}^{(c)}$, $\mathcal{M}_{\text{box}}^{(f)}$, $\mathcal{M}_{\text{box}}^{(g)}$, $\mathcal{M}_{\text{xbox}}^{(h)}$ and $\mathcal{M}_{\text{seagull}}^{(i)}$, we arrive at the following modified integral representations of the LO and NLO amplitudes [60]:

$$\mathcal{M}_{\text{box}}^{(a)} = e^4 \int \frac{d^4 k}{(2\pi)^4 i} \frac{[\bar{u}(p')\gamma^\mu(\not{p} - \not{k} + m_l)\gamma^\nu u(p)] [\chi^\dagger(p'_p)v_\mu v_\nu\chi(p_p)]}{(k^2 + i0)[(Q - k)^2 + i0](k^2 - 2k \cdot p + i0)(v \cdot k + i0)}, \quad (14)$$

$$\mathcal{M}_{\text{xbox}}^{(b)} = e^4 \int \frac{d^4 k}{(2\pi)^4 i} \frac{[\bar{u}(p')\gamma^\mu(\not{p} + \not{k} - \not{Q} + m_l)\gamma^\nu u(p)] [\chi^\dagger(p'_p)v_\mu v_\nu\chi(p_p)]}{(k^2 + i0)[(Q - k)^2 + i0](k^2 + 2k \cdot p' + i0)(v \cdot k + i0)}, \quad (15)$$

$$\widetilde{\mathcal{M}}_{\text{box}}^{(c)} = \frac{e^4}{2M} \int \frac{d^4 k}{(2\pi)^4 i} \frac{[\bar{u}(p')\gamma^\mu(\not{p} - \not{k} + m_l)\gamma^\nu u(p)] [\chi^\dagger(p'_p)v_\mu k_\nu\chi(p_p)]}{(k^2 + i0)[(Q - k)^2 + i0](k^2 - 2k \cdot p + i0)(v \cdot k + i0)}, \quad (16)$$

$$\widetilde{\mathcal{M}}_{\text{xbox}}^{(d)} = \frac{e^4}{2M} \int \frac{d^4 k}{(2\pi)^4 i} \frac{[\bar{u}(p')\gamma^\mu(\not{p} + \not{k} - \not{Q} + m_l)\gamma^\nu u(p)] [\chi^\dagger(p'_p)v_\nu k_\mu\chi(p_p)]}{(k^2 + i0)[(Q - k)^2 + i0](k^2 + 2k \cdot p' + i0)(v \cdot k + i0)} \quad (17)$$

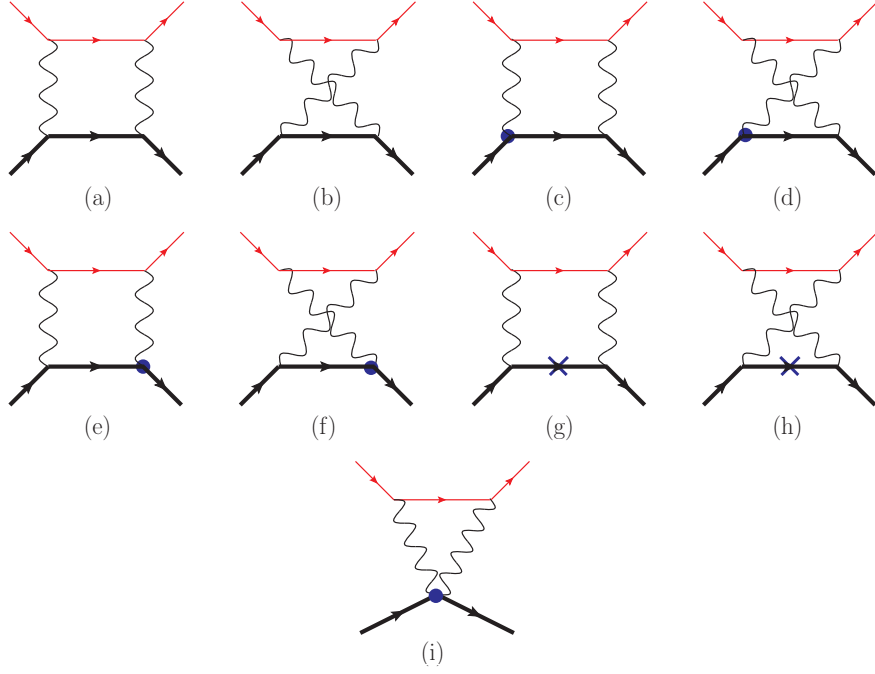


FIG. 1. The LO [i.e., $\mathcal{O}(\alpha^2)$] and NLO [i.e., $\mathcal{O}(\alpha^2/M)$] TPE diagrams contributing to the $\mathcal{O}(\alpha^3/M)$ lepton-proton elastic differential cross-section, are shown. The thick, thin, and wiggly lines denote the proton, lepton, and photon propagators. The blobs and crosses denote the insertions of the NLO proton-photon vertices and $\mathcal{O}(1/M)$ proton propagators, respectively (figure reproduced from Ref. [60]).

$$\widetilde{\mathcal{M}}_{\text{box}}^{(e)} = \frac{e^4}{2M} \int \frac{d^4 k}{(2\pi)^4 i} \frac{[\bar{u}(p')\gamma^\mu(\not{p} - \not{k} + m_l)\gamma^\nu u(p)][\chi^\dagger(p'_p)v_\nu(Q + k)_\mu\chi(p_p)]}{(k^2 + i0)[(Q - k)^2 + i0](k^2 - 2k \cdot p + i0)(v \cdot k + i0)}, \quad (18)$$

$$\widetilde{\mathcal{M}}_{\text{xbbox}}^{(f)} = \frac{e^4}{2M} \int \frac{d^4 k}{(2\pi)^4 i} \frac{[\bar{u}(p')\gamma^\mu(\not{p} + \not{k} - \not{Q} + m_l)\gamma^\nu u(p)][\chi^\dagger(p'_p)v_\mu(k + Q)_\nu\chi(p_p)]}{(k^2 + i0)[(Q - k)^2 + i0](k^2 + 2k \cdot p' + i0)(v \cdot k + i0)}, \quad (19)$$

$$\widetilde{\mathcal{M}}_{\text{box}}^{(g)} = \frac{e^4}{2M} \int \frac{d^4 k}{(2\pi)^4 i} \frac{[\bar{u}(p')\gamma^\mu(\not{p} - \not{k} + m_l)\gamma^\nu u(p)][\chi^\dagger(p'_p)v_\mu v_\nu\chi(p_p)]}{(k^2 + i0)[(Q - k)^2 + i0](k^2 - 2k \cdot p + i0)} \left(-\frac{k^2}{(v \cdot k + i0)^2} \right), \quad (20)$$

$$\widetilde{\mathcal{M}}_{\text{xbbox}}^{(h)} = \frac{e^4}{2M} \int \frac{d^4 k}{(2\pi)^4 i} \frac{[\bar{u}(p')\gamma^\mu(\not{p} + \not{k} - \not{Q} + m_l)\gamma^\nu u(p)][\chi^\dagger(p'_p)v_\mu v_\nu\chi(p_p)]}{(k^2 + i0)[(Q - k)^2 + i0](k^2 + 2k \cdot p' + i0)} \left(-\frac{k^2}{(v \cdot k + i0)^2} \right), \quad (21)$$

$$\text{and} \quad \widetilde{\mathcal{M}}_{\text{seagull}}^{(i)} = -\frac{e^4}{M} \int \frac{d^4 k}{(2\pi)^4 i} \frac{[\bar{u}(p')\gamma^\mu(\not{p} - \not{k} + m_l)\gamma_\mu u(p)][\chi^\dagger(p'_p)\chi(p_p)]}{(k^2 + i0)[(Q - k)^2 + i0](k^2 - 2k \cdot p + i0)}, \quad (22)$$

where m_l denotes the lepton mass in the above integrals. It is noteworthy that the contributions arising from the interference of amplitudes in Eq. (9), namely, $\mathcal{M}_\gamma^{(1)*}\mathcal{M}_{\gamma\gamma}^{(\text{LO})}$, which generate the $\mathcal{O}(\alpha/M^2)$ fractional correction terms to the elastic cross section, $\delta_{\text{box}}^{(a_1)}$ and $\delta_{\text{box}}^{(b_1)}$ [see Eqs. (26) and (27)], are an order beyond the intended NLO accuracy of our previous exact TPE work in Ref. [59].

Now we analytically re-evaluate the the nine TPE diagrams (a) - (i), in order to determine their additional $\mathcal{O}(\alpha/M^2)$ fractional corrections contributing to the elastic differential cross section at our target accuracy of $\mathcal{O}(\alpha^3/M^2)$. We follow the same reduction strategy used in Ref. [59], employing successive applications of integration by parts (IBP) identities and the method of partial fractions to simplify the corresponding Feynman amplitudes. As in Ref. [59], we first present the unexpanded expressions for the fractional contributions arising from the LO and NLO TPE diagrams,

accurate to $\mathcal{O}(\alpha/M^2)$:

$$\delta_{\gamma\gamma}^{(\text{LO+NLO})}(Q^2) = \left[\delta_{\text{box}}^{(a)}(Q^2) + \delta_{\text{xbox}}^{(b)}(Q^2) \right]_{\text{LO}} + \left[\delta_{\text{box}}^{(a_1)}(Q^2) + \delta_{\text{xbox}}^{(b_1)}(Q^2) + \delta_{\text{box}}^{(c)}(Q^2) + \delta_{\text{xbox}}^{(d)}(Q^2) \right. \\ \left. + \delta_{\text{box}}^{(e)}(Q^2) + \delta_{\text{xbox}}^{(f)}(Q^2) + \delta_{\text{box}}^{(g)}(Q^2) + \delta_{\text{xbox}}^{(h)}(Q^2) + \delta_{\gamma\gamma}^{(\text{seagull})}(Q^2) \right]_{\text{NLO}}, \quad (23)$$

where

$$\delta_{\text{box}}^{(a)}(Q^2) = 2\Re e \sum_{\text{spins}} \left[\mathcal{M}_{\gamma}^{(0)*} \mathcal{M}_{\text{box}}^{(a)} \right] \Big/ \sum_{\text{spins}} \left| \mathcal{M}_{\gamma}^{(0)} \right|^2 \\ = -4\pi\alpha \left[\frac{Q^2}{Q^2 + 4EE'} \right] \Re e \left\{ \int \frac{d^4 k}{(2\pi)^4 i} \frac{\text{Tr} [(\not{p} + m_l) \not{v} (\not{p}' + m_l) \not{v} (\not{p} - \not{k} + m_l) \not{v}]}{(k^2 + i0) [(Q - k)^2 + i0] (k^2 - 2k \cdot p + i0) (v \cdot k + i0)} \right\} \\ = -8\pi\alpha \left[\frac{Q^2}{Q^2 + 4EE'} \right] \Re e \left\{ E' I^-(p, 0|0, 1, 1, 1) + E I^-(p, 0|1, 0, 1, 1) - (Q^2 + 8EE') \right. \\ \times I^-(p, 0|1, 1, 1, 0) + E(Q^2 + 8EE') I^-(p, 0|1, 1, 1, 1) \\ \left. - (E + E') I^-(p, 0|1, 1, 0, 1) \right\}, \quad (24)$$

$$\delta_{\text{xbox}}^{(b)}(Q^2) = 2\Re e \sum_{\text{spins}} \left[\mathcal{M}_{\gamma}^{(0)*} \mathcal{M}_{\text{xbox}}^{(b)} \right] \Big/ \sum_{\text{spins}} \left| \mathcal{M}_{\gamma}^{(0)} \right|^2 \\ = -4\pi\alpha \left[\frac{Q^2}{Q^2 + 4EE'} \right] \Re e \left\{ \int \frac{d^4 k}{(2\pi)^4 i} \frac{\text{Tr} [(\not{p} + m_l) \not{v} (\not{p}' + m_l) \not{v} (\not{p} + \not{k} - \not{Q} + m_l) \not{v}]}{(k^2 + i0) [(Q - k)^2 + i0] (k^2 + 2k \cdot p' + i0) (v \cdot k + i0)} \right\}, \\ = -8\pi\alpha \left[\frac{Q^2}{Q^2 + 4EE'} \right] \Re e \left\{ E I^+(p', 0|0, 1, 1, 1) + E' I^+(p', 0|1, 0, 1, 1) + (Q^2 + 8EE') \right. \\ \times I^+(p', 0|1, 1, 1, 0) + E'(Q^2 + 8EE') I^+(p', 0|1, 1, 1, 1) \\ \left. - (E + E') I^+(p', 0|1, 1, 0, 1) \right\}, \quad (25)$$

$$\delta_{\text{box}}^{(a_1)}(Q^2) = 2\Re e \sum_{\text{spins}} \left[\mathcal{M}_{\gamma}^{(1)*} \mathcal{M}_{\text{box}}^{(a)} \right] \Big/ \sum_{\text{spins}} \left| \mathcal{M}_{\gamma}^{(0)} \right|^2 \\ = -\frac{2\pi\alpha}{M} \left[\frac{Q^2}{Q^2 + 4EE'} \right] \left(Q_{\alpha} + v_{\alpha} \frac{Q^2}{2M} \right) \\ \times \Re e \left\{ \int \frac{d^4 k}{(2\pi)^4 i} \frac{\text{Tr} [(\not{p} + m_l) \gamma^{\alpha} (\not{p}' + m_l) \not{v} (\not{p} - \not{k} + m_l) \not{v}]}{(k^2 + i0) [(Q - k)^2 + i0] (k^2 - 2k \cdot p + i0) (v \cdot k + i0)} \right\} = \frac{Q^2}{4M^2} \delta_{\text{box}}^{(a)}(Q^2), \quad (26)$$

$$\delta_{\text{xbox}}^{(b_1)}(Q^2) = 2\Re e \sum_{\text{spins}} \left[\mathcal{M}_{\gamma}^{(1)*} \mathcal{M}_{\text{xbox}}^{(b)} \right] \Big/ \sum_{\text{spins}} \left| \mathcal{M}_{\gamma}^{(0)} \right|^2 \\ = -\frac{2\pi\alpha}{M} \left[\frac{Q^2}{Q^2 + 4EE'} \right] \left(Q_{\alpha} + v_{\alpha} \frac{Q^2}{2M} \right) \\ \times \Re e \left\{ \int \frac{d^4 k}{(2\pi)^4 i} \frac{\text{Tr} [(\not{p} + m_l) \gamma^{\alpha} (\not{p}' + m_l) \not{v} (\not{p} + \not{k} - \not{Q} + m_l) \not{v}]}{(k^2 + i0) [(Q - k)^2 + i0] (k^2 + 2k \cdot p' + i0) (v \cdot k + i0)} \right\} = \frac{Q^2}{4M^2} \delta_{\text{xbox}}^{(b)}(Q^2), \quad (27)$$

$$\delta_{\text{box}}^{(c)}(Q^2) = 2\Re e \sum_{\text{spins}} \left[\mathcal{M}_{\gamma}^{(0)*} \widetilde{\mathcal{M}}_{\text{box}}^{(c)} \right] \Big/ \sum_{\text{spins}} \left| \mathcal{M}_{\gamma}^{(0)} \right|^2 \\ = -\frac{2\pi\alpha}{M} \left[\frac{Q^2}{Q^2 + 4EE'} \right] \Re e \left\{ \int \frac{d^4 k}{(2\pi)^4 i} \frac{\text{Tr} [(\not{p} + m_l) \not{v} (\not{p}' + m_l) \not{v} (\not{p} - \not{k} + m_l) \not{k}]}{(k^2 + i0) [(Q - k)^2 + i0] (k^2 - 2k \cdot p + i0) (v \cdot k + i0)} \right\} \\ = \frac{4\pi\alpha}{M} Q^2 \Re e \left\{ I^-(p, 0|1, 1, 0, 1) \right\}, \quad (28)$$

$$\begin{aligned}
\delta_{\text{box}}^{(d)}(Q^2) &= 2\Re e \sum_{\text{spins}} \left[\mathcal{M}_\gamma^{(0)*} \widetilde{\mathcal{M}}_{\text{box}}^{(d)} \right] \Big/ \sum_{\text{spins}} \left| \mathcal{M}_\gamma^{(0)} \right|^2 \\
&= -\frac{2\pi\alpha}{M} \left[\frac{Q^2}{Q^2 + 4EE'} \right] \Re e \left\{ \int \frac{d^4 k}{(2\pi)^4 i} \frac{\text{Tr} [(\not{p} + m_l) \not{p} (\not{p}' + m_l) \not{k} (\not{p} + \not{k} - \not{Q} + m_l) \not{p}]}{(k^2 + i0) [(Q - k)^2 + i0] (k^2 + 2k \cdot p' + i0) (v \cdot k + i0)} \right\} \\
&= -\frac{4\pi\alpha}{M} Q^2 \Re e \left\{ I^-(p, 0|1, 1, 0, 1) \right\}, \tag{29}
\end{aligned}$$

$$\begin{aligned}
\delta_{\text{box}}^{(e)}(Q^2) &= 2\Re e \sum_{\text{spins}} \left[\mathcal{M}_\gamma^{(0)*} \widetilde{\mathcal{M}}_{\text{box}}^{(e)} \right] \Big/ \sum_{\text{spins}} \left| \mathcal{M}_\gamma^{(0)} \right|^2 \\
&= -\frac{2\pi\alpha}{M} \left[\frac{Q^2}{Q^2 + 4EE'} \right] \Re e \left\{ \int \frac{d^4 k}{(2\pi)^4 i} \frac{\text{Tr} [(\not{p} + m_l) \not{p} (\not{p}' + m_l) (\not{k} + \not{Q}) (\not{p} - \not{k} + m_l) \not{p}]}{(k^2 + i0) [(Q - k)^2 + i0] (k^2 - 2k \cdot p + i0) (v \cdot k + i0)} \right\} \\
&= \frac{4\pi\alpha}{M} \left[\frac{Q^2}{Q^2 + 4EE'} \right] \Re e \left\{ 4E^2 Q^2 I^-(p, 0|1, 1, 1, 1) - 4E^2 I^-(p, 0|1, 0, 1, 1) - (Q^2 - 4E^2) \right. \\
&\quad \times I^-(p, 0|1, 1, 0, 1) + 2(Q^2 + 2EE') I^-(p, 0|0, 1, 1, 1) \\
&\quad \left. - 4EQ^2 I^-(p, 0|1, 1, 1, 0) \right\}, \tag{30}
\end{aligned}$$

$$\begin{aligned}
\delta_{\text{box}}^{(f)}(Q^2) &= 2\Re e \sum_{\text{spins}} \left[\mathcal{M}_\gamma^{(0)*} \widetilde{\mathcal{M}}_{\text{box}}^{(f)} \right] \Big/ \sum_{\text{spins}} \left| \mathcal{M}_\gamma^{(0)} \right|^2 \\
&= -\frac{2\pi\alpha}{M} \left[\frac{Q^2}{Q^2 + 4EE'} \right] \Re e \left\{ \int \frac{d^4 k}{(2\pi)^4 i} \frac{\text{Tr} [(\not{p} + m_l) \not{p} (\not{p}' + m_l) \not{p} (\not{p} + \not{k} - \not{Q} + m_l) (\not{k} + \not{Q})]}{(k^2 + i0) [(Q - k)^2 + i0] (k^2 + 2k \cdot p' + i0) (v \cdot k + i0)} \right\} \\
&= -\frac{4\pi\alpha}{M} \left[\frac{Q^2}{Q^2 + 4EE'} \right] \Re e \left\{ 4E'^2 Q^2 I^+(p', 0|1, 1, 1, 1) - 4E'^2 I^+(p', 0|1, 0, 1, 1) - (Q^2 - 4E'^2) \right. \\
&\quad \times I^+(p', 0|1, 1, 0, 1) + 2(Q^2 + 2EE') I^+(p', 0|0, 1, 1, 1) \\
&\quad \left. + 4E' Q^2 I^+(p', 0|1, 1, 1, 0) \right\}, \tag{31}
\end{aligned}$$

$$\begin{aligned}
\delta_{\text{box}}^{(g)}(Q^2) &= 2\Re e \sum_{\text{spins}} \left[\mathcal{M}_\gamma^{(0)*} \widetilde{\mathcal{M}}_{\text{box}}^{(g)} \right] \Big/ \sum_{\text{spins}} \left| \mathcal{M}_\gamma^{(0)} \right|^2 \\
&= \frac{2\pi\alpha}{M} \left[\frac{Q^2}{Q^2 + 4EE'} \right] \Re e \left\{ \int \frac{d^4 k}{(2\pi)^4 i} \frac{\text{Tr} [(\not{p} + m_l) \not{p} (\not{p}' + m_l) \not{p} (\not{p} - \not{k} + m_l) \not{p}]}{[(Q - k)^2 + i0] (k^2 - 2k \cdot p + i0) (v \cdot k + i0)^2} \right\} \\
&= -\frac{4\pi\alpha}{M} \left[\frac{Q^2}{Q^2 + 4EE'} \right] \Re e \left\{ (Q^2 + 8EE') I^-(p, 0|0, 1, 1, 1) - [EQ^2 + 8E^2 E' + 2m_l^2(E + E')] \right. \\
&\quad \times I^-(p, 0|0, 1, 1, 2) - 2(E' p + E p') \cdot T_1^-(p, 0|0, 1, 1, 2) \Big\}, \quad \text{and} \tag{32}
\end{aligned}$$

$$\begin{aligned}
\delta_{\text{box}}^{(h)}(Q^2) &= 2\Re e \sum_{\text{spins}} \left[\mathcal{M}_\gamma^{(0)*} \widetilde{\mathcal{M}}_{\text{box}}^{(h)} \right] \Big/ \sum_{\text{spins}} \left| \mathcal{M}_\gamma^{(0)} \right|^2 \\
&= \frac{2\pi\alpha}{M} \left[\frac{Q^2}{Q^2 + 4EE'} \right] \Re e \left\{ \int \frac{d^4 k}{(2\pi)^4 i} \frac{\text{Tr} [(\not{p} + m_l) \not{p} (\not{p}' + m_l) \not{p} (\not{p} + \not{k} - \not{Q} + m_l) \not{p}]}{[(Q - k)^2 + i0] (k^2 + 2k \cdot p' + i0) (v \cdot k + i0)^2} \right\} \\
&= \frac{4\pi\alpha}{M} \left[\frac{Q^2}{Q^2 + 4EE'} \right] \Re e \left\{ (Q^2 + 8EE') I^+(p', 0|0, 1, 1, 1) - [EQ^2 - 2E' Q^2 - 8EE'^2 \right. \\
&\quad \left. - 2m_l^2(E + E')] I^+(p', 0|0, 1, 1, 2) - 2(E' p + E p') \cdot T_1^+(p', 0|0, 1, 1, 2) \right\}. \tag{33}
\end{aligned}$$

We note that the contribution $\delta_{\gamma\gamma}^{(\text{seagul})}$ from the seagull diagram (i) has already been evaluated exactly up to $\mathcal{O}(\alpha/M^2)$ in our previous work [60], and hence, not repeated here. There are ten 3-point scalar irreducible loop-integrals (master-integrals) which appear in the above expressions, which are generically defined *via* the following 4-point scalar reducible

loop-integrals, see Ref. [59]:

$$\begin{aligned} I^-(p, \omega | n_1, n_2, n_3, n_4) &= \frac{1}{i} \int \frac{d^4 k}{(2\pi)^4} \frac{1}{(k^2 + i0)^{n_1} [(k - Q)^2 + i0]^{n_2} (k^2 - 2k \cdot p + i0)^{n_3} (v \cdot k + \omega + i0)^{n_4}}, \quad \text{and} \\ I^+(p', \omega | n_1, n_2, n_3, n_4) &= \frac{1}{i} \int \frac{d^4 k}{(2\pi)^4} \frac{1}{(k^2 + i0)^{n_1} [(k - Q)^2 + i0]^{n_2} (k^2 + 2k \cdot p' + i0)^{n_3} (v \cdot k + \omega + i0)^{n_4}}, \end{aligned} \quad (34)$$

where the indices $n_{1,2,3,4} \in \mathbb{Z}$, and ω are arbitrary real-valued parameter. In our case ω can either be taken as zero, or any other finite quantity, e.g., $\omega \rightarrow v \cdot Q = -Q^2/2M$, $\omega \rightarrow v \cdot p = E$, $\omega \rightarrow -v \cdot p' = -E'$, etc., depending on the specific requirement. In Ref. [59], the 3-point loop-integrals were evaluated exactly, however, retaining terms up to $\mathcal{O}(1/M)$ only. Subsequently, In our more recent SPA-based TPE analysis [60], several of these results were extended to include contributions up to $\mathcal{O}(1/M^2)$, consistent with the inclusion of the dynamical NNLO contributions arising from the $\nu = 2$ chiral-order Lagrangian. In this work, we systematically account for all possible kinematically suppressed corrections of $\mathcal{O}(1/M^2)$. These arise not only from the relevant loop-integrals appearing in the LO and NLO fractional contributions to the cross section, Eqs. (24) - (33), but also from phase-space kinematics involving the outgoing lepton energy E' . An example is provided by the recoil expansion of the kinematical pre-factor $Q^2/(Q^2 + 4EE')$ that enters the TPE corrections derived from the LO cross section, Eq. (10) [also see Eq. (1)], namely,

$$\frac{Q^2}{Q^2 + 4EE'} = \left[\frac{Q^2}{Q^2 + 4E^2} \right] - \frac{1}{M} \left[\frac{2EQ^4}{(Q^2 + 4E^2)^2} \right] + \frac{1}{M^2} \left[\frac{4E^2Q^6}{(Q^2 + 4E^2)^3} \right] + \mathcal{O}\left(\frac{1}{M^3}\right). \quad (35)$$

Regarding the 4-point scalar loop-integrals $I^-(p, 0|1, 1, 1, 1)$ and $I^+(p', 0|1, 1, 1, 1)$ appearing in Eqs. (24) - (33), their direct evaluation was found to be technically challenging. Instead, Ref. [59] employs an astute analytical trick, wherein these intricate reducible loop-integrals are evaluated by reducing them to a combination of simpler 3-point master-integrals using a judicious application of partial fraction decomposition and IBP identities to obtain the following results:

$$\begin{aligned} I^-(p, 0|1, 1, 1, 1) &= \frac{1}{Q^2} \left[I^-(p, 0|1, 0, 1, 1) + I^-(p, 0|0, 1, 1, 1) - 2Z^-(\Delta, i\sqrt{-Q^2}/2, m_l, E) \right], \quad \text{and} \\ I^+(p', 0|1, 1, 1, 1) &= \frac{1}{Q^2} \left[I^+(p', 0|1, 0, 1, 1) + I^+(p', 0|0, 1, 1, 1) - 2Z^+(\Delta', i\sqrt{-Q^2}/2, m_l, -E') \right], \end{aligned} \quad (36)$$

where

$$\begin{aligned} Z^-(\Delta, i\sqrt{-Q^2}/2, m_l, E) &= \frac{1}{i} \int \frac{d^4 k}{(2\pi)^4} \frac{1}{[(k + \Delta)^2 - \frac{1}{4}Q^2 + i0] (k^2 - m_l^2 + i0) (v \cdot k + E + i0)}, \quad \text{and} \\ Z^+(\Delta', i\sqrt{-Q^2}/2, m_l, -E') &= \frac{1}{i} \int \frac{d^4 k}{(2\pi)^4} \frac{1}{[(k + \Delta')^2 - \frac{1}{4}Q^2 + i0] (k^2 - m_l^2 + i0) (v \cdot k - E' + i0)}, \end{aligned} \quad (37)$$

are the two additional 3-point master-integrals expressed in term of the four-vectors Δ_μ and Δ'_μ , defined as $\Delta_\mu = -\Delta'_\mu = (p - Q/2)_\mu$. The exact analytical expressions for these two master-integrals, truncated at order $1/M^2$, are provided in Appendix A. In doing so we extend to next order the original $\mathcal{O}(1/M)$ results for the Z^\pm integrals obtained in our previous exact TPE analysis [59].

Regarding the fractional contributions $\delta_{\text{box}}^{(g)}$ and $\delta_{\text{xbbox}}^{(h)}$ arising from the NLO TPE diagrams (g) and (h), these terms additionally involve two 3-point tensor integrals, defined as

$$\begin{aligned} T_1^{-\mu}(p, 0|0, 1, 1, 2) &= \frac{1}{i} \int \frac{d^4 k}{(2\pi)^4} \frac{(k - p)^\mu}{[(k - Q)^2 + i0] (k^2 - 2k \cdot p + i0) (v \cdot k + i0)^2}, \quad \text{and} \\ T_1^{+\mu}(p', 0|0, 1, 1, 2) &= \frac{1}{i} \int \frac{d^4 k}{(2\pi)^4} \frac{(k + p')^\mu}{[(k - Q)^2 + i0] (k^2 + 2k \cdot p' + i0) (v \cdot k + i0)^2}. \end{aligned} \quad (38)$$

At the targeted $\mathcal{O}(1/M^2)$ accuracy, it suffices to evaluate these loop-integrals up to $\mathcal{O}(1/M)$, since the expressions for $\delta_{\text{box}}^{(g), (h)}$ carry an overall $1/M$ pre-factor [see Eqs. (32) and (33)]. The required $\mathcal{O}(1/M)$ expressions for these integrals were already derived analytically in Ref. [59] [cf. Eqs. (B30) and (B31) of Appendix B therein], which we directly adopt in this work.

As noted by Choudhary *et al.* [59], the LO TPE box (a) and crossed-box (b) diagrams are the only ones whose fractional contributions to the elastic cross section, $\delta_{\text{box}}^{(a)}$, Eq. (24), and $\delta_{\text{xbbox}}^{(b)}$, Eq. (25), contain infrared (IR) divergences.

These divergences originate from the IR-singular behavior of the loop-integrals $I^-(p, 0|1, 0, 1, 1)$ and $I^+(p', 0|1, 0, 1, 1)$. However, it was shown that when the two contributions are combined in the sum $\delta_{\gamma\gamma}^{(ab)}$, the LO [i.e., $\mathcal{O}(\alpha M^0)$] IR-divergent terms cancel, leaving only a residual, kinematically suppressed $\mathcal{O}(\alpha/M)$ divergence consistent with NLO contributions. These NLO IR-divergent terms are exactly canceled by corresponding divergences arising from the inclusion of the charge-odd lepton-proton interference bremsstrahlung contributions, as explicitly demonstrated in our earlier work in Ref. [57] and subsequently in Ref. [80]. *En passant*, it is worth noting that the expressions $\delta_{\text{box}}^{(e)}$, Eq. (30), and $\delta_{\text{box}}^{(f)}$, Eq. (31), corresponding to the NLO TPE box (e) and crossed-box (f) diagrams, also contain terms involving the same IR-divergent integrals $I^-(p, 0|1, 0, 1, 1)$ and $I^+(p', 0|1, 0, 1, 1)$. In this case, however, both get canceled by the accompanying 4-point loop-functions $I^-(p, 0|1, 1, 1, 1)$ and $I^+(p', 0|1, 1, 1, 1)$, which themselves are expressed in terms of the same IR-divergent integrals [see Eqs. (36)].

In what follows we will display the analytical expressions for the finite parts of the TPE contributions arising from LO and NLO pairs of box and crossed-box amplitudes (a) - (g), as well as the seagull amplitude (i) [cf. Fig. 1], accounting for all kinematically suppressed terms up to $\mathcal{O}(\alpha/M^2)$ in each case. Particularly in our analytical results at this recoil order, we find it legitimate to replace all appearances of E' and β' by E and β , respectively, since no further recoil order terms are needed. It is noteworthy that diagrams (a) - (d) exhibit substantial cancellations between the box and crossed-box contributions, driven by the underlying analytic structure of the corresponding \pm type of loop-integrals in each case. In fact the total contribution from the (c) and (d) diagrams vanishes altogether, as was also found in Ref. [59], i.e., $\delta_{\gamma\gamma}^{(cd)}(Q^2) = \delta_{\text{box}}^{(c)}(Q^2) + \delta_{\text{box}}^{(d)}(Q^2) = 0$. This behavior, however, do not pertain to diagrams (e) - (h), which predominantly contribute constructively leading to sizable enhancements of the cross section. The finite results are enumerated below:

- First, we express the total finite contribution from the LO TPE box (a) and crossed-box (b) diagrams as²:

$$\begin{aligned} \overline{\delta_{\gamma\gamma}^{(ab)}}(Q^2) &= \delta_{\text{box}}^{(a)}(Q^2) + \delta_{\text{box}}^{(b)}(Q^2) - \delta_{\text{IR}}^{(\text{box})}(Q^2) \\ &\equiv \delta_{\gamma\gamma}^{(0)}(Q^2) + \overline{\delta_{\gamma\gamma}^{(ab;1/M)}}(Q^2) + \overline{\delta_{\gamma\gamma}^{(ab;1/M^2)}}(Q^2) + \mathcal{O}\left(\frac{\alpha}{M^3}\right), \quad \text{where} \end{aligned} \quad (39)$$

$$\begin{aligned} \delta_{\text{IR}}^{(\text{box})}(Q^2) &= \frac{\alpha}{\pi\beta} \left[\frac{1}{\epsilon} - \gamma_E + \ln\left(\frac{4\pi\mu^2}{m_l^2}\right) \right] \left\{ \ln\sqrt{\frac{1+\beta}{1-\beta}} - \frac{\beta}{\beta'} \ln\sqrt{\frac{1+\beta'}{1-\beta'}} \right\} \\ &= -\frac{\alpha Q^2}{2\pi M E \beta^2} \left[\frac{1}{\epsilon} - \gamma_E + \ln\left(\frac{4\pi\mu^2}{m_l^2}\right) \right] \left\{ 1 + \left(\beta - \frac{1}{\beta}\right) \ln\sqrt{\frac{1+\beta}{1-\beta}} \right\} \\ &\quad + \frac{3\alpha Q^4}{8\pi M^2 E^2 \beta^4} \left[\frac{1}{\epsilon} - \gamma_E + \ln\left(\frac{4\pi\mu^2}{m_l^2}\right) \right] \left\{ 1 - \frac{2}{3}\beta^2 + \left(\beta - \frac{1}{\beta}\right) \ln\sqrt{\frac{1+\beta}{1-\beta}} \right\} + \mathcal{O}\left(\frac{\alpha}{M^3}\right). \end{aligned} \quad (40)$$

Here, we have isolated IR divergence using dimensional regularization (DR) by analytically continuing the integrals to D -dimensional space-time with pole, $\epsilon = (4 - D)/2 < 0$. $\gamma_E = 0.577216\dots$ is the Euler-Mascheroni constant, and μ is an arbitrary subtraction scale. As mentioned, the genuine LO [i.e., $\mathcal{O}(\alpha M^0)$] terms exhibit significant cancellations between $\delta_{\text{box}}^{(a)}$ and $\delta_{\text{box}}^{(b)}$, leaving a residual term solely arising from the 3-point master-integral $I(Q|1, 1, 0, 1) \equiv I^-(p, 0|1, 1, 0, 1) = I^+(p', 0|1, 1, 0, 1)$. Unlike the SPA approach, as demonstrated in Ref. [59], these terms yield a non-vanishing LO TPE contribution akin to the well-known McKinley and Feshbach [73] result:

$$\delta_{\gamma\gamma}^{(0)}(Q^2) = 32\pi\alpha E \left[\frac{Q^2}{Q^2 + 4E^2} \right] \mathbb{R}e \left[I^{(0)}(Q|1, 1, 0, 1) \right] = \pi\alpha \frac{\sqrt{-Q^2}}{2E} \left[\frac{1}{1 + \frac{Q^2}{4E^2}} \right], \quad (41)$$

where the loop-function, $I^{(0)}(Q|1, 1, 0, 1) \sim \mathcal{O}(M^0)$, denotes the leading recoil order component of the loop-integral $I(Q|1, 1, 0, 1)$. Its analytical expression up to $\mathcal{O}(1/M^2)$ in the recoil expansion is evaluated in Eq. (A9) of Appendix A. In our previous exact TPE work of Ref. [59] only the $\mathcal{O}(\alpha/M)$ contribution to the cross section stemming from the LO TPE diagrams was derived. Here, we reproduce the same result for completeness:

² Henceforth, an overbar on the fractional TPE contributions $\delta_{\gamma\gamma}$ will denote only the finite part, with the IR-divergent terms proportional to $\left[\frac{1}{\epsilon} - \gamma_E + \ln\left(\frac{4\pi\mu^2}{m_l^2}\right) \right]$ subtracted according to the standard $\overline{\text{MS}}$ scheme.

$$\begin{aligned}
\overline{\delta_{\gamma\gamma}^{(ab;1/M)}}(Q^2) = & -16\pi\alpha E \mathbb{R}e \left\{ \overline{\delta^{(1/M)} I^+}(p', 0|1, 0, 1, 1) + \delta^{(1/M)} I^-(p, 0|0, 1, 1, 1) + \delta^{(1/M)} I^+(p', 0|0, 1, 1, 1) \right. \\
& - \left[\frac{Q^2 + 8E^2}{Q^2 + 4E^2} \right] \left(\delta^{(1/M)} Z^-(\Delta, i\sqrt{-Q^2}/2, m_l, E) \right. \\
& \left. \left. + \delta^{(1/M)} Z^+(\Delta', i\sqrt{-Q^2}/2, m_l, -E') \right) \right. \\
& - \left[\frac{2Q^2}{Q^2 + 4E^2} \right] \delta^{(1/M)} I(Q|1, 1, 0, 1) \Big\} \\
& + 8\pi\alpha \frac{Q^2}{M} \mathbb{R}e \left\{ \overline{I^{(0)}}(p, 0|1, 0, 1, 1) + \left[\frac{4E^2}{Q^2 + 4E^2} \right] I^{(0)}(p, 0|0, 1, 1, 1) + \left[\frac{Q^2(Q^2 - 4E^2)}{(Q^2 + 4E^2)^2} \right] \right. \\
& \left. \times I^{(0)}(Q|1, 1, 0, 1) - \left[\frac{Q^2 + 8E^2}{Q^2 + 4E^2} \right] Z^{(0)}(\Delta, i\sqrt{-Q^2}/2, m_l, E) \right\}. \quad (42)
\end{aligned}$$

The kinematically suppressed $\mathcal{O}(\alpha/M^2)$ component represents our new extension of the above IR-finite part, and is given by the following expression:

$$\begin{aligned}
\overline{\delta_{\gamma\gamma}^{(ab;1/M^2)}}(Q^2) = & -16\pi\alpha E \mathbb{R}e \left\{ \overline{\delta^{(1/M^2)} I^+}(p', 0|1, 0, 1, 1) + \delta^{(1/M^2)} I^-(p, 0|0, 1, 1, 1) + \delta^{(1/M^2)} I^+(p', 0|0, 1, 1, 1) \right. \\
& - \left[\frac{2Q^2}{Q^2 + 4E^2} \right] \delta^{(1/M^2)} I(Q|1, 1, 0, 1) - \left[\frac{Q^2 + 8E^2}{Q^2 + 4E^2} \right] \\
& \times \left(\delta^{(1/M^2)} Z^-(\Delta, i\sqrt{-Q^2}/2, m_l, E) + \delta^{(1/M^2)} Z^+(\Delta', i\sqrt{-Q^2}/2, m_l, -E') \right) \Big\} \\
& - \frac{4\pi\alpha Q^2}{M(Q^2 + 4E^2)} \mathbb{R}e \left\{ 2(Q^2 + 4E^2) \overline{\delta^{(1/M)} I^+}(p', 0|1, 0, 1, 1) + Q^2 \delta^{(1/M)} I^-(p, 0|0, 1, 1, 1) \right. \\
& + (Q^2 + 8E^2) \delta^{(1/M)} I^+(p', 0|0, 1, 1, 1) - 2 \left[\frac{Q^2(Q^2 - 4E^2)}{Q^2 + 4E^2} \right] \\
& \times \delta^{(1/M)} I(Q|1, 1, 0, 1) - \left[\frac{8Q^2 E^2}{Q^2 + 4E^2} \right] \delta^{(1/M)} Z^-(\Delta, i\sqrt{-Q^2}/2, m_l, E) \\
& - 2 \left[\frac{Q^4 + 16Q^2 E^2 + 32E^4}{Q^2 + 4E^2} \right] \delta^{(1/M)} Z^+(\Delta', i\sqrt{-Q^2}/2, m_l, -E') \Big\} \\
& - \frac{16\pi\alpha Q^6 E}{M^2(Q^2 + 4E^2)^2} \mathbb{R}e \left\{ \left[\frac{Q^2 - 4E^2}{Q^2 + 4E^2} \right] I^{(0)}(Q|1, 1, 0, 1) - I^{(0)}(p, 0|0, 1, 1, 1) \right. \\
& \left. + Z^{(0)}(\Delta', i\sqrt{-Q^2}/2, m_l, -E') \right\} \quad (43)
\end{aligned}$$

All the 3-point master-integrals appearing in the above expressions were originally evaluated analytically up to $\mathcal{O}(1/M)$ in the work of Choudhary *et al.* [59]. As for the master-integrals, $I^-(p, 0|0, 1, 1, 1)$, $I^+(p', 0|0, 1, 1, 1)$, $I^-(p, 0|1, 0, 1, 1)$, $I^+(p', 0|1, 0, 1, 1)$, $I^-(p, 0|1, 1, 0, 0)$, and $I^+(p', 0|1, 1, 0, 0)$, their $\mathcal{O}(1/M^2)$ extensions were subsequently obtained in the SPA-based TPE work by Goswami *et al.* [60]. Whereas, the $\mathcal{O}(1/M^2)$ extensions to the 3-point master-integrals $Z^-(\Delta, i\sqrt{-Q^2}/2, m_l, E)$, $Z^+(\Delta', i\sqrt{-Q^2}/2, m_l, -E')$, $I^-(p, 0|1, 1, 0, 1)$, and $I^+(p', 0|1, 1, 0, 1)$, are evaluated for the first time in this work and presented in Appendix A. Note that the functions $I^{(0)}$ and $Z^{(0)}$ denote the LO [i.e., $\mathcal{O}(M^0)$] components of the corresponding I^\pm and Z^\pm integrals, respectively (up to an overall sign); see Ref. [59] for details. In particular, $\overline{I^{(0)}}$, $\overline{\delta^{(1/M)} I^+}(p', 0|1, 0, 1, 1)$, and $\overline{\delta^{(1/M^2)} I^+}(p', 0|1, 0, 1, 1)$ in the above expressions denote the IR-finite parts of the corresponding IR-divergent master-integral $I^+(p', 0|1, 0, 1, 1)$, truncated at $\mathcal{O}(1/M^2)$ (also see

Appendix A of Ref. [60]), namely,

$$\begin{aligned} I^+(p', 0|1, 0, 1, 1) &= \frac{1}{i} \int \frac{d^4 k}{(2\pi)^4} \frac{1}{(k^2 + i0)(k^2 + 2k \cdot p' + i0)(v \cdot k + i0)} \\ &= \frac{1}{(4\pi)^2 \beta' E'} \left[\left\{ \frac{1}{\epsilon} - \gamma_E + \ln \left(\frac{4\pi\mu^2}{m_l^2} \right) \right\} \ln \sqrt{\frac{1+\beta'}{1-\beta'}} - i\pi \left\{ \frac{1}{\epsilon} - \gamma_E + \ln \left(\frac{4\pi\mu^2}{m_l^2} \right) \right\} \right] \\ &\quad - \overline{I^{(0)}}(p, 0|1, 0, 1, 1) + \overline{\delta^{(1/M)} I^+}(p', 0|1, 0, 1, 1) + \overline{\delta^{(1/M^2)} I^+}(p', 0|1, 0, 1, 1) + \mathcal{O}\left(\frac{1}{M^3}\right), \quad (44) \end{aligned}$$

where the IR-finite parts, after expressing the outgoing lepton energy E' and velocity β' in terms of the corresponding incident energy E and velocity β , are given by

$$\overline{I^{(0)}}(p, 0|1, 0, 1, 1) = \frac{1}{(4\pi)^2 \beta E} \left[\text{Li}_2 \left(\frac{2\beta}{1+\beta} \right) + \ln^2 \sqrt{\frac{1+\beta}{1-\beta}} \right], \quad (45)$$

$$\overline{\delta^{(1/M)} I^+}(p', 0|1, 0, 1, 1) = \frac{Q^2}{2(4\pi)^2 M E^2 \beta^3} \left[\text{Li}_2 \left(\frac{2\beta}{1+\beta} \right) + \ln^2 \sqrt{\frac{1+\beta}{1-\beta}} - 2 \ln \sqrt{\frac{1+\beta}{1-\beta}} \right], \text{ and} \quad (46)$$

$$\begin{aligned} \overline{\delta^{(1/M^2)} I^+}(p', 0|1, 0, 1, 1) &= -\frac{Q^4}{8(4\pi)^2 M^2 E^3 \beta^5} \left[2\beta + (3 - \beta^2) \text{Li}_2 \left(\frac{2\beta}{1+\beta} \right) + (3 - \beta^2) \ln^2 \sqrt{\frac{1+\beta}{1-\beta}} \right. \\ &\quad \left. + 2(\beta^2 - 4) \ln \sqrt{\frac{1+\beta}{1-\beta}} \right]. \quad (47) \end{aligned}$$

The function Li_2 in the above equations represents the standard di-logarithm or Spence function defined as

$$\text{Li}_2(z) = - \int_0^z dt \frac{\ln(1-t)}{t}, \quad \forall z \in \mathbb{C}. \quad (48)$$

- Second, the finite part of the contribution arising from the interference of the NLO OPE amplitude $M_\gamma^{(1)}$ with the LO box (a) and crossed-box (b) TPE amplitudes, after subtracting the residual $\mathcal{O}(\alpha/M^3)$ IR divergence, is given by

$$\overline{\delta_{\gamma\gamma}^{(a_1 b_1)}}(Q^2) = \delta_{\text{box}}^{(a_1)}(Q^2) + \delta_{\text{xbox}}^{(b_1)}(Q^2) - \frac{Q^2}{4M^2} \delta_{\text{IR}}^{(\text{box})}(Q^2) = \overline{\delta_{\gamma\gamma}^{(a_1 b_1; 1/M^2)}}(Q^2) + \mathcal{O}\left(\frac{\alpha}{M^3}\right), \quad (49)$$

where

$$\begin{aligned} \overline{\delta_{\gamma\gamma}^{(a_1 b_1; 1/M^2)}}(Q^2) &= \frac{Q^2}{4M^2} \delta_{\gamma\gamma}^{(0)}(Q^2) \\ &= -\frac{\pi\alpha(-Q^2)^{3/2}}{8M^2 E} \left[\frac{1}{1 + \frac{Q^2}{4E^2}} \right]. \quad (50) \end{aligned}$$

In other words, since the leading TPE IR divergence scales as $\delta_{\text{IR}}^{(\text{box})} \sim \mathcal{O}(\alpha/M)$ [see Eq. (40)], no new $\mathcal{O}(\alpha/M^2)$ divergence is generated by the contribution $\overline{\delta_{\gamma\gamma}^{(a_1 b_1)}}$, other than those terms originating from the $1/M$ -recoil expansion of $\delta_{\text{IR}}^{(\text{box})}$ itself originating from the contribution $\overline{\delta_{\gamma\gamma}^{(ab)}}$ already considered.

- Third, the largest corrections originate from the NLO TPE box (e) and crossed-box (f) diagrams, whose contributions add constructively and may be expressed as

$$\begin{aligned} \delta_{\gamma\gamma}^{(ef)}(Q^2) &= \delta_{\text{box}}^{(e)}(Q^2) + \delta_{\text{xbox}}^{(f)}(Q^2) \\ &\equiv \delta_{\gamma\gamma}^{(ef; 1/M)}(Q^2) + \delta_{\gamma\gamma}^{(ef; 1/M^2)}(Q^2) + \mathcal{O}\left(\frac{\alpha}{M^3}\right), \quad (51) \end{aligned}$$

where the $\mathcal{O}(\alpha/M)$ component $\delta_{\gamma\gamma}^{(ef; 1/M)}$, previously derived in Ref. [59], is reproduced below for completeness. Whereas, the kinematically suppressed $\mathcal{O}(\alpha/M^2)$ component $\delta_{\gamma\gamma}^{(ef; 1/M^2)}$ constitutes the necessary extension of that

result in the present work. Thus, we have

$$\delta_{\gamma\gamma}^{(ef;1/M)}(Q^2) = \frac{16\pi\alpha Q^2}{M(Q^2 + 4E^2)} \mathbb{R}e \left\{ (Q^2 + 4E^2) I^{(0)}(p, 0|0, 1, 1, 1) - 2Q^2 EI(Q|1, 1, 1, 0) \right. \\ \left. - 4E^2 Z^{(0)}(\Delta, i\sqrt{-Q^2}/2, m_l, E) \right\}, \quad (52)$$

and

$$\delta_{\gamma\gamma}^{(ef;1/M^2)}(Q^2) = \frac{8\pi\alpha Q^2}{M(Q^2 + 4E^2)} \mathbb{R}e \left\{ (Q^2 + 4E^2) \left(\delta^{(1/M)} I^-(p, 0|0, 1, 1, 1) - \delta^{(1/M)} I^+(p', 0|0, 1, 1, 1) \right) \right. \\ \left. - 4E^2 \left(\delta^{(1/M)} Z^-(\Delta, i\sqrt{-Q^2}/2, m_l, E) \right. \right. \\ \left. \left. - \delta^{(1/M)} Z^+(\Delta', i\sqrt{-Q^2}/2, m_l, -E') \right) \right\} \\ - \frac{8\pi\alpha Q^4}{M^2(Q^2 + 4E^2)^2} \mathbb{R}e \left\{ 2(Q^2 + 4E^2) EI^{(0)}(Q|1, 1, 0, 1) + Q^2(Q^2 - 4E^2) I^{(0)}(p, 0|1, 1, 1, 0) \right. \\ \left. + 4Q^2 E Z^{(0)}(\Delta, i\sqrt{-Q^2}/2, m_l, E) \right\}. \quad (53)$$

- Fourth, the total contribution from the NLO TPE box (g) and crossed-box (h) diagrams can be expressed as follows:

$$\delta_{\gamma\gamma}^{(gh)}(Q^2) = \delta_{\text{box}}^{(g)}(Q^2) + \delta_{\text{box}}^{(h)}(Q^2) \\ = \delta_{\gamma\gamma}^{(gh;1/M)}(Q^2) + \delta_{\gamma\gamma}^{(gh;1/M^2)}(Q^2) + \mathcal{O}\left(\frac{\alpha}{M^3}\right), \quad (54)$$

where the $\mathcal{O}(\alpha/M)$ component $\delta_{\gamma\gamma}^{(gh;1/M)}$, previously derived in Ref. [59], is reproduced below for completeness, namely,

$$\delta_{\gamma\gamma}^{(gh);1/M}(Q^2) = -\frac{4\pi\alpha Q^2}{M(Q^2 + 4E^2)} \mathbb{R}e \left\{ 2 \left[Q^2 \left(1 + \frac{1}{\beta^2} \right) + 8E^2 \right] I^{(0)}(p, 0|0, 1, 1, 1) \right. \\ \left. + \left[\frac{Q^2 + 4E^2 \beta^2}{E\beta^2} \right] \left(I(Q|0, 1, 0, 2) - I^{(0)}(p, 0|0, 0, 1, 2) \right) \right\} \\ - \frac{2\pi\alpha Q^4}{M(Q^2 + 4E^2)} \left[Q^2 \left(1 + \frac{2}{\beta^2} \right) + 8E^2 \right] \mathbb{R}e \left[I^{(0)}(p, 0|0, 1, 1, 2) \right] \\ - \frac{\alpha Q^2}{\pi M E \beta^3} \left[\ln \sqrt{\frac{1+\beta}{1-\beta}} - \beta \right]. \quad (55)$$

Here, the function $I^{(0)}(p, 0|0, 0, 1, 2)$ denotes the $\mathcal{O}(M^0)$ component of 2-point master-integrals $I^-(p, 0|0, 0, 1, 2)$ and $I^+(p', 0|0, 0, 1, 2)$, as evaluated in Ref. [59]. The 2-point master-integral $I(Q|0, 1, 0, 2)$, which is also computed in the same reference, contains the same UV-divergent pieces as $I^{(0)}(p, 0|0, 0, 1, 2)$. These divergences cancel identically when the two contributions are combined in the above expression, yielding a finite result. The term $\delta_{\gamma\gamma}^{(gh;1/M^2)}$ denotes the $\mathcal{O}(\alpha/M^2)$ extension of the above results obtained in the present work, which, for brevity, is presented in

the unexpanded form in terms of the relevant loop-functions as

$$\begin{aligned}
\delta_{\gamma\gamma}^{(gh;1/M^2)}(Q^2) = & \frac{4\pi\alpha Q^2}{M(Q^2+4E^2)} \mathbb{R}e \left\{ 2E(Q^2+4E^2) \left(\delta^{(1/M)} I^-(p,0|0,1,1,2) + \delta^{(1/M)} I^+(p',0|0,1,1,2) \right) \right. \\
& + \left[Q^2 \left(1 + \frac{1}{\beta^2} \right) + 8E^2 \right] \left(\delta^{(1/M)} I^+(p',0|0,1,1,1) \right. \\
& \left. \left. - \delta^{(1/M)} I^-(p,0|0,1,1,1) \right) \right. \\
& + \left. \left(2E + \frac{Q^2}{2E\beta^2} \right) \delta^{(1/M)} I^+(p',0|0,0,1,2) \right\} \\
& + \frac{\pi\alpha Q^4}{M^2 E^2 \beta^4 (Q^2+4E^2)^2} \left\{ 2\beta^2 E^2 \left(32\beta^2 E^4 + (4E^2 + 16E^2\beta^2) Q^2 + Q^4(1+2\beta^2) \right) \right. \\
& \times \delta^{(M^0)} I^+(p',0|0,1,1,2) + 4EQ^2(1-\beta^2) \left(Q^2 + 4E^2(1+\beta^2) \right) \\
& \times I^{(0)}(p,0|0,1,1,1) + 2E^2\beta^2(1-\beta^2)(Q^2-4E^2) \\
& \times \left. \left(I(Q|0,1,0,2) - I^{(0)}(p,0|0,0,1,2) \right) \right\} \\
& + \frac{2\pi\alpha Q^8}{M^2 E \beta^4 (Q^2+4E^2)^2} \left(2E^2(2-\beta^4) + Q^2(1-\beta^2) \right) \mathbb{R}e \left[I^{(0)}(p,0|0,1,1,2) \right]. \tag{56}
\end{aligned}$$

The 3-point master-integrals $I^-(p,0|0,1,1,2)$ and $I^+(p',0|0,1,1,2)$ needed in the above results, contain “super-leading-order” contributions proportional to the function $I^{(0)}(p,0|0,1,1,2)$ that scale as $\mathcal{O}(M)$, as we first demonstrated in Ref. [59]. The same functions also appears in our recent SPA-based TPE analysis [60], where a slightly modified notation is introduced to denote the various $1/M$ -recoil order components, which we adopt here, namely,

$$\begin{aligned}
I^-(p,0|0,1,1,2) = & \frac{1}{i} \int \frac{d^4k}{(2\pi)^4} \frac{1}{[(k-Q)^2+i0]} \frac{1}{(k^2-2k\cdot p+i0)(v\cdot k+i0)^2} \\
\equiv & MI^{(0)}(p,0|0,1,1,2) + \delta^{(1/M)} I^-(p,0|0,1,1,2) + \mathcal{O}\left(\frac{1}{M^2}\right), \tag{57}
\end{aligned}$$

where

$$I^{(0)}(p,0|0,1,1,2) = -\frac{4}{(4\pi)^2 Q^2 E \beta} \ln \sqrt{\frac{1+\beta}{1-\beta}}, \quad \text{and} \tag{58}$$

$$\delta^{(1/M)} I^-(p,0|0,1,1,2) = -\frac{3Q^2}{(4\pi)^2 M E^3 \beta^4}. \tag{59}$$

Likewise, the expression of the loop-integral $I^+(p',0|0,1,1,2) \sim \mathcal{O}(M)$ is given as

$$\begin{aligned}
I^+(p',0|0,1,1,2) = & \frac{1}{i} \int \frac{d^4k}{(2\pi)^4} \frac{1}{[(k-Q)^2+i0]} \frac{1}{(k^2+2k\cdot p'+i0)(v\cdot k+i0)^2} \\
\equiv & -MI^{(0)}(p,0|0,1,1,2) + \delta^{(M^0)} I^+(p',0|0,1,1,2) + \delta^{(1/M)} I^+(p',0|0,1,1,2) + \mathcal{O}\left(\frac{1}{M^2}\right), \tag{60}
\end{aligned}$$

where

$$\delta^{(M^0)} I^+(p',0|0,1,1,2) = -\frac{2}{(4\pi)^2 E^2 \beta^3} \left[\ln \sqrt{\frac{1+\beta}{1-\beta}} - \beta \right], \quad \text{and} \tag{61}$$

$$\delta^{(1/M)} I^+(p',0|0,1,1,2) = \frac{Q^2}{2(4\pi)^2 M E^3 \beta^5} \left(-3\beta + (3-\beta^2) \ln \sqrt{\frac{1+\beta}{1-\beta}} \right). \tag{62}$$

- Fifth, the total contribution from the NLO TPE seagull diagram (i) is evaluated exactly in our earlier SPA-based analysis [60]:

$$\delta_{\gamma\gamma}^{(\text{seagull})}(Q^2) \equiv \delta_{\gamma\gamma}^{(\text{seagull};1/M)}(Q^2) + \delta_{\gamma\gamma}^{(\text{seagull};1/M^2)}(Q^2) + \mathcal{O}\left(\frac{\alpha}{M^3}\right), \quad (63)$$

where the $\mathcal{O}(\alpha/M)$ and the kinematically suppressed $\mathcal{O}(\alpha/M^2)$ components are reproduced below:

$$\begin{aligned} \delta_{\gamma\gamma}^{(\text{seagull};1/M)}(Q^2) &= \frac{16\alpha m_l^2 E}{\pi M(Q^2 + 4E^2)\nu_l^2} \\ &\times \left[\left(\frac{1 + \nu_l^2}{2\nu_l} \right) \left\{ \frac{\pi^2}{3} + \ln^2 \sqrt{\frac{\nu_l + 1}{\nu_l - 1}} + \text{Li}_2 \left(\frac{\nu_l - 1}{\nu_l + 1} \right) \right\} - \ln \sqrt{-\frac{Q^2}{m_l^2}} \right], \end{aligned} \quad (64)$$

and

$$\begin{aligned} \delta_{\gamma\gamma}^{(\text{seagull};1/M^2)}(Q^2) &= -\frac{32\alpha m_l^2 Q^2 E^2}{\pi M^2(Q^2 + 4E^2)^2 \nu_l^2} \\ &\times \left[\left(\frac{1 + \nu_l^2}{2\nu_l} \right) \left\{ \frac{\pi^2}{3} + \ln^2 \sqrt{\frac{\nu_l + 1}{\nu_l - 1}} + \text{Li}_2 \left(\frac{\nu_l - 1}{\nu_l + 1} \right) \right\} - \ln \sqrt{-\frac{Q^2}{m_l^2}} \right] \\ &+ \frac{\alpha Q^4}{\pi M^2(Q^2 + 4E^2)\nu_l^2} \\ &\times \left[\frac{2m_l^2}{Q^2\nu_l} \left\{ \frac{\pi^2}{3} + \ln^2 \sqrt{\frac{\nu_l + 1}{\nu_l - 1}} + \text{Li}_2 \left(\frac{\nu_l - 1}{\nu_l + 1} \right) \right\} + 2 \ln \sqrt{-\frac{Q^2}{m_l^2}} \right], \end{aligned} \quad (65)$$

respectively, and where $\nu_l = \sqrt{1 - 4m_l^2/Q^2}$. The latter correction is also included in the total $\mathcal{O}(\alpha/M^2)$ TPE contribution $\delta_{\gamma\gamma}^{(\text{LO+NLO};2)}$, as considered below. The seagull contribution, which depends primarily on the square of the lepton mass, m_l , is exceedingly small in the case of electron-proton scattering when compared with the other non-vanishing contributions from the NLO diagram.

To conclude this section we display in Fig. 2 the relevant kinematically suppressed $\mathcal{O}(\alpha/M^2)$ components resulting from the LO and NLO diagrams entering their total contribution to the elastic cross section, i.e.,

$$\begin{aligned} \delta_{\gamma\gamma}^{(\text{LO+NLO};2)}(Q^2) &\equiv \overline{\delta_{\gamma\gamma}^{(ab;1/M^2)}(Q^2)} + \overline{\delta_{\gamma\gamma}^{(a_1 b_1;1/M^2)}(Q^2)} + \delta_{\gamma\gamma}^{(ef;1/M^2)}(Q^2) \\ &+ \delta_{\gamma\gamma}^{(gh;1/M^2)}(Q^2) + \delta_{\gamma\gamma}^{(\text{seagull};1/M^2)}(Q^2). \end{aligned} \quad (66)$$

In the following section we turn to the genuine dynamical TPE contributions that incorporate the proton–photon NNLO interaction at $\nu = 2$, leading to the finite size modifications of the elastic differential cross section.

IV. DYNAMICAL NNLO CORRECTIONS BY INCLUDING TPE DIAGRAMS UP TO NNLO

We restrict our attention to the four dominant “reducible” two-loop TPE diagrams at chiral-order $\nu = 2$, where one of the loops is a pion-loop at the proton-photon vertex. In this case the pion-loop contribution factorizes, leading to a renormalization of the photon–proton vertices and effectively reduce the topologies to one-loop TPE diagrams dressed with the proton’s Dirac (F_1^p) and Pauli (F_2^p) form factors [79], parameterizing the finite-size of the proton (cf. Fig. 3). In other words, we here treat only our “effective one-loop” approximation. Below we then extend the NLO results presented in the previous section to incorporate all one-loop dynamical NNLO corrections to the TPE arising from the interference between the TPE and the OPE Feynman diagrams, which explicitly scale as $\mathcal{O}(\alpha/M^2)$. The extension also include insertions of the proton’s propagator up to $\mathcal{O}(1/M^2)$, as given in Eq.(7). To this end, the NNLO extension of Eq. (9) is given as

$$\left[\frac{d\sigma_{el}(Q^2)}{d\Omega'_l} \right]_{\text{NNLO}}^{(\ell^\mp)} = \pm \left[\frac{d\sigma_{el}(Q^2)}{d\Omega'_l} \right]_0 \delta_{\gamma\gamma}^{(\text{NNLO})}(Q^2), \quad (67)$$

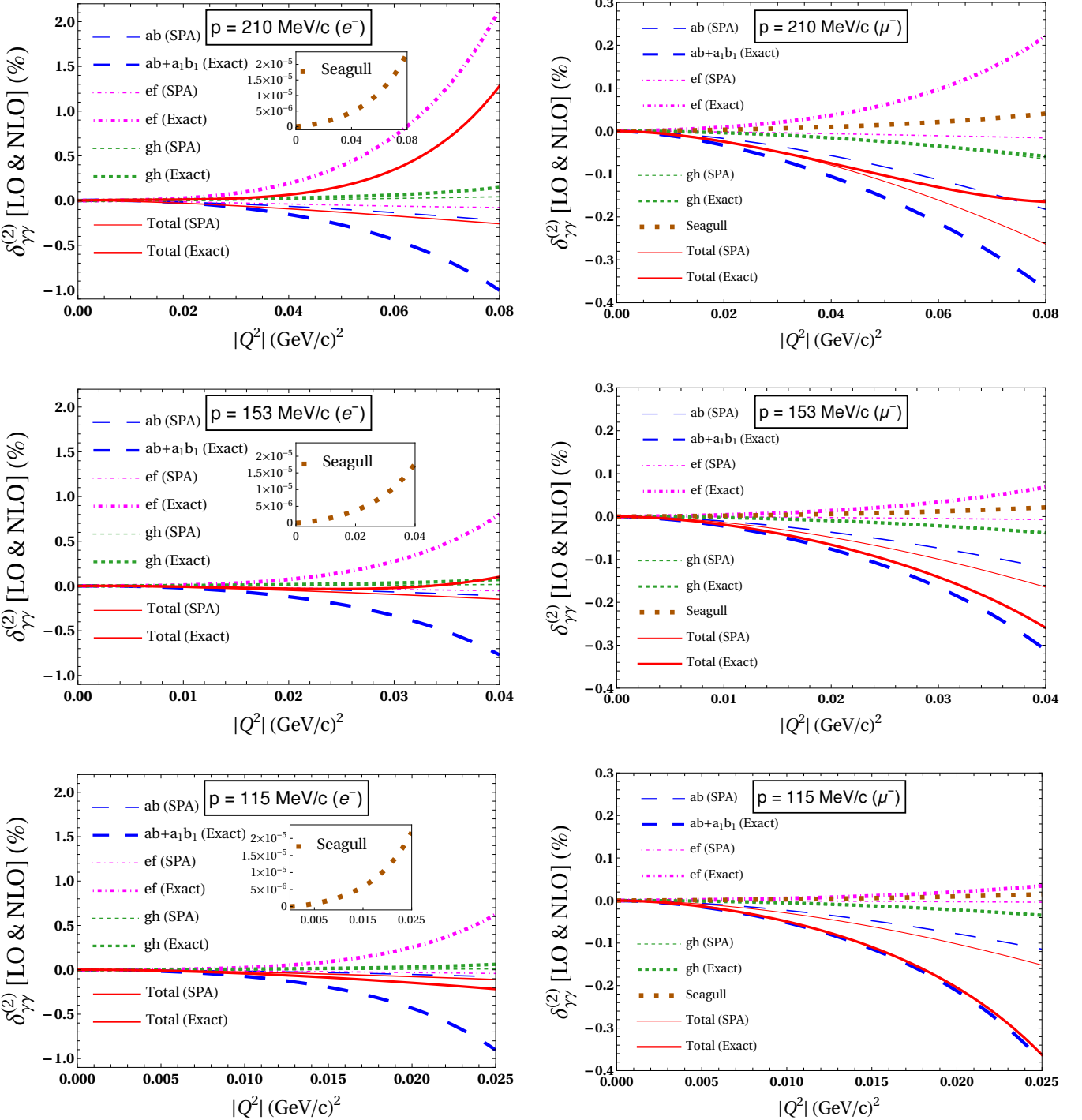


FIG. 2. The box and crossed-box pairs of finite fractional kinematical NNLO corrections arising from the LO and NLO TPE diagrams (a) - (h), are shown together with the contributions arising from the NLO seagull diagram (i) and the interference of the NLO Born (OPE) amplitude $\mathcal{M}_\gamma^{(1)}$ with the LO TPE diagrams (a) and (b), entering the $\mathcal{O}(\alpha/M^2)$ component $\delta_{\gamma\gamma}^{(\text{LO+NLO};2)}$ [see Eq. (66)] of the corrections to the elastic lepton–proton differential cross section. Note that in the figure, we present the combined $\mathcal{O}(\alpha/M^2)$ contribution from the LO pair of TPE diagrams (a) and (b), i.e., $\overline{\delta_{\gamma\gamma}^{(ab;1/M^2)}} + \overline{\delta_{\gamma\gamma}^{(a_1b_1;1/M^2)}}$, which is labeled as “ab+a₁b₁ (Exact)”. For comparison, the corresponding SPA results of Goswami *et al.* [60] are also displayed. It is noteworthy that the tiny seagull contribution (inset panel) has no SPA counterpart. The results for e–p (μ –p) elastic scattering are shown in the left (right) panel as functions of the squared four-momentum transfer $|Q^2|$, for three MUSE incident lepton beam momenta: 210 MeV/c, 153 MeV/c, and 115 MeV/c. All fractional corrections are given relative to the LO OPE differential cross section.

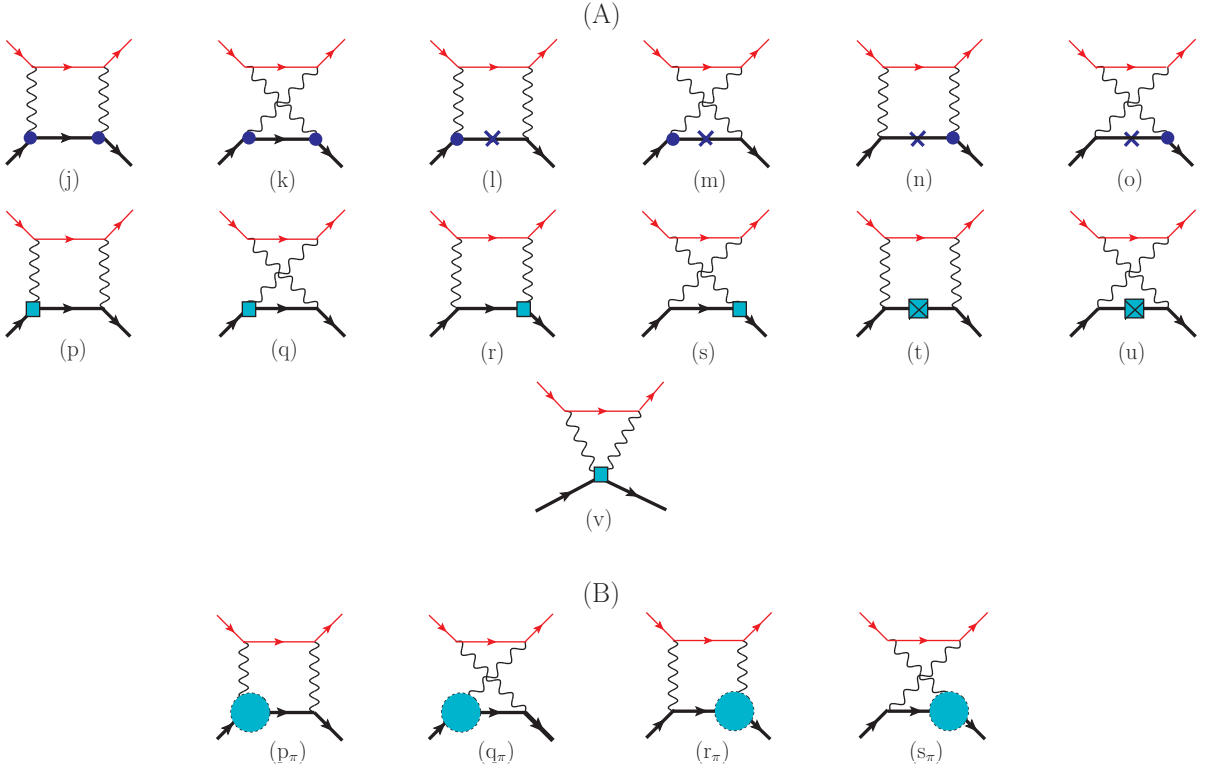


FIG. 3. The one-loop NNLO [i.e., $\mathcal{O}(\alpha^2/M^2)$] TPE diagrams contributing to the $\mathcal{O}(\alpha^3/M^2)$ lepton-proton elastic differential cross section, are shown. The thick, thin, and wiggly lines denote the proton, lepton and photon propagators. The small solid circles and square green boxes denote the insertions of NLO ($\nu = 1$) and NNLO ($\nu = 2$) proton-photon interaction vertices, respectively. The crosses and green-square boxes represent the insertions of the $\mathcal{O}(1/M)$ and $\mathcal{O}(1/M^2)$ proton propagator components. Panel (A) contains the true TPE one-loop diagrams, while panel (B) shows the reducible two-loop TPE diagrams involving pion-loops and counter terms (not explicitly shown above, instead see Fig. 1 of Ref. [80]) at the proton-photon vertices, as depicted by the large green blobs. These pion-loop insertions renormalize the diagrams (p) – (s) with NNLO proton-photon vertex corrections, effectively reducing them to one-loop graphs *dressed* with proton form factors.

where

$$\begin{aligned}
 \delta_{\gamma\gamma}^{(\text{NNLO})}(Q^2) &= \frac{2\mathcal{R}e \sum_{\text{spins}} \left[\mathcal{M}_\gamma^{(0)*} \mathcal{M}_{\gamma\gamma}^{(\text{NNLO})} + \mathcal{M}_\gamma^{(1)*} \mathcal{M}_{\gamma\gamma}^{(\text{NLO})} + \mathcal{M}_\gamma^{(2)*} \mathcal{M}_{\gamma\gamma}^{(\text{LO})} \right]}{\sum_{\text{spins}} \left| \mathcal{M}_\gamma^{(0)} \right|^2} \\
 &= \frac{2\mathcal{R}e \sum_{\text{spins}} \left[\mathcal{M}_\gamma^{(0)*} \mathcal{M}_{\gamma\gamma}^{(\text{NNLO})} + \mathcal{M}_\gamma^{(2)*} \mathcal{M}_{\gamma\gamma}^{(\text{LO})} \right]}{\sum_{\text{spins}} \left| \mathcal{M}_\gamma^{(0)} \right|^2} + \mathcal{O}\left(\frac{\alpha}{M^3}\right). \quad (68)
 \end{aligned}$$

Note that the interference of $\mathcal{M}_\gamma^{(1)*}$ and $\mathcal{M}_{\gamma\gamma}^{(\text{NLO})}$ in the equation above leads to $\mathcal{O}(\alpha/M^3)$ terms, which are beyond our NNLO order calculation. They are therefore explicitly omitted in this analysis. As previously mentioned, if $+\delta_{\gamma\gamma}^{(\text{NNLO})}$ represents to the TPE corrections for lepton-proton scattering, $-\delta_{\gamma\gamma}^{(\text{NNLO})}$ will corresponds to antilepton-proton scattering. In other words, the overall sign reflects the charge-odd nature of the radiative corrections. The last term $\mathcal{M}_\gamma^{(2)}$ in the above expression denotes the NNLO OPE amplitude [57, 60, 80]:

$$\begin{aligned}
 \mathcal{M}_\gamma^{(2)} &= -\frac{e^2}{8M^2Q^2} [\bar{u}_l(p') \gamma^\mu u_l(p)] \left[\chi^\dagger(p'_p) \left\{ (2(v \cdot Q)^2 - Q^2) v_\mu - (v \cdot Q) Q_\mu \right\} \chi(p_p) \right] \\
 &\quad - \frac{e^2}{Q^2} [\bar{u}_l(p') \gamma^\mu u_l(p)] \left[\chi^\dagger(p'_p) \mathcal{V}_\mu^{(2)} \chi(p_p) \right], \quad (69)
 \end{aligned}$$

where

$$\begin{aligned} \mathcal{V}_\mu^{(2)} = & (F_1^p - 1)v_\mu + \frac{1}{2M} \left\{ (F_1^p - 1) \left(Q_\mu + \frac{Q^2}{2M} v_\mu \right) + 2(F_1^p + F_2^p - 1 - \kappa_p) [S_\mu, S \cdot Q] \right\} \\ & - \frac{Q^2}{8M^2} (F_1^p - 2F_2^p - 1)v_\mu + \mathcal{O} \left(\frac{1}{M^3} \right), \end{aligned} \quad (70)$$

where the vertex factor $\mathcal{V}_\mu^{(2)}$ in Eq. (70) encodes the proton's hadronic structure *via* its form factors. It renormalizes the NNLO interactions originating from the $\mathcal{L}_{\pi N}^{(2)}$ chiral Lagrangian.

The term $\mathcal{M}_{\gamma\gamma}^{(\text{NNLO})}$ denotes the sum of the box, the crossed-box and the seagull NNLO TPE amplitudes, labeled (j) - (v) in the upper panel (A) of Fig. 3. In particular, the diagrams (p) - (s), which involve NNLO insertions at the proton-photon vertices, in addition receive contributions from the the so-called “form-factor-type” graphs, (p_π) - (s_π), as depicted in the lower panel (B) of the same figure. Thus we have

$$\mathcal{M}_{\gamma\gamma}^{(\text{NNLO})} = \mathcal{M}_{\text{box}}^{(j)} + \cdots + \mathcal{M}_{\text{xbox}}^{(u)} + \mathcal{M}_{\text{seagull}}^{(v)} + \left[\mathcal{M}_{\text{box}}^{(p_\pi)} + \cdots + \mathcal{M}_{\text{xbox}}^{(s_\pi)} \right]_{\text{form factors}}. \quad (71)$$

The form factors displayed in Eq. (70) admit the following low-energy Taylor expansion which to $\mathcal{O}(1/M^2)$ can be expressed in terms of proton's Dirac and Pauli mean square radii, $\langle r_{1,2}^2 \rangle \sim \mathcal{O}(1/M^2)$, and the anomalous magnetic moment $\kappa_p \sim \mathcal{O}(M^0)$ (see Ref. [79] for details):

$$F_1^p(Q^2) = 1 + \frac{Q^2}{6} \langle r_1^2 \rangle + \mathcal{O} \left(\frac{1}{M^3} \right), \quad \text{and} \quad F_2^p(Q^2) = \kappa_p + \frac{Q^2}{6} \langle r_2^2 \rangle + \mathcal{O} \left(\frac{1}{M^3} \right). \quad (72)$$

However, for the radiatively corrected cross section evaluated up to $\mathcal{O}(\alpha/M^2)$, only the mean-square Dirac radius $\langle r_1^2 \rangle$ contributes, while the mean-square Pauli radius $\langle r_2^2 \rangle$ enters beyond $\mathcal{O}(1/M^4)$. One can relate $\langle r_1^2 \rangle$ to the proton's root-mean-square (rms) electric or charge radius $r_p \equiv \langle r_E^2 \rangle^{1/2}$ *via*

$$\langle r_1^2 \rangle = \langle r_E^2 \rangle - \frac{3\kappa_p}{2M^2} + \mathcal{O}(M^{-3}). \quad (73)$$

The general frame-independent integral representations of the NNLO amplitudes, namely, $\mathcal{M}_{\text{box}}^{(j)}, \dots, \mathcal{M}_{\text{xbox}}^{(s_\pi)}$, along with their mutual partial cancellations when specialized to the lab frame, were presented without approximation in our recent SPA-based analysis [60]. In particular, the tilde notation over some of these amplitudes denotes their residual parts after several terms proportional to $v_\mu v_\nu$ cancel among them in the lab frame, as detailed in that reference. Here, instead, we directly present the exact expressions for the lepton-proton fractional TPE corrections to the lab frame cross section, as defined in Eqs. 67 and 68. The lab frame amplitudes (t) and (u) cancel exactly, i.e., $\mathcal{M}_{\text{xbox}}^{(t)} + \mathcal{M}_{\text{xbox}}^{(u)} = 0$, as was also found in our SPA analysis [60]. Furthermore, it was shown therein that the NNLO seagull diagram (v) contributes at $\mathcal{O}(\alpha/M^3)$ and thus omitted in that analysis. Consequently, the expressions of the amplitudes (t), (u), and (v) are omitted in the following analysis. The complete expression for the fractional contributions arising from the NNLO TPE diagrams, together with the interference between the NNLO OPE amplitude $\mathcal{M}_\gamma^{(2)}$ and LO TPE diagrams (a) and (b), accurate to $\mathcal{O}(\alpha/M^2)$, is expressed as

$$\begin{aligned} \delta_{\gamma\gamma}^{(\text{NNLO})}(Q^2) = & \delta_{\text{box}}^{(j)}(Q^2) + \delta_{\text{xbox}}^{(k)}(Q^2) + \delta_{\text{box}}^{(l)}(Q^2) + \delta_{\text{xbox}}^{(m)}(Q^2) + \delta_{\text{box}}^{(n)}(Q^2) + \delta_{\text{xbox}}^{(o)}(Q^2) + \delta_{\text{box}}^{(p+p_\pi)}(Q^2) \\ & + \delta_{\text{xbox}}^{(q+q_\pi)}(Q^2) + \delta_{\text{box}}^{(r+r_\pi)}(Q^2) + \delta_{\text{xbox}}^{(s+s_\pi)}(Q^2) + \delta_{\text{box}}^{(a_2)}(Q^2) + \delta_{\text{xbox}}^{(b_2)}(Q^2) + \mathcal{O} \left(\frac{\alpha}{M^3} \right), \end{aligned} \quad (74)$$

where

$$\begin{aligned} \delta_{\text{box}}^{(j)}(Q^2) &= 2\mathbb{R}e \sum_{\text{spins}} \left[\mathcal{M}_{\gamma}^{(0)*} \widetilde{\mathcal{M}}_{\text{box}}^{(j)} \right] \Big/ \sum_{\text{spins}} \left| \mathcal{M}_{\gamma}^{(0)} \right|^2 \\ &= -\frac{e^2}{8M^2} \left[\frac{Q^2}{Q^2 + 4EE'} \right] \mathbb{R}e \left\{ \int \frac{d^4k}{(2\pi)^4 i} \frac{\text{Tr}[(\not{p}' + m_l)\gamma^\mu(\not{p} - \not{k} + m_l)\gamma^\nu(\not{p} + m_l)\not{p}]}{(k^2 + i0)[(Q - k)^2 + i0](k^2 - 2k \cdot p + i0)(v \cdot k + i0)} \right. \\ &\quad \times \left. \left[(k + Q)_\mu k_\nu - v_\mu k_\nu v \cdot (Q + k) - (Q + k)_\mu v_\nu (v \cdot k) \right] \right\} \end{aligned} \quad (75)$$

$$\begin{aligned} &= -\frac{e^2}{2M^2} \left[\frac{Q^2}{Q^2 + 4EE'} \right] \mathbb{R}e \left\{ 4(E' + E)p_\mu p_\nu I_1^{-\mu\nu}(p, 0|1, 1, 1, 1) - 4Q^2 E v \cdot I_1^-(p, 0|1, 1, 1, 0) \right. \\ &\quad - (Q^2 - 4E^2 - 4EE')I^-(p, 0|1, 1, 0, 0) - 4E^2 I^-(p, 0|1, 0, 1, 0) \\ &\quad + 4Q^2 E^2 I^-(p, 0|1, 1, 1, 0) - EI^-(p, 0|1, 0, 0, 1) \\ &\quad + (2E + E')I^-(p, 0|0, 1, 0, 1) - (E + E')I_2^-(p, 0|0, 1, 1, 1) \\ &\quad + (2Q^2 E - Q^2 E' + 4E^2 E' - 4EE'^2) I^-(p, 0|1, 1, 0, 1) \\ &\quad \left. + 2(Q^2 + 2EE')I^-(p, 0|0, 1, 1, 0) \right\}, \end{aligned} \quad (76)$$

$$\begin{aligned} \delta_{\text{xbox}}^{(k)}(Q^2) &= 2\mathbb{R}e \sum_{\text{spins}} \left[\mathcal{M}_{\gamma}^{(0)*} \widetilde{\mathcal{M}}_{\text{xbox}}^{(k)} \right] \Big/ \sum_{\text{spins}} \left| \mathcal{M}_{\gamma}^{(0)} \right|^2 \\ &= -\frac{e^2}{8M^2} \left[\frac{Q^2}{Q^2 + 4EE'} \right] \mathbb{R}e \left\{ \int \frac{d^4k}{(2\pi)^4 i} \frac{\text{Tr}[(\not{p}' + m_l)\gamma^\mu(\not{p} + \not{k} - \not{Q} + m_l)\gamma^\nu(\not{p} + m_l)\not{p}]}{(k^2 + i0)[(Q - k)^2 + i0](k^2 + 2k \cdot p' + i0)(v \cdot k + i0)} \right. \\ &\quad \times \left. \left[(k + Q)_\nu k_\mu - v_\nu k_\mu v \cdot (Q + k) - (Q + k)_\nu v_\mu (v \cdot k) \right] \right\} \\ &= -\frac{e^2}{2M^2} \left[\frac{Q^2}{Q^2 + 4EE'} \right] \mathbb{R}e \left\{ 4(E' + E)p'_\mu p'_\nu I_1^{+\mu\nu}(p', 0|1, 1, 1, 1) - 4Q^2 E' v \cdot I_1^+(p', 0|1, 1, 1, 0) \right. \\ &\quad + (Q^2 - 4E'^2 - 4EE')I^+(p', 0|1, 1, 0, 0) + 4E'^2 I^+(p', 0|1, 0, 1, 0) \\ &\quad - 4Q^2 E'^2 I^+(p', 0|1, 1, 1, 0) - E'I^+(p', 0|1, 0, 0, 1) \\ &\quad + (2E' + E)I^+(p', 0|0, 1, 0, 1) - (E + E')I_2^+(p', 0|0, 1, 1, 1) \\ &\quad + (2Q^2 E' - Q^2 E + 4EE'^2 - 4E^2 E') I^+(p', 0|1, 1, 0, 1) \\ &\quad \left. - 2(Q^2 + 2EE')I^+(p', 0|0, 1, 1, 0) \right\}, \end{aligned} \quad (77)$$

$$\begin{aligned} \delta_{\text{box}}^{(l)}(Q^2) &= 2\mathbb{R}e \sum_{\text{spins}} \left[\mathcal{M}_{\gamma}^{(0)*} \widetilde{\mathcal{M}}_{\text{box}}^{(l)} \right] \Big/ \sum_{\text{spins}} \left| \mathcal{M}_{\gamma}^{(0)} \right|^2 \\ &= \frac{-e^2}{8M^2} \left[\frac{Q^2}{Q^2 + 4EE'} \right] \mathbb{R}e \left\{ \int \frac{d^4k}{(2\pi)^4 i} \frac{\text{Tr}[(\not{p}' + m_l)\not{p}(\not{p} - \not{k} + m_l)\not{k}(\not{p} + m_l)\not{p}]}{(k^2 + i0)[(Q - k)^2 + i0](k^2 - 2k \cdot p + i0)} \left(1 - \frac{k^2}{(v \cdot k)^2} \right) \right\} \\ &= \frac{e^2 Q^2}{2M^2} \mathbb{R}e \left\{ I^-(p, 0|1, 1, 0, 0) - I^-(p, 0|0, 1, 0, 2) \right\}, \end{aligned} \quad (78)$$

$$\begin{aligned} \delta_{\text{xbox}}^{(m)}(Q^2) &= 2\mathbb{R}e \sum_{\text{spins}} \left[\mathcal{M}_{\gamma}^{(0)*} \widetilde{\mathcal{M}}_{\text{xbox}}^{(m)} \right] \Big/ \sum_{\text{spins}} \left| \mathcal{M}_{\gamma}^{(0)} \right|^2 \\ &= \frac{-e^2}{8M^2} \left[\frac{Q^2}{Q^2 + 4EE'} \right] \mathbb{R}e \left\{ \int \frac{d^4k}{(2\pi)^4 i} \frac{\text{Tr}[(\not{p}' + m_l)\not{k}(\not{p} + \not{k} - \not{Q} + m_l)\not{p}(\not{p} + m_l)\not{p}]}{(k^2 + i0)[(Q - k)^2 + i0](k^2 + 2k \cdot p' + i0)} \left(1 - \frac{k^2}{(v \cdot k)^2} \right) \right\} \\ &= -\frac{e^2 Q^2}{2M^2} \mathbb{R}e \left\{ I^+(p', 0|1, 1, 0, 0) - I^+(p', 0|0, 1, 0, 2) \right\}, \end{aligned} \quad (79)$$

$$\begin{aligned}
\delta_{\text{box}}^{(n)}(Q^2) &= 2\mathbb{R}e \sum_{\text{spins}} \left[\mathcal{M}_\gamma^{(0)*} \widetilde{\mathcal{M}}_{\text{box}}^{(n)} \right] \Big/ \sum_{\text{spins}} \left| \mathcal{M}_\gamma^{(0)} \right|^2 \\
&= \frac{-e^2}{8M^2} \left[\frac{Q^2}{Q^2 + 4EE'} \right] \mathbb{R}e \left\{ \int \frac{d^4k}{(2\pi)^4 i} \frac{\text{Tr}[(\not{p}' + m_l)(\not{Q} + \not{k})(\not{p} - \not{k} + m_l)\not{\psi}(\not{p} + m_l)\not{\psi}]}{(k^2 + i0)[(Q - k)^2 + i0](k^2 - 2k \cdot p + i0)} \right. \\
&\quad \times \left(1 - \frac{k^2}{(v \cdot k)^2} \right) \\
&\quad + \left. \int \frac{d^4k}{(2\pi)^4 i} \frac{\text{Tr}[(\not{p}' + m_l)\not{\psi}(\not{p} - \not{k} + m_l)\not{\psi}(\not{p} + m_l)\not{\psi}]}{[(Q - k)^2 + i0](k^2 - 2k \cdot p + i0)(v \cdot k + i0)} \right\} \\
&= \frac{e^2}{2M^2} \left[\frac{Q^2}{Q^2 + 4EE'} \right] \mathbb{R}e \left\{ 3(Q^2 + 4EE')I^-(p, 0|0, 1, 1, 0) + 4Q^2E^2I^-(p, 0|1, 1, 1, 0) \right. \\
&\quad + E(3Q^2 - 8EE')I^-(p, 0|0, 1, 1, 1) + 4E^2I^-(p, 0|0, 0, 1, 2) \\
&\quad - 4Q^2Ev \cdot I_1^-(p, 0|1, 1, 1, 0) - E'I_2^-(p, 0|0, 1, 1, 1) \\
&\quad + (Q^2 - 4E^2)I^-(p, 0|0, 1, 0, 2) - EI^-(p, 0|0, 0, 1, 1) \\
&\quad - 4Q^2E^2I^-(p, 0|0, 1, 1, 2) - 4E^2I^-(p, 0|1, 0, 1, 0) \\
&\quad - 2(Q^2 + 2EE')I_2^-(p, 0|0, 1, 1, 2) + (E + E')I^-(p, 0|0, 1, 0, 1) \\
&\quad \left. - (Q^2 - 4E^2)I^-(p, 0|1, 1, 0, 0) \right\}, \tag{80}
\end{aligned}$$

$$\begin{aligned}
\delta_{\text{xbox}}^{(o)}(Q^2) &= 2\mathbb{R}e \sum_{\text{spins}} \left[\mathcal{M}_\gamma^{(0)*} \widetilde{\mathcal{M}}_{\text{xbox}}^{(o)} \right] \Big/ \sum_{\text{spins}} \left| \mathcal{M}_\gamma^{(0)} \right|^2 \\
&= -\frac{e^2}{8M^2} \left[\frac{Q^2}{Q^2 + 4EE'} \right] \mathbb{R}e \left\{ \int \frac{d^4k}{(2\pi)^4 i} \frac{\text{Tr}[(\not{p}' + m_l)\not{\psi}(\not{p} + \not{k} - \not{Q} + m_l)(\not{Q} + \not{k})(\not{p} + m_l)\not{\psi}]}{(k^2 + i0)[(Q - k)^2 + i0](k^2 + 2k \cdot p' + i0)} \right. \\
&\quad \times \left(1 - \frac{k^2}{(v \cdot k)^2} \right) \\
&\quad + \left. \int \frac{d^4k}{(2\pi)^4 i} \frac{\text{Tr}[(\not{p}' + m_l)\not{\psi}(\not{p} + \not{k} - \not{Q} + m_l)\not{\psi}(\not{p} + m_l)\not{\psi}]}{[(Q - k)^2 + i0](k^2 + 2k \cdot p' + i0)(v \cdot k + i0)} \right\} \\
&= -\frac{e^2}{2M^2} \left[\frac{Q^2}{Q^2 + 4EE'} \right] \mathbb{R}e \left\{ 3(Q^2 + 4EE')I^+(p', 0|0, 1, 1, 0) + 4Q^2E'^2I^+(p', 0|1, 1, 1, 0) \right. \\
&\quad - E'(3Q^2 - 8EE')I^+(p', 0|0, 1, 1, 1) + 4E'^2I^+(p', 0|0, 0, 1, 2) \\
&\quad + 4Q^2E'v \cdot I_1^+(p', 0|1, 1, 1, 0) + EI_2^+(p', 0|0, 1, 1, 1) \\
&\quad + (Q^2 - 4E'^2)I^+(p', 0|0, 1, 0, 2) + E'I^+(p', 0|0, 0, 1, 1) \\
&\quad - 4E'^2Q^2I^+(p', 0|0, 1, 1, 2) - 4E'^2I^+(p', 0|1, 0, 1, 0) \\
&\quad - 2(Q^2 + 2EE')I_2^+(p', 0|0, 1, 1, 2) - (E' + E)I^+(p', 0|0, 1, 0, 1) \\
&\quad \left. - (Q^2 - 4E'^2)I^+(p', 0|1, 1, 0, 0) \right\}, \tag{81}
\end{aligned}$$

$$\begin{aligned}
\delta_{\text{box}}^{(p+p_\pi)}(Q^2) &= 2\mathbb{R}e \sum_{\text{spins}} \left[\mathcal{M}_\gamma^{(0)*} \left(\mathcal{M}_{\text{box}}^{(p)} + \mathcal{M}_{\text{box}}^{(p_\pi)} \right) \right] \Big/ \sum_{\text{spins}} \left| \mathcal{M}_\gamma^{(0)} \right|^2 \\
&= -4\pi\alpha \left[\frac{Q^4}{Q^2 + 4EE'} \right] \left(\frac{\langle r_1^2 \rangle}{6} + \frac{\kappa_p}{4M^2} - \frac{1}{8M^2} \right) \\
&\quad \times \mathbb{R}e \left\{ \int \frac{d^4k}{(2\pi)^4 i} \frac{\text{Tr}[(\not{p}' + m_l)\not{\psi}(\not{p} - \not{k} + m_l)\not{\psi}(\not{p} + m_l)\not{\psi}]}{(k^2 + i0)[(Q - k)^2 + i0](k^2 - 2k \cdot p + i0)(v \cdot k + i0)} \right\} \\
&= Q^2 \left(\frac{\langle r_1^2 \rangle}{6} + \frac{\kappa_p}{4M^2} - \frac{1}{8M^2} \right) \delta_{\text{box}}^{(a)}(Q^2), \tag{82}
\end{aligned}$$

$$\begin{aligned}
\delta_{\text{xbbox}}^{(q+q\pi)}(Q^2) &= 2\mathbb{R}e \sum_{\text{spins}} \left[\mathcal{M}_\gamma^{(0)*} \left(\mathcal{M}_{\text{xbbox}}^{(q)} + \mathcal{M}_{\text{xbbox}}^{(q\pi)} \right) \right] \Big/ \sum_{\text{spins}} \left| \mathcal{M}_\gamma^{(0)} \right|^2 \\
&= -4\pi\alpha \left[\frac{Q^4}{Q^2 + 4EE'} \right] \left(\frac{\langle r_1^2 \rangle}{6} + \frac{\kappa_p}{4M^2} - \frac{1}{8M^2} \right) \\
&\quad \times \mathbb{R}e \left\{ \int \frac{d^4k}{(2\pi)^4 i} \frac{\text{Tr}[(\not{p}' + m_l)\not{\psi}(\not{p} + \not{k} - \not{Q} + m_l)\not{\psi}(\not{p} + m_l)\not{\psi}]}{(k^2 + i0)[(Q - k)^2 + i0](k^2 + 2k \cdot p' + i0)(v \cdot k + i0)} \right\} \\
&= Q^2 \left(\frac{\langle r_1^2 \rangle}{6} + \frac{\kappa_p}{4M^2} - \frac{1}{8M^2} \right) \delta_{\text{xbbox}}^{(b)}(Q^2), \tag{83}
\end{aligned}$$

$$\begin{aligned}
\delta_{\text{box}}^{(r+r\pi)}(Q^2) &= 2\mathbb{R}e \sum_{\text{spins}} \left[\mathcal{M}_\gamma^{(0)*} \left(\mathcal{M}_{\text{box}}^{(r)} + \mathcal{M}_{\text{box}}^{(r\pi)} \right) \right] \Big/ \sum_{\text{spins}} \left| \mathcal{M}_\gamma^{(0)} \right|^2 \\
&= -4\pi\alpha \left[\frac{Q^4}{Q^2 + 4EE'} \right] \left(\frac{\langle r_1^2 \rangle}{6} + \frac{\kappa_p}{4M^2} - \frac{1}{8M^2} \right) \\
&\quad \times \mathbb{R}e \left\{ \int \frac{d^4k}{(2\pi)^4 i} \frac{\text{Tr}[(\not{p}' + m_l)\not{\psi}(\not{p} - \not{k} + m_l)\not{\psi}(\not{p} + m_l)\not{\psi}]}{(k^2 + i0)[(Q - k)^2 + i0](k^2 - 2k \cdot p + i0)(v \cdot k + i0)} \right\} \\
&= Q^2 \left(\frac{\langle r_1^2 \rangle}{6} + \frac{\kappa_p}{4M^2} - \frac{1}{8M^2} \right) \delta_{\text{box}}^{(a)}(Q^2), \tag{84}
\end{aligned}$$

$$\begin{aligned}
\delta_{\text{xbbox}}^{(s+s\pi)}(Q^2) &= 2\mathbb{R}e \sum_{\text{spins}} \left[\mathcal{M}_\gamma^{(0)*} \left(\mathcal{M}_{\text{xbbox}}^{(s)} + \mathcal{M}_{\text{xbbox}}^{(s\pi)} \right) \right] \Big/ \sum_{\text{spins}} \left| \mathcal{M}_\gamma^{(0)} \right|^2 \\
&= -4\pi\alpha \left[\frac{Q^4}{Q^2 + 4EE'} \right] \left(\frac{\langle r_1^2 \rangle}{6} + \frac{\kappa_p}{4M^2} - \frac{1}{8M^2} \right) \\
&\quad \times \mathbb{R}e \left\{ \int \frac{d^4k}{(2\pi)^4 i} \frac{\text{Tr}[(\not{p}' + m_l)\not{\psi}(\not{p} + \not{k} - \not{Q} + m_l)\not{\psi}(\not{p} + m_l)\not{\psi}]}{(k^2 + i0)[(Q - k)^2 + i0](k^2 + 2k \cdot p' + i0)(v \cdot k + i0)} \right\} \\
&= Q^2 \left(\frac{\langle r_1^2 \rangle}{6} + \frac{\kappa_p}{4M^2} - \frac{1}{8M^2} \right) \delta_{\text{xbbox}}^{(b)}(Q^2). \tag{85}
\end{aligned}$$

It is noteworthy that the last four NNLO box and crossed-box contributions, Eqs. (82)–(85), are proportional to contributions $\delta_{\text{box}}^{(a)}$ and $\delta_{\text{xbbox}}^{(b)}$ arising from the LO TPE diagrams (a) and (b), respectively. Since the latter exactly vanish at LO [i.e., $\mathcal{O}(\alpha M^0)$] in the SPA analysis, it follows that the $\mathcal{O}(\alpha/M^2)$ contributions from the (p) – (s) diagrams also vanish in SPA, as shown in Ref. [60]. In contrast our exact TPE analysis exhibits non-zero proton structure effects at NNLO as manifested through the LEC such as κ_p and $\langle r_1^2 \rangle$ (equivalently the proton radius r_p).³ The additional interference between the NNLO OPE amplitude $\mathcal{M}_\gamma^{(2)}$ and the LO TPE diagrams generate the following two contributions:

$$\begin{aligned}
\delta_{\text{box}}^{(a_2)}(Q^2) &= 2\mathbb{R}e \sum_{\text{spins}} \left[\mathcal{M}_\gamma^{(2)*} \mathcal{M}_{\text{box}}^{(a)} \right] \Big/ \sum_{\text{spins}} \left| \mathcal{M}_\gamma^{(0)} \right|^2 \\
&= -4\pi\alpha \left[\frac{Q^4}{Q^2 + 4EE'} \right] \left(\frac{\langle r_1^2 \rangle}{6} + \frac{\kappa_p}{4M^2} - \frac{1}{8M^2} \right) \\
&\quad \times \mathbb{R}e \left\{ \int \frac{d^4k}{(2\pi)^4 i} \frac{\text{Tr}[(\not{p} + m_l)\not{\psi}(\not{p}' + m_l)\not{\psi}(\not{p} - \not{k} + m_l)\not{\psi}]}{(k^2 + i0)[(Q - k)^2 + i0](k^2 - 2k \cdot p + i0)(v \cdot k + i0)} \right\} + \mathcal{O}\left(\frac{\alpha}{M^3}\right) \\
&= Q^2 \left(\frac{\langle r_1^2 \rangle}{6} + \frac{\kappa_p}{4M^2} - \frac{1}{8M^2} \right) \delta_{\text{box}}^{(a)}(Q^2) + \mathcal{O}\left(\frac{\alpha}{M^3}\right), \tag{86}
\end{aligned}$$

³ It is worth re-emphasizing that in standard HB χ PT power counting arguments, the proton's $\langle r_1^2 \rangle \sim \mathcal{O}(1/M^2)$, whereas κ_p scales as $\mathcal{O}(M^0)$. Consequently, the NNLO results in Eqs. (82) – (85) are consistent with the expected $\mathcal{O}(1/M^2)$ scaling.

and

$$\begin{aligned}
\delta_{\text{xbox}}^{(b_2)}(Q^2) &= 2\Re e \sum_{\text{spins}} \left[\mathcal{M}_\gamma^{(2)*} \mathcal{M}_{\text{xbox}}^{(b)} \right] \Big/ \sum_{\text{spins}} \left| \mathcal{M}_\gamma^{(0)} \right|^2 \\
&= -4\pi\alpha \left[\frac{Q^4}{Q^2 + 4EE'} \right] \left(\frac{\langle r_1^2 \rangle}{6} + \frac{\kappa_p}{4M^2} - \frac{1}{8M^2} \right) \\
&\quad \times \Re e \left\{ \int \frac{d^4 k}{(2\pi)^4 i} \frac{\text{Tr} [(\not{p} + m_l) \not{p} (\not{p}' + m_l) \not{p} (\not{p} + \not{k} - \not{Q} + m_l) \not{p}]}{(k^2 + i0) [(Q - k)^2 + i0] (k^2 + 2k \cdot p' + i0) (v \cdot k + i0)} \right\} + \mathcal{O} \left(\frac{\alpha}{M^3} \right), \\
&= Q^2 \left(\frac{\langle r_1^2 \rangle}{6} + \frac{\kappa_p}{4M^2} - \frac{1}{8M^2} \right) \delta_{\text{xbox}}^{(b)}(Q^2) + \mathcal{O} \left(\frac{\alpha}{M^3} \right). \tag{87}
\end{aligned}$$

As discussed in the previous section, the IBP decomposition and partial fractioning reduce each of these NNLO fractional contributions to a sequence of 2-, 3-, and 4-point scalar and tensor loop-integrals. This reduction involves not only the loop-integrals already encountered in the preceding works of Refs. [59] and [60], but also an additional set of fourteen 2- and 3-point master-integrals, as well as five reducible 3- and 4-point tensor loop-integrals. These loop-integrals are analytically evaluated and their expressions are given in Appendix B. All such 2-point master-integrals appearing above exhibit UV divergence, with the exception of $I^-(p, 0|1, 0, 0, 1) = I^+(p', 0|1, 0, 0, 1)$, which correspond to scaleless integrals that vanish in DR.

Our analytical expressions for the finite parts of the TPE contributions arise from the pairs of box and crossed-box NNLO amplitudes (j) - (s_π) [cf. Fig. 3] and incorporate all corrections up to $\mathcal{O}(\alpha/M^2)$ in each case. As in the previous section, we replace $E' \rightarrow E$ and $\beta' \rightarrow \beta$ in all $\mathcal{O}(\alpha/M^2)$ terms. As noted among the LO and NLO diagrams (a) - (d), a substantial cancellation occur between the NNLO box and cross-box pairs (the exception is the (n) and (o) pair of diagrams), leading to markedly simplified results. In fact the total contribution from the box (l) and crossed-box (m) diagrams vanishes identically, as obtained in our SPA analysis in Ref. [60], i.e., $\delta_{\gamma\gamma}^{(lm)}(Q^2) = \delta_{\text{box}}^{(l)}(Q^2) + \delta_{\text{xbox}}^{(m)}(Q^2) = 0$. It is also noteworthy that the additional IR-divergences appearing at NNLO, namely, contributions arising from diagrams (p), (p_π), ⋯ (s) and (s_π), as well as the interference of the NNLO OPE amplitude $\mathcal{M}_\gamma^{(2)}$ with the LO TPE diagrams (a) and (b), cancel at $\mathcal{O}(\alpha/M^2)$. Their remnants constitute only residual divergences at $\mathcal{O}(\alpha/M^3)$, which is beyond our accuracy, and therefore not needed in this analysis. The remaining non-vanishing finite results are discussed below:

- First, the total contribution from the box (j) and crossed-box (k) diagrams is expressed as

$$\delta_{\gamma\gamma}^{(jk)}(Q^2) = \delta_{\gamma\gamma}^{(jk;1/M^2)}(Q^2) + \mathcal{O} \left(\frac{\alpha}{M^3} \right), \quad \text{where} \tag{88}$$

$$\delta_{\gamma\gamma}^{(jk;1/M^2)}(Q^2) = \frac{Q^2}{8M^2} \delta_{\gamma\gamma}^{(0)}(Q^2) = -\frac{\pi\alpha(-Q^2)^{3/2}}{16M^2 E} \left[\frac{1}{1 + \frac{Q^2}{4E^2}} \right]. \tag{89}$$

where $\delta_{\gamma\gamma}^{(0)}$ is the finite $\mathcal{O}(\alpha M^0)$ contribution of the LO TPE diagrams (a) and (b); see Eq. (41).

- Second, the total contribution arising from the box (n) and crossed-box (o) diagrams is given by

$$\begin{aligned}
\delta_{\gamma\gamma}^{(no)}(Q^2) &= \delta_{\text{box}}^{(n)}(Q^2) + \delta_{\text{xbox}}^{(o)}(Q^2) \\
&\equiv \delta_{\gamma\gamma}^{(no;1/M)}(Q^2) + \delta_{\gamma\gamma}^{(no;1/M^2)}(Q^2) + \mathcal{O} \left(\frac{\alpha}{M^3} \right), \tag{90}
\end{aligned}$$

where

$$\delta_{\gamma\gamma}^{(no;1/M)}(Q^2) = -\frac{8\pi\alpha Q^4}{M} \Re e \left[I^{(0)}(p, 0|0, 1, 1, 2) \right], \tag{91}$$

and

$$\begin{aligned}
\delta_{\gamma\gamma}^{(no;1/M^2)}(Q^2) &= \frac{2\pi\alpha Q^2}{M^2 E^2 \beta^2 (Q^2 + 4E^2)} \Re e \left\{ 2E^2 Q^2 \beta^2 (Q^2 + 4E^2) \delta^{(M^0)} I^+(p', 0|0, 1, 1, 2) \right. \\
&\quad \left. + (Q^2 + 2E^2)(Q^2 + 2E^2 \beta^2) \left(I^{(0)}(p, 0|0, 0, 1, 2) - I(Q|0, 1, 0, 2) \right) \right\}. \tag{92}
\end{aligned}$$

Note the surprising appearance of the kinematically enhanced term $\delta_{\gamma\gamma}^{(no;1/M)} \sim \mathcal{O}(\alpha/M)$ which arise in the NNLO diagrammatic contributions. This originates from the 3-point reducible loop-integrals $I_2^-(p, 0|0, 1, 1, 2)$ and $I_2^+(p', 0|0, 1, 1, 2)$, as demonstrated in Appendix B, and are expressed in terms of the master-integrals $I^-(p, 0|0, 1, 1, 2)$ and $I^+(p', 0|0, 1, 1, 2)$, respectively. The latter integrals contain contributions proportional to $MI^{(0)}(p, 0|0, 1, 1, 2) \sim \mathcal{O}(M)$, as discussed in the last section [see Eqs. (57) and (60)].

- Third, the total finite contribution arising from diagrams (p) - (s) and their pionic counterparts (p_π) - (s_π) (after subtracting the residual $\mathcal{O}(\alpha/M^3)$ IR divergence) is given by

$$\begin{aligned} \overline{\delta_{\gamma\gamma}^{(p+p_\pi, \dots, s+s_\pi)}}(Q^2) &= \delta_{\text{box}}^{(p+p_\pi)}(Q^2) + \delta_{\text{xbox}}^{(q+q_\pi)}(Q^2) + \delta_{\text{box}}^{(r+r_\pi)}(Q^2) + \delta_{\text{xbox}}^{(s+s_\pi)}(Q^2) \\ &\quad - 2Q^2 \left(\frac{r_p^2}{6} - \frac{1}{8M^2} \right) \delta_{\text{IR}}^{(\text{box})}(Q^2) \\ &= \overline{\delta_{\gamma\gamma}^{(p+p_\pi, \dots, s+s_\pi; 1/M^2)}}(Q^2) + \mathcal{O}\left(\frac{\alpha}{M^3}\right), \end{aligned} \quad (93)$$

where

$$\overline{\delta_{\gamma\gamma}^{(p+p_\pi, \dots, s+s_\pi; 1/M^2)}}(Q^2) = -\frac{\pi\alpha(-Q^2)^{3/2}}{E} \left(\frac{r_p^2}{6} - \frac{1}{8M^2} \right) \left[\frac{1}{1 + \frac{Q^2}{4E^2}} \right]. \quad (94)$$

- Fourth, the total contribution arising from the interference of the NNLO OPE amplitude $\mathcal{M}_\gamma^{(2)}$ with the LO TPE diagrams (a) and (b) (after subtracting the residual $\mathcal{O}(\alpha/M^3)$ IR divergence) is given by

$$\begin{aligned} \overline{\delta_{\gamma\gamma}^{(a_2 b_2)}}(Q^2) &= \delta_{\text{box}}^{(a_2)}(Q^2) + \delta_{\text{xbox}}^{(b_2)}(Q^2) - Q^2 \left(\frac{r_p^2}{6} - \frac{1}{8M^2} \right) \delta_{\text{IR}}^{(\text{box})}(Q^2) \\ &= \overline{\delta_{\gamma\gamma}^{(a_2 b_2; 1/M^2)}}(Q^2) + \mathcal{O}\left(\frac{\alpha}{M^3}\right), \end{aligned} \quad (95)$$

where

$$\overline{\delta_{\gamma\gamma}^{(a_2 b_2; 1/M^2)}}(Q^2) = -\frac{\pi\alpha(-Q^2)^{3/2}}{2E} \left(\frac{r_p^2}{6} - \frac{1}{8M^2} \right) \left[\frac{1}{1 + \frac{Q^2}{4E^2}} \right]. \quad (96)$$

Note that, in presenting the above results, we have eliminated the proton's iso-vector mean-square radius $\langle r_1^2 \rangle$ and anomalous magnetic moment κ_p in favor of the proton mean square charge radius, $r_p^2 \equiv \langle r_E^2 \rangle$ [see Eq. (73)], which is treated as a phenomenologically fixed input parameter in our analysis.

We finally present the consolidated analytical expression for the finite fractional part of the dynamical NNLO TPE contributions to the elastic differential cross section, retaining all terms up to $\mathcal{O}(\alpha/M^2)$, as obtained from Eqs. (88) - (95):

$$\begin{aligned} \overline{\delta_{\gamma\gamma}^{(\text{NNLO})}}(Q^2) &= \delta_{\gamma\gamma}^{(\text{NNLO})}(Q^2) - 3Q^2 \left(\frac{r_p^2}{6} - \frac{1}{8M^2} \right) \delta_{\text{IR}}^{(\text{box})}(Q^2) \\ &= \delta_{\gamma\gamma}^{(\text{NNLO}; 1)}(Q^2) + \delta_{\gamma\gamma}^{(\text{NNLO}; 2)}(Q^2) + \mathcal{O}\left(\frac{\alpha}{M^3}\right), \end{aligned} \quad (97)$$

where the $\mathcal{O}(\alpha/M)$ enhanced components arise solely from the NNLO TPE box (n) and crossed-box (o) pair of diagrams and are collected in

$$\delta_{\gamma\gamma}^{(\text{NNLO}; 1)}(Q^2) \equiv \delta_{\gamma\gamma}^{(no; 1/M)}(Q^2) = \frac{2\alpha Q^2}{\pi M E \beta} \ln \sqrt{\frac{1+\beta}{1-\beta}}. \quad (98)$$

We emphasize that, in presenting our final consolidated numerical results in the next section (see later in Fig. 6), the above terms involving the NNLO TPE diagrams will be grouped along with the NLO modifications to the elastic corrections rather than being treated as NNLO contributions. By contrast, the genuine NNLO components [i.e.,

$\mathcal{O}(\alpha/M^2)$] components involving the NNLO TPE diagrams are collected in the term

$$\begin{aligned}
\delta_{\gamma\gamma}^{(\text{NNLO};2)}(Q^2) &\equiv \delta_{\gamma\gamma}^{(jk)}(Q^2) + \delta_{\gamma\gamma}^{(no;1/M^2)}(Q^2) + \overline{\delta_{\gamma\gamma}^{(p+p_\pi, \dots, s+s_\pi)}}(Q^2) + \overline{\delta_{\gamma\gamma}^{(a_2b_2)}}(Q^2) \\
&= -\frac{\alpha Q^4}{2\pi M^2 E^2 (Q^2 + 4E^2)^2} \left\{ \left(8E^2(Q^2 + 2E^2)\beta^2 - Q^4(1 - \beta^2) \right) \ln \sqrt{\frac{1 + \beta}{1 - \beta}} \right. \\
&\quad \left. - \beta^3(Q^2 + 4E^2)^2 \right\} - \frac{\pi\alpha E(-Q^2)^{3/2}}{4M^2(Q^2 + 4E^2)} \\
&\quad - \frac{3\pi\alpha(-Q^2)^{3/2}}{2E} \left(\frac{r_p^2}{6} - \frac{1}{8M^2} \right) \left[\frac{1}{1 + \frac{Q^2}{4E^2}} \right]. \tag{99}
\end{aligned}$$

In these exact NNLO TPE results we find non-vanishing, structure-dependent proton corrections at $\mathcal{O}(\alpha/M^2)$ from the form factor-type diagrams (p) – (s $_\pi$), whereas in the corresponding SPA-based evaluation of Ref. [60], they are kinematically suppressed. Fig. 4 displays the exactly evaluated numerical results for each of these box and crossed-box paired contributions, along with their total fractional contribution $\delta_{\gamma\gamma}^{(\text{NNLO};2)}$. We also compare these results with the corresponding SPA-based results reported in Ref. [60].

V. RESULTS AND DISCUSSION

Here we present our numerical evaluations of the exact TPE and the SPA versions of the corrections to the lepton-proton elastic differential cross section. We incorporate all radiative effects modified by the dominant proton chiral structure-dependent corrections up to $\mathcal{O}(\alpha/M^2)$ (NNLO accuracy) in $\text{HB}\chi\text{PT}$, which is of relevance to the low energy MUSE kinematical regime [27]. This analysis supersedes the earlier $\mathcal{O}(1/M)$ NLO analysis of Choudhary *et al.* [59] where, for example, no finite-size proton effects appeared, effectively treating the proton as point-like. As detailed in the two preceding sections, the NNLO TPE contributions to the elastic cross section, i.e., $\mathcal{O}(\alpha/M^2)$, arise from the following two principal sources:

1. The kinematical NNLO recoil contributions generated by the interference of the TPE and OPE amplitudes at LO and NLO when the outgoing lepton kinematical variables (E' , β') are re-expressed in terms of the incoming ones (E , β) by using Eq. (1).
2. The dynamical NNLO contributions originating from the interference of TPE and OPE amplitudes that involve NNLO chiral order Feynman diagrams.

While point 1 involves either two NLO γpp vertex insertions or a single NLO γpp vertex combined with a $\mathcal{O}(1/M)$ correction to the proton propagator, point 2 originates from contributions involving either a single NNLO γpp vertex insertion or a $\mathcal{O}(1/M^2)$ correction to the proton propagator. The numerical results correspond to each of the two types of contributions.

However, before turning to the $\mathcal{O}(\alpha/M^2)$ discussion of the TPE contributions, for completeness, we first revisit the $\mathcal{O}(\alpha/M)$ corrections to the cross section. As discussed in Sec. III, these terms arise from the LO and NLO TPE diagrams (a) – (i), evaluated in the exact TPE analysis of Choudhary *et al.* [59]. However, as demonstrated in Sec. IV, there exists an additional and significant recoil contribution arising from the kinematically enhanced NNLO component $\delta_{\gamma\gamma}^{(no;1/M)}$, Eq. (91), which are associated with the box (n) and crossed-box (o) diagrams. This term modifies the result of Ref. [59]. Figure 5 displays the numerical values of all the relevant NLO [i.e., $\mathcal{O}(\alpha/M)$] finite fractional contributions to the elastic differential cross section arising from the exactly evaluated TPE diagrams in this work. The corresponding total NLO contribution is defined as:

$$\delta_{\gamma\gamma}^{(1)}(Q^2) \equiv \overline{\delta_{\gamma\gamma}^{(ab;1/M)}}(Q^2) + \delta_{\gamma\gamma}^{(ef;1/M)}(Q^2) + \delta_{\gamma\gamma}^{(gh;1/M)}(Q^2) + \delta_{\gamma\gamma}^{(\text{seagull};1/M)}(Q^2) + \delta_{\gamma\gamma}^{(no;1/M)}(Q^2). \tag{100}$$

The first four NLO radiative corrections were first resolved in Ref. [59], whereas the last term (91) contains a term first evaluated in this paper. In other words, Fig. 5 provides an updated version the our previous NLO results published in Choudhary *et al.* [59]. As noted before, the exact TPE loop-integrals contributing to the corrections $\delta_{\gamma\gamma}^{(ef)}$ and $\delta_{\gamma\gamma}^{(gh)}$, due to the four diagrams (e) – (h), add a positive contribution, constructively – unlike the other box and crossed-box pairs. Therefore, we find that the (e) – (h) diagrams add sizable contributions to the e-p cross section. The large numerical size of these evaluated contributions are partly driven by the sizable 3-point scalar loop-integrals, such as $Z^-(\Delta, i\sqrt{-Q^2}/2, m_l, E)$, $Z^+(\Delta', i\sqrt{-Q^2}/2, m_l, -E')$, $I^-(p, 0|0, 1, 1, 2)$ and $I^+(p', 0|0, 1, 1, 2)$

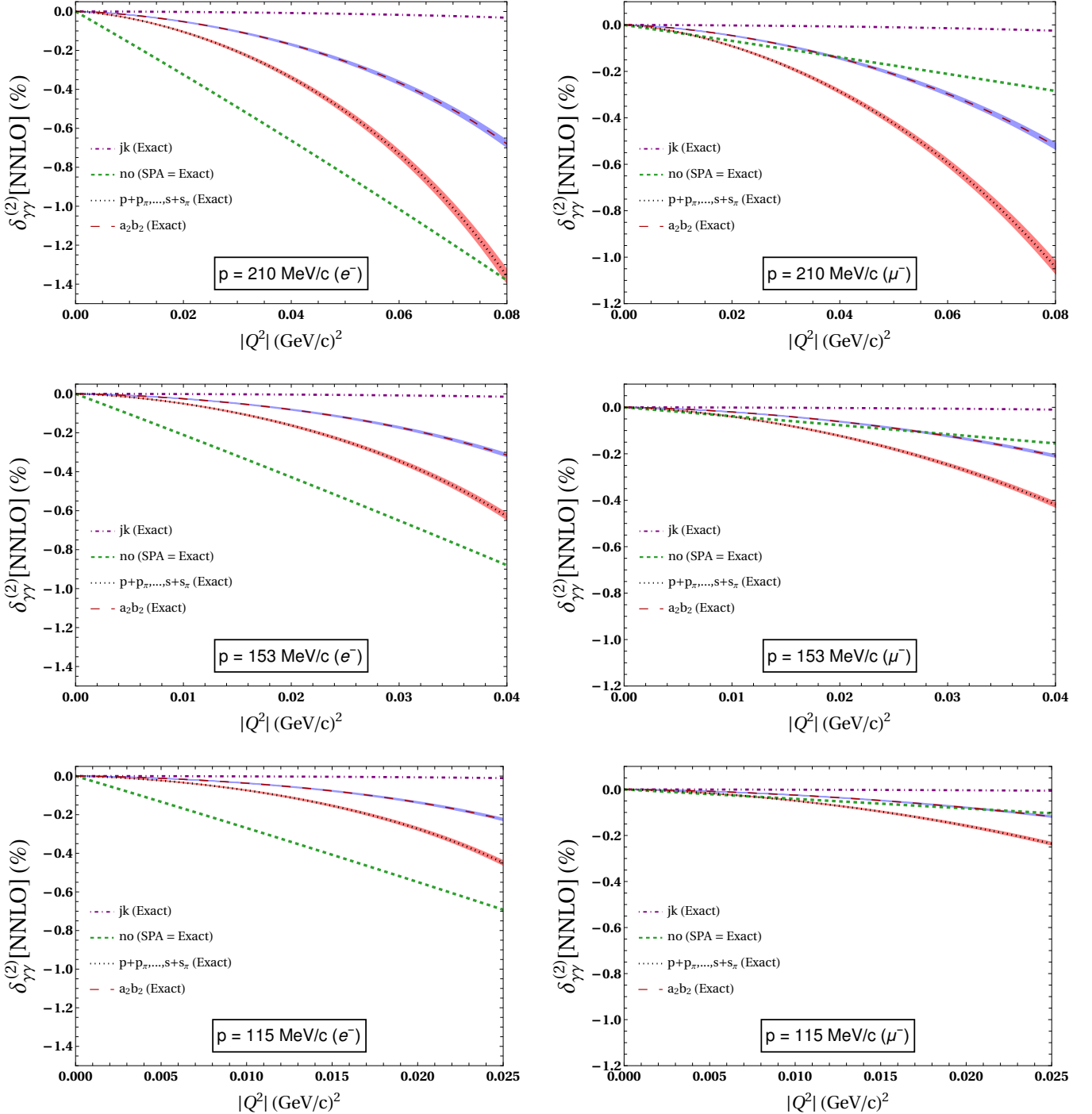


FIG. 4. The box and crossed-box pairs of finite fractional dynamic NNLO corrections arising from the NNLO TPE diagrams, (j) – (s_π), are shown together with the interference of the NNLO OPE amplitude $\mathcal{M}_\gamma^{(2)}$ with the LO TPE diagrams (a) and (b), entering the $\mathcal{O}(\alpha/M^2)$ component $\delta_{\gamma\gamma}^{(\text{NNLO};2)}$ [Eq. (99)] of the electron-proton (left panel) and muon-proton (right panel) elastic differential cross sections. For comparison the corresponding SPA results of Goswami *et al.* [60] are also shown. Within the SPA evaluation the only non-vanishing NNLO TPE contribution arises from diagrams (n) and (o). The result is identical to the one obtained in our exact calculation, as indicated by the label “no (SPA = Exact)” for the curves. The purple and red shaded bands reflect the uncertainties associated with varying the proton rms radius across the range spanned by the CREMA determination [$r_p = 0.84087(39)$ fm] [76, 77] and the MAMI-ISR measurement [$r_p = 0.87 \pm (0.014)\text{stat.} \pm (0.024)\text{syst.} \pm (0.003)\text{mod.}$ fm] [75]. The central curve in each band corresponds to result obtained using the mean value, $\overline{r_p} \sim 0.855$ fm. All fractional corrections are given relative to the LO OPE differential cross section relevant to MUSE kinematical range.

(cf. Appendices for their analytic expressions) that enter them. For the same reason the individual contributions from the LO TPE diagrams $\delta_{\text{box}}^{(a)}$ and $\delta_{\text{xbox}}^{(b)}$ are also quite sizable; however, their mutual cancellation substantially reduces the net magnitude of their IR-finite combination, $\overline{\delta_{\gamma\gamma}^{(ab)}}$. It is also worth noting that the absence of such sizable loop-integrals, most notably the Z^\pm functions, in our SPA-based treatments [56, 60], is the primary reason why the SPA results are substantially smaller than those obtained from the exact treatment. In Fig. 5, we compare our recently obtained SPA results of Ref. [60] with the present exact numerical evaluation of the $\mathcal{O}(\alpha/M)$ corrections. Furthermore, in Fig. 5 we remark that in our HB χ PT framework, the contributions arising from the (n) and (o) diagrams turn out equal in both the SPA and exact evaluations. The other qualitative features visible in Fig. 5 are enumerated as follows.

1. The exact evaluations reveal substantial cancellations among the various contributions. This is in sharp contrast to the SPA results where such cancellations are less pronounced.
2. Our results for muon scattering are about a magnitude smaller than for the electron case.
3. For electron scattering prominent contributions originate from the exact (e) and (f) diagrams, which exhibit a sign change as Q^2 increases across the MUSE kinematic range. The magnitude of the remaining corrections increase monotonically with increasing momentum transfer Q^2 . These contributions also show the largest discrepancy between the exact and the SPA results at the highest Q^2 values.
4. The muon scattering results are in stark contrast to the electron results. The only prominent contribution in our exact evaluation are the positive contributions from the (g) and (h) diagrams. However, for our SPA evaluation from the (e) and (f) diagrams, the contributions are negative, which become more negative with increasing Q^2 . We find similar behavior (but smaller in magnitude) for the contributions from diagrams (n) and (o) which become increasing more negative with increasing $|Q^2|$. The other contributions are quite small.

We now turn to the $\mathcal{O}(\alpha/M^2)$ kinematical TPE results, which are presented in Fig. 2. Here we display the kinematically suppressed NLO contributions to the cross section arising from the LO and NLO diagrams (a) – (i), and compare them with our NLO part of the previously obtained SPA results of Goswami *et al.* [60]. The salient features of these NNLO corrections, as evident from Fig. 2 are enumerated as below:

1. The exact evaluation reveals sizable cancellations among the individual positive and negative contributions, rendering the net results numerically smaller than the corresponding $\mathcal{O}(\alpha/M)$ corrections shown in Fig. 5. Such cancellations are not manifest in the corresponding SPA results.
2. The $\mathcal{O}(\alpha/M^2)$ contribution from the box (e) and crossed-box (f) diagrams constitutes the dominant part of the correction. Moreover the exact results are significantly larger in magnitude and opposite in sign compared to the corresponding SPA results.
3. Regarding the contributions from the box (a) and crossed-box (b) diagrams, the SPA results are smaller than those from the exact evaluation. In the exact case the amplitudes receive additional contributions from the interference between the NLO OPE amplitude and the LO TPE diagrams,

$$\mathcal{M}_\gamma^{(1)*} (\mathcal{M}_{\text{box}}^{(a)} + \mathcal{M}_{\text{xbox}}^{(b)}) ,$$

[denoted as $a_1 b_1$ in the figure]. These contributions are absent in the SPA treatment. Notably the above interference terms are numerically tiny compared to the dominant contributions arising from interference of the LO OPE amplitude $\mathcal{M}_\gamma^{(0)}$ with the (a) and (b) TPE diagrams.

4. The result from the box (g) and crossed-box (h) diagrams is also tiny relative to the other TPE terms. In this case, the SPA and exact results are numerically very close, while exhibiting opposite signs for electron and muon scattering across all beam momenta.
5. As discussed earlier, the seagull contributions exhibit a strong dependence on the lepton mass. Thus, the seagull term is extremely small for electrons but becomes noticeably larger for muons.

Next, we consider our exactly evaluated $\mathcal{O}(\alpha/M^2)$ dynamical TPE contributions from the NNLO diagrams (j) – (s $_\pi$), which include non-vanishing proton structure effects arising from the pion-loop diagrams (p $_\pi$) – (s $_\pi$). These results stand in contrast to the SPA results of Ref. [60], where all such $\mathcal{O}(\alpha/M^2)$ contributions from the diagrams above canceled once the residual $\mathcal{O}(\alpha/M^3)$ terms were dropped. We adopt the strategy of Ref. [60] to estimate the proton structure-dependent corrections parameterized by the rms charge radius r_p , and we select a representative range of

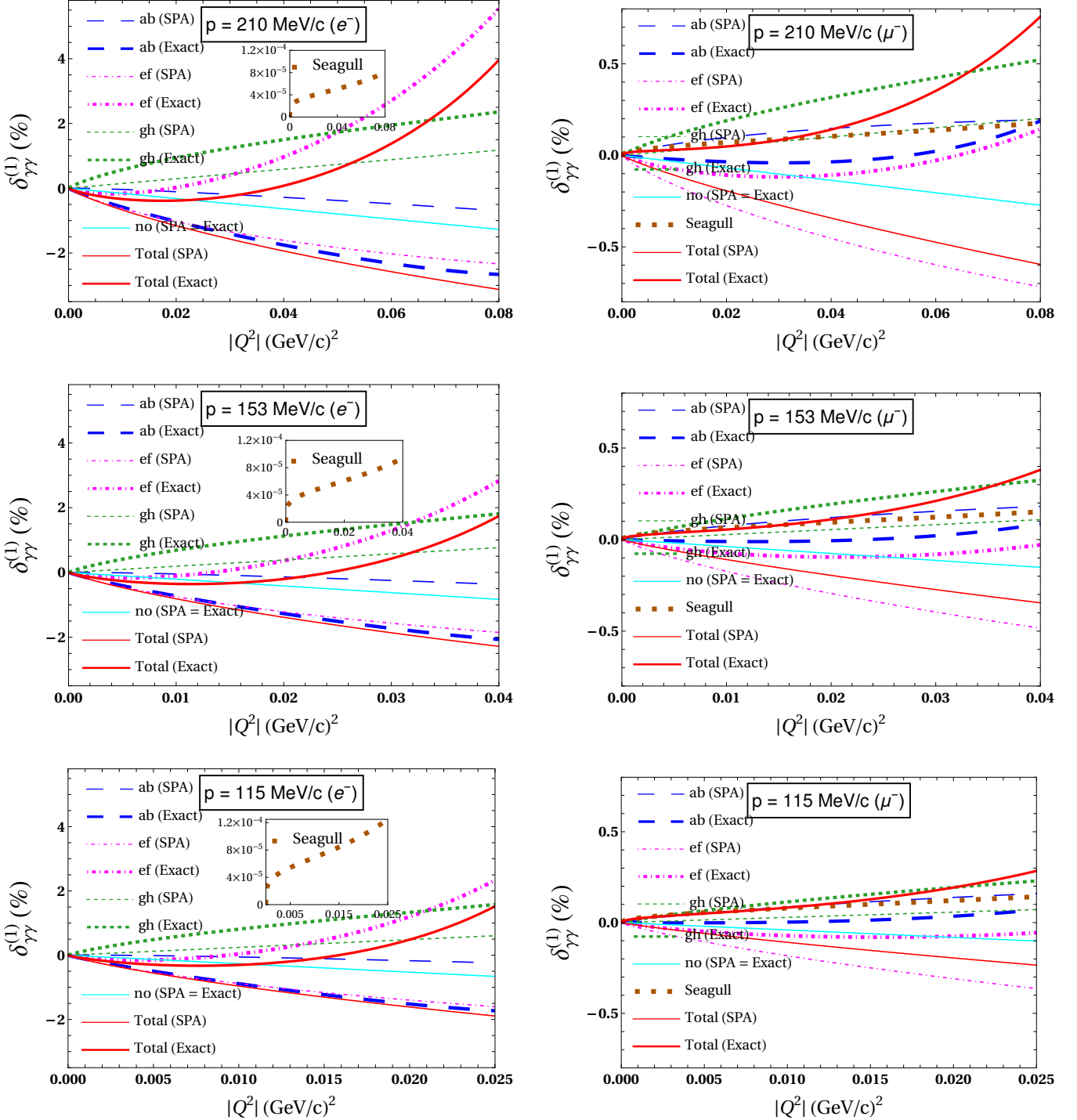


FIG. 5. The finite fractional NLO [i.e., $\mathcal{O}(\alpha/M)$] corrections $\delta_{\gamma\gamma}^{(1)}$ [see Eq. (100)] arising from relevant box and crossed-box pairs of TPE diagrams, contributing to the elastic lepton-proton differential cross section up-to-and-including NLO [i.e., $\mathcal{O}(\alpha^3/M)$] accuracy, is presented. For comparison the NLO SPA results of Goswami *et al.* [60] are also displayed. The results for e-p (μ -p) elastic scattering are shown in the left (right) panel as functions of the squared four-momentum transfer $|Q^2|$, for three MUSE incident lepton beam momenta: 210 MeV/c, 153 MeV/c, and 115 MeV/c. All corrections are given relative to the LO OPE differential cross section.

recently extracted experimental values. This allows us to quantify the sensitivity of our NNLO results to the existing phenomenological discrepancy associated with the charge-radius puzzle [16–23]. We vary our results over a reasonably wide range of proton charge-radius values, specifically between $r_p = 0.87 \pm (0.014)\text{stat.} \pm (0.024)\text{syst.} \pm (0.003)\text{mod.}$ fm and $0.84087(39)$ fm. The former corresponds to the recent extraction from electron proton scattering ISR measurements by the A1 Collaboration (MAMI) [75], while the latter reflects the high precision muonic hydrogen spectroscopy determination reported about a decade ago by the CREMA Collaboration (PSI) [76, 77]. The corresponding results for the dynamical NNLO results are displayed in Fig. 4, which exhibit the following features enumerated as below:

1. Unlike the kinematical NNLO corrections shown in Fig. 2, a notable feature of the dynamical NNLO corrections is that they are all negative and add constructively, thereby yielding net contributions that are larger in magnitude than the former. Moreover, they exhibit only a weak dependence on the lepton mass, with the sole exception of the contribution from diagrams (n) and (o), which displays a pronounced sensitivity to the lepton mass.
2. In SPA, the only non-vanishing dynamical contribution at this order arises from the (n) and (o) diagrams, and this contribution is identical to that obtained in our exact evaluation.
3. The dynamical contributions at $\mathcal{O}(\alpha/M^2)$ are numerically comparable in size to the corresponding kinematical corrections with sole exception of vanishingly small contribution from diagrams (j) and (k).
4. A distinguishing feature between the SPA and the exact TPE evaluations is that only in the latter approach there are additional dynamical contributions from the interference between the NNLO OPE and LO TPE amplitudes,

$$\mathcal{M}_\gamma^{(2)*} (\mathcal{M}_{\text{box}}^{(a)} + \mathcal{M}_{\text{xbox}}^{(b)}) ,$$

[denoted as a_2b_2 in the figure]. In contrast to the tiny $\mathcal{O}(\alpha/M^2)$ kinematical suppressed interference contribution involving the NLO OPE amplitude $\mathcal{M}_\gamma^{(1)*}$ and the LO TPE diagrams, apparent from Fig. 2 (labeled as a_1b_1), the a_2b_2 interference contribution is numerically sizable.

Finally, in Fig. 6 we consolidate all our exact TPE results obtained from the analysis of the LO, NLO and NNLO TPE diagrams contributing to the charge-odd component of the virtual radiative corrections to the elastic ℓ^\mp -p differential cross section up to NNLO [i.e., $\mathcal{O}(\alpha/M^2)$], i.e.,

$$\begin{aligned} \left[\frac{d\sigma_{el}(Q^2)}{d\Omega'_l} \right]_{\gamma\gamma;\text{odd}}^{(\ell^\mp)} &= \left[\frac{d\sigma_{el}(Q^2)}{d\Omega'_l} \right]_{\text{LO+NLO}}^{(\ell^\mp)} + \left[\frac{d\sigma_{el}(Q^2)}{d\Omega'_l} \right]_{\text{NNLO}}^{(\ell^\mp)} \\ &= \left[\frac{d\sigma_{el}(Q^2)}{d\Omega'_l} \right]_0 \delta_{\text{TPE}}^{(\ell^\mp)}(Q^2) , \end{aligned} \quad (101)$$

where the total fractional TPE radiative corrections is given by

$$\begin{aligned} \delta_{\text{TPE}}^{(\ell^-)}(Q^2) = -\delta_{\text{TPE}}^{(\ell^+)}(Q^2) &= \delta_{\gamma\gamma}^{(\text{LO+NLO})}(Q^2) + \delta_{\gamma\gamma}^{(\text{NNLO})}(Q^2) \\ &\equiv \delta_{\gamma\gamma}^{(0)}(Q^2) + \delta_{\gamma\gamma}^{(1)}(Q^2) + \delta_{\gamma\gamma}^{(2)}(Q^2) + o\left(\frac{\alpha}{M^2}\right) . \end{aligned} \quad (102)$$

The last term, denoted by “o”, represents additional $\mathcal{O}(\alpha/M^2)$ correction terms that can arise from the inclusion of irreducible two-loop pionic TPE diagrams, which were omitted in the present analysis, as discussed in Sec. I.

Fig. 6 displays the numerical values of the “true” LO, NLO and NNLO TPE corrections $\delta_{\gamma\gamma}^{(0,1,2)}$ to the elastic differential cross section, namely, the different $1/M$ -recoil order radiative corrections, where $\delta_{\gamma\gamma}^{(0)} \sim \mathcal{O}(\alpha M^0)$ and $\delta_{\gamma\gamma}^{(1)} \sim \mathcal{O}(\alpha/M)$ are given in Eqs. (41) and (100), respectively, and $\delta_{\gamma\gamma}^{(2)} \sim \mathcal{O}(\alpha/M^2)$ is given by the sum of Eqs. (66) and (99):

$$\delta_{\gamma\gamma}^{(2)}(Q^2) = \delta_{\gamma\gamma}^{(\text{LO+NLO};2)}(Q^2) + \delta_{\gamma\gamma}^{(\text{NNLO};2)}(Q^2) . \quad (103)$$

The following features are extracted from Fig. 6.

1. The LO corrections $\delta_{\gamma\gamma}^{(0)}$ exhibit a roughly linear dependence on the $|Q^2|$ but depend only weakly on the incident lepton beam momentum and the lepton mass.
2. For electron scattering the NLO corrections $\delta_{\gamma\gamma}^{(1)}$ are negative for very low- Q^2 values and turn positive at higher momentum transfers. In contrast for muon scattering the NLO corrections remain positive throughout and grow monotonically with $|Q^2|$ across the entire MUSE kinematic range.

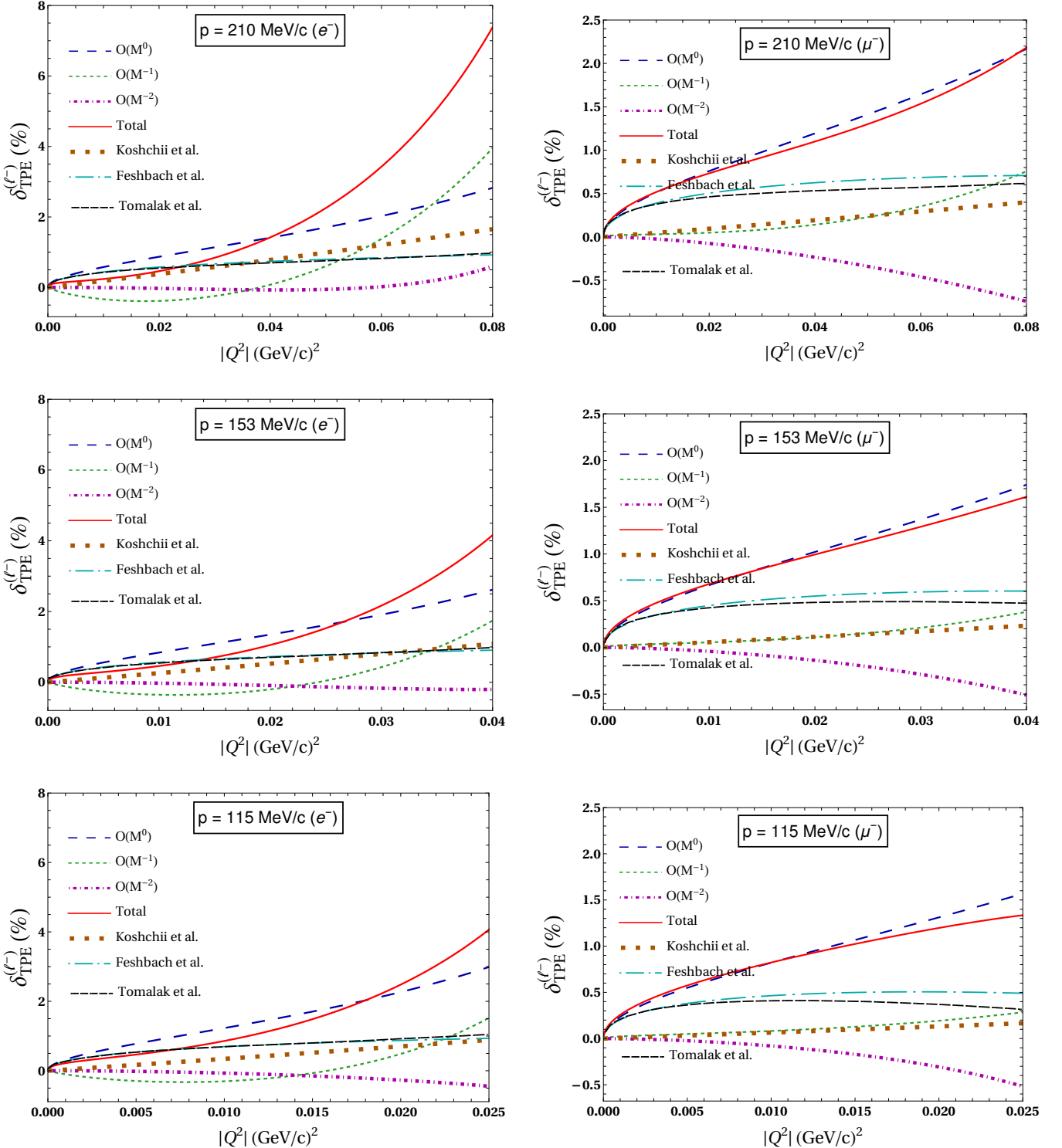


FIG. 6. Our HB χ PT results for the LO [i.e., $\mathcal{O}(\alpha M^0)$], NLO [i.e., $\mathcal{O}(\alpha/M)$] and NNLO [i.e., $\mathcal{O}(\alpha/M^2)$] finite fractional TPE corrections to the electron-proton (left panel) and muon-proton (right panel) elastic differential cross sections up to NNLO [i.e., $\mathcal{O}(\alpha^3/M^2)$] accuracy, is presented. The figure incorporates all LO, NLO and NNLO TPE diagrams considered in this work. In particular, the hadronic structure-dependent $\mathcal{O}(\alpha/M^2)$ corrections, relying on the proton rms charge radius (r_p) are evaluated by fixing its value to $r_p = \overline{r_p} \sim 0.855 \text{ fm}$. This choice corresponds to the mean of the CREMA determination [$r_p = 0.84087(39) \text{ fm}$] [76, 77] and the MAMI-ISR extraction [$r_p = 0.87 \pm (0.014)\text{stat.} \pm (0.024)\text{syst.} \pm (0.003)\text{mod.} \text{ fm}$] [75]. Our “Total” result (solid red line) is compared with the well known potential scattering result of McKinley and Feshbach [73], the SPA-based hadronic model result of Koshchii and Afanasev [38] and the dispersion technique based result of Tomalak and Vanderhaeghen [36, 37]. The fractional contributions are considered relative to the LO Born differential cross section relevant to MUSE kinematical range.

3. The net NNLO (kinematical and dynamical) corrections $\delta_{\gamma\gamma}^{(2)}$ are negative and much smaller in magnitude compared to the lower orders. Thus, we conclude that the TPE results exhibit a reasonable perturbative convergence.
4. It is noteworthy that the total TPE corrections $\delta_{\text{TPE}}^{(e^-, \mu^-)}$ for electrons and muons turn out to be roughly of the same magnitude. For electron scattering, we observe delicate cancellations among several large contributions, whereas for muon scattering the dominant terms add constructively, resulting in a net correction of comparable magnitude in both cases. The total corrections increase with both Q^2 and beam momentum, reaching values of approximately 7.5% for electron scattering and 4.4% for muon scattering.
5. A comparison with other recent TPE predictions, such as Refs. [36–38], which are largely based on the assumption of elastic proton–intermediate–state dominance, indicates that our analytical $\text{HB}\chi\text{PT}$ -based exact TPE calculation yields corrections of substantially larger magnitudes. In particular, for electron scattering, the predicted total correction increases markedly at the highest beam momentum, in clear contrast to the behavior observed in these alternative approaches. By comparison, the corresponding correction for muon scattering exhibits only a mild dependence on the incident beam momentum.

VI. SUMMARY AND CONCLUSION

In this work, we have presented a comprehensive and fully analytic evaluation of TPE corrections to elastic lepton–proton scattering within the framework of $\text{SU}(2)$ $\text{HB}\chi\text{PT}$. Our analysis extended the previous studies of the exact analytical evaluation of the fractional TPE corrections to the elastic differential cross section up-to-and-including NLO by Choudhary *et al.* [59]. Here we have additionally incorporated the kinematically suppressed NNLO corrections from the LO and NLO TPE diagrams, as well as the dynamical NNLO corrections from the NNLO TPE diagrams. The latter includes the proton’s hadronic structure-dependent corrections arising from the dominant reducible two-loop form factor TPE diagrams with factorizable pion-loops. Our previous exact TPE analysis in Ref. [59] demonstrated that the inclusion of the NLO diagrams (c) – (i) leads to sizable corrections compared with those that arise from the LO diagrams (a) and (b). The large NLO effect raised concerns regarding the efficacy of low-energy perturbative convergence of the $\text{HB}\chi\text{PT}$ expansion scheme. This concern motivated a more robust investigation into the behavior of the NNLO perturbative corrections of TPE, as pursued in this work.

Firstly, we demonstrated that the exact evaluation yields NLO results that differ substantially from those obtained in our earlier $\text{HB}\chi\text{PT}$ SPA analyses of Refs. [56] and [60]. Besides resolving the inherent shortcoming associated with the SPA formulation within $\text{HB}\chi\text{PT}$, namely, that the Feshbach-type correction [73] is absent at LO, our results clearly demonstrate that the net NNLO (kinematical and dynamical) contributions are numerically small compared to the LO and NLO contributions, thereby exhibit good convergence in the $1/M$ -recoil expansion, while the genuine NNLO dynamical corrections are uniformly negative and yield non-negligible contributions to the elastic differential cross section. In particular, the net NNLO corrections were found to be approximately 0.5% (0.8%) of the LO Born contribution for electron–proton (muon–proton) scattering in the MUSE kinematic range. In other words, we find a rather nominal sensitivity to lepton mass effects arising at NNLO. In addition, our exactly evaluated results identifies several contrasting features between the kinematical and dynamical NNLO corrections which are qualitatively very different for the corresponding SPA results reported in Ref. [60]. Especially, the exact treatment yields non-vanishing proton structure-dependent $\mathcal{O}(\alpha/M^2)$ correction terms, which were found to cancel at this order in the SPA analysis, where they are instead kinematically suppressed and effectively pushed beyond $\mathcal{O}(\alpha/M^3)$. Finally, we demonstrate that no additional IR-divergent contributions to the cross section arise from the NNLO TPE diagrams beyond those already present at LO. Specifically, the IR divergences originating from the box (a) and crossed-box (b) diagrams are fully accounted for and are systematically canceled by the inclusion of the corresponding soft-photon bremsstrahlung contributions, as explicitly shown in our recent work in Ref. [80].

Despite these advances, the present calculation up to NNLO accuracy does not yet constitute a fully systematic treatment. In particular, we have neglected contributions from irreducible pionic two-loop TPE diagrams, whose exact analytical evaluation is substantially more involved. Furthermore, according to the $\text{HB}\chi\text{PT}$ power counting, additional NNLO contributions arise from TPE diagrams involving inelastic intermediate excited nucleon states, most notably the $\Delta(1232)$ resonance. Such effects are known to become increasingly important at higher energies and momentum transfers and may yield non-negligible corrections, especially in muon–proton scattering at kinematics relevant to the MUSE experiment. A comprehensive investigation of these missing contributions, and their implications for future high-precision extractions of lepton–proton TPE corrections, is therefore essential and will be addressed in a forthcoming work.

In conclusion, we find that an SPA-based analysis of the TPE suffers from serious shortcomings due to an improper treatment of the kinematics associated with the loop-integrations in the box and crossed-box diagrams. In particular,

we demonstrate that significant contributions arise from kinematical regions of the loop-momentum where both exchanged photons are hard, i.e., far off their mass-shell, and are therefore not reliably captured within the SPA framework.

ACKNOWLEDGMENTS

RG and UR acknowledges financial support from the Science and Engineering Research Board, Republic of India, (Grant No. CRG/2022/000027). RG also acknowledges the organizers of the HADRON2025 International Conference at Osaka University for their financial support and hospitality during the conference.

Appendix A: Loop-integrals entering the kinematical NNLO recoil corrections

In Sec. 3, we analyzed the NNLO [i.e., $\mathcal{O}(\alpha/M^2)$] kinematical TPE corrections to the elastic lepton–proton differential cross section. This required an exact analytic evaluation of the LO and NLO TPE box and crossed-box diagrams. The resulting expressions can be written in terms of a set of master integrals, which are discussed in the main text. Several of these integrals were previously evaluated using dimensional regularization (DR) up to $\mathcal{O}(1/M^2)$ in our SPA-based TPE analysis of Ref. [60]. The remaining loop integrals, which did not appear in that work, are listed below to $\mathcal{O}(1/M^2)$ accuracy. In particular, a subset of latter already appeared in our earlier exact TPE study in Ref. [59], where they were computed to $\mathcal{O}(1/M)$ accuracy. Their $\mathcal{O}(1/M^2)$ extended results are also included here.

The kinematics of the elastic lepton-proton scattering is defined in terms of the incoming and outgoing lepton four-momenta $p_\mu = (E, \mathbf{p})$ and $p'_\mu = (E', \mathbf{p}')$, respectively, with $|\mathbf{p}| = \beta E$ and $|\mathbf{p}'| = \beta' E'$, such that the four-momentum transfer is $Q_\mu = (p - p')_\mu$, while k_μ represents the TPE loop four-momentum. First we present the result of the 3-point master-integral $Z^-(\Delta, i\sqrt{-Q^2}/2, m_l, E)$, computed up to $\mathcal{O}(1/M^2)$ as follows:

$$\begin{aligned} Z^-(\Delta, i\sqrt{-Q^2}/2, m_l, E) &= Z^{(0)}(\Delta, i\sqrt{-Q^2}/2, m_l, E) + \delta^{(1/M)} Z^-(\Delta, i\sqrt{-Q^2}/2, m_l, E) \\ &\quad + \delta^{(1/M^2)} Z^-(\Delta, i\sqrt{-Q^2}/2, m_l, E) + \mathcal{O}\left(\frac{1}{M^3}\right) \end{aligned} \quad (\text{A1})$$

where the four-vector $\Delta_\mu = (p - Q/2)_\mu$, and the $\mathcal{O}(M^0)$, $\mathcal{O}(1/M)$, and $\mathcal{O}(1/M^2)$ components are respectively given by

$$\begin{aligned} Z^{(0)}(\Delta, i\sqrt{-Q^2}/2, m_l, E) &= -\frac{1}{(4\pi)^2 \sqrt{E^2 - \Delta^2}} \left[\frac{1}{2} \text{Li}_2\left(\frac{\Delta^2}{\Delta^2 - m_l^2}\right) - \frac{1}{2} \text{Li}_2\left(\frac{\Delta^2 - m_l^2}{\eta^2}\right) \right. \\ &\quad - \frac{1}{2} \text{Li}_2\left(\frac{\eta^2}{\Delta^2 - m_l^2}\right) + \text{Li}_2\left(1 + \frac{E(1 + \beta)}{\eta}\right) \\ &\quad \left. + \text{Li}_2\left(1 + \frac{E(1 - \beta)}{\eta}\right) \right], \end{aligned} \quad (\text{A2})$$

$$\begin{aligned} \delta^{(1/M)} Z^-(\Delta, i\sqrt{-Q^2}/2, m_l, E) &= \frac{-Q^2}{4(4\pi)^2 M(E^2 - \Delta^2)} \left[(4\pi)^2 E Z^{(0)} - \sqrt{\frac{\Delta^2}{\Delta^2 - m_l^2}} \ln\left(\frac{\sqrt{\Delta^2} + \sqrt{\Delta^2 - m_l^2}}{\sqrt{\Delta^2} - \sqrt{\Delta^2 - m_l^2}}\right) \right. \\ &\quad \left. - \ln\left(\frac{m_l^2}{\Delta^2 - m_l^2}\right) - i\pi \left(1 + \frac{\sqrt{\Delta^2} + E}{\sqrt{\Delta^2 - m_l^2}}\right) \right], \end{aligned} \quad (\text{A3})$$

and

$$\begin{aligned}
\delta^{(1/M^2)} Z^- \left(\Delta, i\sqrt{-Q^2}/2, m_l, E \right) = & \frac{Q^4 \Delta^2 Z^{(0)}}{32M^2(E^2 - \Delta^2)^2} - \frac{EQ^2}{4M(E^2 - \Delta^2)} \delta^{(1/M)} Z^- \left(\Delta, i\sqrt{-Q^2}/2, m_l, E \right) \\
& + \frac{Q^4}{32(4\pi)^2 M^2(E^2 - \Delta^2)^2} \left[- \frac{2E(E^2 - \Delta^2)}{\Delta^2 - m_l^2} \right. \\
& - \left(2E - \frac{2E^2}{\eta} - \frac{m_l^2 \sqrt{E^2 - \Delta^2}}{\Delta^2 - m_l^2} \right) \ln \left(\frac{m_l^2}{\Delta^2 - m_l^2} \right) \\
& + \frac{E(E + \sqrt{E^2 - \Delta^2})(\sqrt{E^2 - \Delta^2} - \beta^2 E)}{\Delta^2 - m_l^2} \ln \left(\frac{\Delta^2 - m_l^2}{\eta^2} \right) \\
& - \frac{2E\sqrt{\Delta^2}}{\sqrt{\Delta^2 - m_l^2}} \ln \left(\frac{\sqrt{\Delta^2} + \sqrt{\Delta^2 - m_l^2}}{\sqrt{\Delta^2} - \sqrt{\Delta^2 - m_l^2}} \right) + E(E + \sqrt{E^2 - \Delta^2}) \\
& \times \left\{ \frac{1 + \beta}{\sqrt{E^2 - \Delta^2} + \beta E} \ln \left(- \frac{E(1 + \beta)}{\eta} \right) - \frac{1 - \beta}{\sqrt{E^2 - \Delta^2} - \beta E} \right. \\
& \left. \left. \times \ln \left(- \frac{E(1 - \beta)}{\eta} \right) \right\} \right], \tag{A4}
\end{aligned}$$

where $\eta = -E + \sqrt{E^2 - \Delta^2}$, $\Delta^2 = (p - Q/2)^2 = m_l^2 - Q^2/4$, and

$$\text{Li}_2(z) = - \int_0^z dt \frac{\ln(1-t)}{t}, \quad \forall z \in \mathbb{C}, \tag{A5}$$

is the standard dilogarithm (or Spence) function.

Next we present the result of the 3-point master-integral $Z^+ \left(\Delta', i\sqrt{-Q^2}/2, m_l, -E' \right)$ computed up to $\mathcal{O}(1/M^2)$:

$$\begin{aligned}
Z^+ \left(\Delta', i\sqrt{-Q^2}/2, m_l, -E' \right) = & -Z^{(0)} \left(\Delta, i\sqrt{-Q^2}/2, m_l, E \right) + \delta^{(1/M)} Z^+ \left(\Delta', i\sqrt{-Q^2}/2, m_l, -E' \right) \\
& + \delta^{(1/M^2)} Z^+ \left(\Delta', i\sqrt{-Q^2}/2, m_l, -E' \right) + \mathcal{O} \left(\frac{1}{M^3} \right), \tag{A6}
\end{aligned}$$

where the four-vector $\Delta'_\mu = -\Delta_\mu = -(p - Q/2)_\mu$, and the $\mathcal{O}(1/M)$, and $\mathcal{O}(1/M^2)$ components are respectively given by

$$\begin{aligned}
\delta^{(1/M)} Z^+ \left(\Delta', i\sqrt{-Q^2}/2, m_l, -E' \right) = & \frac{Q^2}{4(4\pi)^2 M(E^2 - \Delta^2)} \left[(4\pi)^2 E Z^{(0)} + \sqrt{\frac{\Delta^2}{\Delta^2 - m_l^2}} \right. \\
& \times \ln \left(\frac{\sqrt{\Delta^2} + \sqrt{\Delta^2 - m_l^2}}{\sqrt{\Delta^2} - \sqrt{\Delta^2 - m_l^2}} \right) - \frac{4}{\beta} \ln \sqrt{\frac{1 + \beta}{1 - \beta}} - \ln \left(\frac{m_l^2}{\Delta^2 - m_l^2} \right) \\
& \left. + i\pi \left(\frac{\sqrt{\Delta^2} - E}{\sqrt{\Delta^2 - m_l^2}} - 3 \right) \right], \tag{A7}
\end{aligned}$$

and

$$\begin{aligned}
\delta^{(1/M^2)} Z^+ \left(\Delta', i\sqrt{-Q^2}/2, m_l, -E' \right) = & \frac{Q^4}{32M^2(4\pi)^2(E^2 - \Delta^2)^{5/2}} \left[(4\pi)^2 Z^{(0)} \sqrt{E^2 - \Delta^2} (2E^2 + \Delta^2) \right. \\
& - \frac{8(4\pi)^2 M E}{Q^2} (E^2 - \Delta^2)^{3/2} \delta^{(1/M)} Z^+ \left(\Delta', i\sqrt{-Q^2}/2, m_l, -E' \right) \\
& - \frac{2E\sqrt{\Delta^2(E^2 - \Delta^2)}}{\sqrt{\Delta^2 - m_l^2}} \ln \left(\frac{\sqrt{\Delta^2} + \sqrt{\Delta^2 - m_l^2}}{\sqrt{\Delta^2} - \sqrt{\Delta^2 - m_l^2}} \right) \\
& - \frac{2(E^2 - \Delta^2)^{3/2}}{E\beta^2} \left(4 - \frac{E^2\beta^2}{\Delta^2 - m_l^2} \right) + \frac{16(E^2 - \Delta^2)}{\beta} \ln \sqrt{\frac{1+\beta}{1-\beta}} \\
& + \left(\frac{4(E^2 - \Delta^2)(1+\beta^2)}{\beta^2} - \frac{m_l^2(E^2 - \Delta^2)}{\Delta^2 - m_l^2} - 2E\sqrt{E^2 - \Delta^2} \right) \\
& \times \ln \left(\frac{m_l^2}{\eta^2} \right) + \frac{\sqrt{E^2 - \Delta^2}}{\Delta^2 - m_l^2} \ln \left(\frac{\Delta^2 - m_l^2}{\eta^2} \right) \left\{ \left(\sqrt{E^2 - \Delta^2} - 3E \right) \right. \\
& \times \left. (\Delta^2 - m_l^2) - \Delta^2 \sqrt{E^2 - \Delta^2} \right\} - \frac{E(1-\beta)}{\sqrt{E^2 - \Delta^2} - \beta E} \left\{ 5(E^2 - \Delta^2) \right. \\
& \times \ln \left(-\frac{E(1-\beta)}{\eta} \right) - 3E\sqrt{E^2 - \Delta^2} - \frac{8(E^2 - \Delta^2)^{3/2}}{\beta E} \\
& + \left. \frac{4(1-\beta)(E^2 - \Delta^2)^2}{E^2\beta^3} \right\} - \frac{E(1+\beta)}{\sqrt{E^2 - \Delta^2} + \beta E} \ln \left(-\frac{E(1+\beta)}{\eta} \right) \\
& \times \left\{ 5(E^2 - \Delta^2) - 3E\sqrt{E^2 - \Delta^2} + \frac{8(E^2 - \Delta^2)^{3/2}}{\beta E} \right. \\
& \left. - \frac{4(1-\beta)(E^2 - \Delta^2)^2}{E^2\beta^3} \right\}. \tag{A8}
\end{aligned}$$

Finally we require the 3-point master-integral $I(Q|1, 1, 0, 1) = I^-(p, 0|1, 1, 0, 1) = I^+(p', 0|1, 1, 0, 1)$ for the kinematical $\mathcal{O}(\alpha/M^2)$ corrections. The integral was previously evaluated only up to $\mathcal{O}(1/M)$ accuracy in Ref. [56]. Its $\mathcal{O}(1/M^2)$ extension is given as below

$$\begin{aligned}
I^-(p, 0|1, 1, 0, 1) &= \frac{1}{i} \int \frac{d^4 k}{(2\pi)^4} \frac{1}{(k^2 + i0)[(k - Q)^2 + i0](v \cdot k + i0)} \\
&= I^{(0)}(Q|1, 1, 0, 1) + \delta^{(1/M)} I(Q|1, 1, 0, 1) + \delta^{(1/M^2)} I(Q|1, 1, 0, 1) + \mathcal{O}\left(\frac{1}{M^3}\right), \tag{A9}
\end{aligned}$$

where

$$I^{(0)}(Q|1, 1, 0, 1) = -\frac{1}{16} \sqrt{\frac{1}{-Q^2}}, \tag{A10}$$

$$\delta^{(1/M)} I(Q|1, 1, 0, 1) = -\frac{1}{8M\pi^2} \left[1 - \ln \left(-\frac{\sqrt{-Q^2}}{M} + \frac{Q^2}{M^2} \right) \right], \quad \text{and} \tag{A11}$$

$$\delta^{(1/M^2)} I(Q|1, 1, 0, 1) = \frac{\sqrt{-Q^2}}{M^2} \left(\frac{1}{128} - \frac{1}{8\pi^2} \right). \tag{A12}$$

Appendix B: Loop-integrals entering the dynamical NNLO corrections

In Sec. 4 the evaluation of the genuine $\mathcal{O}(\alpha/M^2)$ dynamical TPE corrections requires incorporating a new set 2-, 3-, and 4-point scalar and tensor loop-integrals, that were not present in the earlier TPE analyses of Choudhary *et al.* [59] and Goswami *et al.* [60]. We first consider the two 4-point tensor loop-integrals appearing in the fractional

contributions $\delta_{\gamma\gamma}^{(j)}$ and $\delta_{\gamma\gamma}^{(k)}$ from the box (j) and crossed-box (k) diagrams [see Eqs. (75) and (77)], namely,

$$I_1^{-\mu\nu}(p, 0|1, 1, 1, 1) = \frac{1}{i} \int \frac{d^4 k}{(2\pi)^4} \frac{k^\mu k^\nu}{(k^2 + i0)[(k - Q)^2 + i0](k^2 - 2k \cdot p + i0)(v \cdot k + i0)}, \quad \text{and} \quad (\text{B1})$$

$$I_1^{+\mu\nu}(p, 0|1, 1, 1, 1) = \frac{1}{i} \int \frac{d^4 k}{(2\pi)^4} \frac{k^\mu k^\nu}{(k^2 + i0)[(k - Q)^2 + i0](k^2 + 2k \cdot p' + i0)(v \cdot k + i0)}, \quad (\text{B2})$$

respectively. In order to compute the sum of the box-crossed-box pair of fractional contributions to the cross section, $\delta_{\gamma\gamma}^{(jk)} \sim \mathcal{O}(\alpha/M^2)$, we are required to evaluate only to LO [i.e., $\mathcal{O}(M^0)$] accuracy in the recoil expansion:

$$\begin{aligned} p_\mu p_\nu I_1^{-\mu\nu}(p, 0|1, 1, 1, 1) &+ p'_\mu p'_\nu I_1^{+\mu\nu}(p, 0|1, 1, 1, 1) \\ &= \frac{1}{2} \left[p \cdot T_1^-(p, 0|0, 1, 1, 1) - p' \cdot T_1^+(p', 0|0, 1, 1, 1) - Q \cdot I_1(Q|1, 1, 0, 1) \right. \\ &\quad \left. + m_l^2 \left(I^-(p, 0|0, 1, 1, 1) + I^+(p', 0|0, 1, 1, 1) \right) \right] \\ &= -\frac{Q^2}{4} I^{(0)}(Q|1, 1, 0, 1) + \mathcal{O}\left(\frac{1}{M}\right). \end{aligned} \quad (\text{B3})$$

The above scalar product $Q \cdot I_1(Q|1, 1, 0, 1)$ can be further reduced *via* partial-fraction decomposition into an appropriate combination of 2- and 3-point scalar integrals, namely,

$$\begin{aligned} Q \cdot I_1(Q|1, 1, 0, 1) &= \frac{1}{i} \int \frac{d^4 k}{(2\pi)^4} \frac{k \cdot Q}{(k^2 + i0)[(k - Q)^2 + i0](v \cdot k + i0)} \\ &= \frac{1}{2} \left[I^-(p, 0|0, 1, 0, 1) + Q^2 I^-(p, 0|1, 1, 0, 1) - I^-(p, 0|1, 0, 0, 1) \right]. \end{aligned} \quad (\text{B4})$$

The following 2-point functions are evaluated in dimensional regularization *via* analytic continuation to D -dimensional space-time:

$$I(Q|1, 0, 0, 1) \equiv I^-(p, 0|1, 0, 0, 1) \equiv I^+(p', 0|1, 0, 0, 1) = 0, \quad \text{and} \quad (\text{B5})$$

$$\begin{aligned} I(Q|0, 1, 0, 1) &\equiv I^-(p, 0|0, 1, 0, 1) \equiv I^+(p', 0|0, 1, 0, 1) \\ &= \frac{Q^2}{16\pi^2 M} \left[\frac{1}{\epsilon} + \gamma_E - \ln\left(\frac{4\pi\mu^2}{m_l^2}\right) - \ln\left(\frac{m_l^2 M^2}{Q^4}\right) - 2 \right], \end{aligned} \quad (\text{B6})$$

where $\gamma_E = 0.577216\dots$ denotes the Euler-Mascheroni constant and $\epsilon = (4 - D)/2 < 0$. The former scaleless loop-integrals vanish identically in dimensional regularization, while the latter UV-divergent integral $I(Q|0, 1, 0, 1) \sim \mathcal{O}(1/M)$ generates only $\mathcal{O}(\alpha/M^3)$ contributions to $\delta_{\gamma\gamma}^{(jk)}$. These lie beyond our working accuracy, therefore they may be safely discarded. The two 3-point tensor integrals $T_1^{\pm\mu}$ are reduced into a combination of 2- and 3-point function using the well-known *Passarino-Veltman decomposition* [81]:

$$T_1^{-\mu}(p, 0|0, 1, 1, 1) = \frac{1}{i} \int \frac{d^4 k}{(2\pi)^4} \frac{(k - p)^\mu}{[(k - Q)^2 + i0](k^2 - 2k \cdot p + i0)(v \cdot k + i0)} = v^\mu B_1^- + p'^\mu B_2^-, \quad \text{and} \quad (\text{B7})$$

$$T_1^{+\mu}(p', 0|0, 1, 1, 1) = \frac{1}{i} \int \frac{d^4 k}{(2\pi)^4} \frac{(k + p')^\mu}{[(k - Q)^2 + i0](k^2 + 2k \cdot p' + i0)(v \cdot k + i0)} = v^\mu B_1^+ + p^\mu B_2^+, \quad (\text{B8})$$

where

$$\begin{aligned}
B_1^- &= \left[1 - \frac{1}{\beta'^2} \right] I^-(p, 0|0, 1, 1, 0) - \left[E - \frac{E}{\beta'^2} + \frac{m_l^2}{E'\beta'^2} \right] I^-(p, 0|0, 1, 1, 1) \\
&\quad + \frac{1}{2E'\beta'^2} [I^-(p, 0|0, 0, 1, 1) - I(Q|0, 1, 0, 1)] , \\
B_2^- &= \frac{1}{E'\beta'^2} I^-(p, 0|0, 1, 1, 0) - \left[\frac{E}{E'\beta'^2} - \frac{m_l^2}{E'^2\beta'^2} \right] I^-(p, 0|0, 1, 1, 1) \\
&\quad - \frac{1}{2E'^2\beta'^2} [I^-(p, 0|0, 0, 1, 1) - I(Q|0, 1, 0, 1)] , \\
B_1^+ &= \left[1 - \frac{1}{\beta^2} \right] I^+(p', 0|0, 1, 1, 0) + \left[E' - \frac{E'}{\beta^2} + \frac{m_l^2}{E\beta^2} \right] I^+(p', 0|0, 1, 1, 1) \\
&\quad - \frac{1}{2E\beta^2} [I^+(p', 0|0, 0, 1, 1) - I(Q|0, 1, 0, 1)] , \\
B_2^+ &= \frac{1}{E\beta^2} I^+(p', 0|0, 1, 1, 0) + \left[\frac{E'}{E\beta^2} - \frac{m_l^2}{E^2\beta^2} \right] I^+(p', 0|0, 1, 1, 1) \\
&\quad + \frac{1}{2E^2\beta^2} [I^+(p', 0|0, 0, 1, 1) - I(Q|0, 1, 0, 1)] . \tag{B9}
\end{aligned}$$

While the 3-point scalar integrals $I^-(p, 0|0, 1, 1, 1)$ and $I^+(p', 0|0, 1, 1, 0)$ were already evaluated in our earlier works, Refs. [59] and [60], the 2-point scalar master-integrals entering the B^\pm functions are evaluated in DR, yielding the following UV-divergent expressions:

$$\begin{aligned}
I^-(p, 0|0, 1, 1, 0) &\equiv I^+(p', 0|0, 1, 1, 0) \equiv I^-(p, 0|1, 0, 1, 0) \equiv I^+(p', 0|1, 0, 1, 0) \\
&= -\frac{1}{(4\pi)^2} \left[\frac{1}{\epsilon} + \gamma_E - \ln \left(\frac{4\pi\mu^2}{m_l^2} \right) - 2 \right] , \tag{B10}
\end{aligned}$$

$$I^-(p, 0|0, 0, 1, 1) = -\frac{2E}{(4\pi)^2} \left[\left\{ \frac{1}{\epsilon} + \gamma - \ln \left(\frac{4\pi\mu^2}{m_l^2} \right) \right\} - 2 + 2\beta \ln \sqrt{\frac{1+\beta}{1-\beta}} \right] , \tag{B11}$$

$$I^+(p', 0|0, 0, 1, 1) = \frac{2E'}{(4\pi)^2} \left[\left\{ \frac{1}{\epsilon} + \gamma - \ln \left(\frac{4\pi\mu^2}{m_l^2} \right) \right\} - 2 + 2\beta' \ln \sqrt{\frac{1+\beta'}{1-\beta'}} \right] . \tag{B12}$$

There is one additional 2-point master-integral $I(Q|1, 1, 0, 0)$, appearing in the TPE diagrams (j), (k), (n) and (o), which is likewise UV-divergent and evaluated to yield

$$I(Q|1, 1, 0, 0) \equiv I^-(p, 0|1, 1, 0, 0) \equiv I^+(p', 0|1, 1, 0, 0) = -\frac{1}{(4\pi)^2} \left[\frac{1}{\epsilon} + \gamma_E - \ln \left(-\frac{4\pi\mu^2}{Q^2} \right) - 2 \right] . \tag{B13}$$

Finally we evaluate several new 3-point loop-integrals, which also contribute to the cross section at NNLO. These reducible functions are decomposed into combinations of UV-divergent 2- and 3-point scalar master-integrals as follows:

$$\begin{aligned}
I_1^{+\mu}(p', 0|1, 1, 1, 0) &= \frac{1}{i} \int \frac{d^4 k}{(2\pi)^4} \frac{k^\mu}{(k^2 + i0)[(k - Q)^2 + i0](k^2 + 2k \cdot p' + i0)} \\
&= \frac{1}{8\pi^2 Q^2 \nu^2} \left[\left(p'^\mu + \frac{1}{2} Q^\mu \right) \ln \left(-\frac{Q^2}{m_l^2} \right) - 8\pi^2 (Q^2 p'^\mu + 2m_l^2 Q^\mu) I(Q|1, 1, 1, 0) \right] , \tag{B14}
\end{aligned}$$

$$\begin{aligned}
I_2^-(p, 0|0, 1, 1, 1) &= \frac{1}{i} \int \frac{d^4 k}{(2\pi)^4} \frac{k^2}{[(k-Q)^2 + i0](k^2 - 2k \cdot p + i0)(v \cdot k + i0)} \\
&= I^-(p, 0|0, 1, 0, 1) + 2p \cdot T_1^-(p, 0|0, 1, 1, 1) + 2m_l^2 I^-(p, 0|0, 1, 1, 1), \tag{B15}
\end{aligned}$$

$$\begin{aligned}
I_2^+(p', 0|0, 1, 1, 1) &= \frac{1}{i} \int \frac{d^4 k}{(2\pi)^4} \frac{k^2}{[(k-Q)^2 + i0](k^2 + 2k \cdot p' + i0)(v \cdot k + i0)} \\
&= I^-(p, 0|0, 1, 0, 1) - 2p' \cdot T_1^+(p', 0|0, 1, 1, 1) + 2m_l^2 I^+(p', 0|0, 1, 1, 1), \tag{B16}
\end{aligned}$$

$$\begin{aligned}
I_2^-(p, 0|0, 1, 1, 2) &= \frac{1}{i} \int \frac{d^4 k}{(2\pi)^4} \frac{k^2}{[(k-Q)^2 + i0](k^2 - 2k \cdot p + i0)(v \cdot k + i0)^2} \\
&= I^-(Q|0, 1, 0, 2) + 2p \cdot T_1^-(p, 0|0, 1, 1, 2) + 2m_l^2 I^-(p, 0|0, 1, 1, 2), \tag{B17}
\end{aligned}$$

$$\begin{aligned}
I_2^+(p', 0|0, 1, 1, 2) &= \frac{1}{i} \int \frac{d^4 k}{(2\pi)^4} \frac{k^2}{[(k-Q)^2 + i0](k^2 + 2k \cdot p' + i0)(v \cdot k + i0)^2} \\
&= I^-(Q|0, 1, 0, 2) - 2p' \cdot T_1^+(p', 0|0, 1, 1, 2) + 2m_l^2 I^+(p', 0|0, 1, 1, 2). \tag{B18}
\end{aligned}$$

Here $I^-(p, 0|0, 1, 1, 2)$ and $I^+(p', 0|0, 1, 1, 2)$ are given in Eqs. (57) and (60), respectively. The expression for $I(Q|0, 1, 0, 2)$ can be found in Ref. [59]. We emphasize that although each of these scalar integrals contains UV divergences, all such divergences cancel exactly once the box and crossed-box TPE diagram pairs are combined. The net contribution from these diagrams to the cross section is therefore finite.

[1] M. N. Rosenbluth, Phys. Rev. **79**, 615 (1950).

[2] A. I. Akhiezer, M. P. Rekalo, Fiz. Elem. Chast. Atom. Yadra **4**, 662 (1973).

[3] R. G. Arnold and C. E. Carlson and F. Gross, Phys. Rev. C **23**, 363 (1981).

[4] O. Gayou, *et al.*, Phys. Rev. C **64**, 038202 (2001).

[5] M. K. Jones *et al.*, Phys. Rev. Lett. **84**, 1398 (2000).

[6] C. F. Perdrisat, V. Punjabi, M. Vanderhaeghen, Prog. Part. Nucl. Phys. **59**, 694 (2007).

[7] V. Punjabi *et al.*, Eur. Phys. J. A **51**, 79 (2015).

[8] A. J. R. Puckett, *et al.*, Phys. Rev. Lett. **104**, 242301 (2010).

[9] J. Arrington, Phys. Rev. C **68**, 034325 (2003).

[10] P. A. M. Guichon and M. Vanderhaeghen, Phys. Rev. Lett. **91**, 142303 (2003).

[11] P. G. Blunden, W. Melnitchouk and J. A. Tjon, Phys. Rev. Lett. **91**, 142304 (2003).

[12] M. P. Rekalo and E. Tomasi-Gustafsson, Nucl. Phys. A **742**, 322 (2004).

[13] P. G. Blunden, W. Melnitchouk, and J. A. Tjon, Phys. Rev. C **72**, 034612 (2005).

[14] C. E. Carlson and M. Vanderhaeghen, Ann. Rev. Nucl. Part. Sci. **57**, 171 (2007).

[15] J. Arrington, P. G. Blunden, and W. Melnitchouk, Prog. Part. Nucl. Phys. **66**, 782 (2011).

[16] R. Pohl *et al.*, [CREMA Collaboration] Nature **466** 213, 2010.

[17] R. Pohl, R. Gilman, G. A. Miller, and K. Pachucki, Ann. Rev. Nucl. Part. Sci. **63**, 175 (2013).

[18] P. J. Mohr, *et al.*, “CODATA Recommended Values of the Fundamental Physical Constants: 2010*”, Rev. Mod. Phys. **84**, 1527 (2012).

[19] A. Antognini, *et al.*, Science **339**, 417 (2013).

[20] J. C. Bernauer and R. Pohl, Scientific American **310**, 32 (2014).

[21] C. E. Carlson, Prog. Part. Nucl. Phys. **82**, 59 (2015).

[22] J. C. Bernauer, EPJ Web Conf. **234**, 01001 (2020).

[23] H. Gao and M. Vanderhaeghen, Rev. Mod. Phys. **94**, 015002, (2022).

[24] B. S. Henderson *et al.*, [OLYMPUS Collaboration (DESY)] Phys. Rev. Lett. **118**, 092501 (2017).

[25] I. A. Rachev *et al.*, [VEPP-3 Collaboration (Novosibirsk)] Phys. Rev. Lett. **114**, 062005 (2015).

[26] D. Rimal *et al.*, [CLAS Collaboration (Jefferson Lab)] Phys. Rev. C **95**, 065201 (2017).

[27] R. Gilman *et al.*, [MUSE Collaboration (PSI)] AIP Conf. Proc. **1563**, 167 (2013).

[28] Y. C. Chen *et al.*, Phys. Rev. Lett. **93**, 122301 (2004).

[29] M. Gorchtein, P. A. M. Guichon, and M. Vanderhaeghen, Nucl. Phys. A **741**, 234 (2004).

[30] S. Kondratyuk, and P.G. Blunden, Phys. Rev. C **75**, 038201 (2007).

[31] A. Afanasev, M. Strikman, and C. Weiss, Phys. Rev. D **77** 014028 (2008).

[32] L. C. Maximon and J. A. Tjon, Phys. Rev. C **62**, 054320 (2000).

[33] M. Vanderhaeghen *et al.*, Phys. Rev. C **62**, 025501 (2000).

[34] O. Tomalak and M. Vanderhaeghen, Phys. Rev. D **90**, 013006 (2014).

[35] G. Lee, J. R. Arrington, and R. J. Hill, Phys. Rev. D **92**, 013013 (2015).

[36] O. Tomalak and M. Vanderhaeghen, Phys. Rev. D **93**, 013023 (2016).

[37] O. Tomalak and M. Vanderhaeghen, Eur. Phys. J. C **76**, 125 (2016).

[38] O. Koshchii and A. Afanasev, Phys. Rev. D **96**, 016005 (2017).

[39] R.-D. Bucoveanu, and H. Spiesberger, Eur. Phys. J. A **55**, 57 (2019).

[40] Q. Q. Guo and H. Q. Zhou, Phys. Rev. C **106**, 015203 (2022).

[41] H. W. Hammer, and Ulf-G. Meißner, Eur. Phys. J. A **20**, 469 (2004).

[42] M. Gorchtein, Phys. Lett. B **644**, 322 (2007).

[43] D. Borisyuk and A. Kobushkin, Phys. Rev. C **78**, 025208 (2008).

[44] O. Tomalak and M. Vanderhaeghen, Eur. Phys. J. A **51**, 24 (2015).

[45] I. T. Lorenz, Ulf-G. Meißner, H.-W. Hammer, Y.-B. Dong, Phys. Rev. D **91**, 014023 (2015).

[46] O. Tomalak, B. Pasquini, M. Vanderhaeghen, Phys. Rev. D **95**, 096001 (2017).

[47] O. Tomalak, Eur. Phys. J. C **77**, 858 (2017).

[48] O. Tomalak and M. Vanderhaeghen, Eur. Phys. J. C **78**, 514 (2018).

[49] R. J. Hill, and G. Paz, Phys. Rev. Lett. **107**, 160402 (2011).

[50] C. Pesimal, A. Pineda and O. Tomalak, Prog. Part. Nucl. Phys. **121**, 103901 (2021).

[51] D. Nevado, and A. Pineda, Phys. Rev. C **77**, 035202 (2008).

[52] M. C. Birse, and J. A. McGovern, Eur. Phys. J. A **48**, 120 (2012).

[53] J. M. Alarcon, V. Lensky, and V. Pascalutsa, Eur. Phys. J. C **74**, 2852 (2014).

[54] C. Pesimal, and A. Pineda, Eur. Phys. J. A **51**, 156 (2015).

[55] J. M. Alarcon, F. Hagelstein, V. Lensky, V. Pascalutsa, Phys. Rev. D **102**, 014006 (2020).

[56] P. Talukdar, V. C. Shastry, U. Raha and F. Myhrer, Phys. Rev. D **101**, 013008 (2020).

[57] P. Talukdar, V. C. Shastry, U. Raha, and F. Myhrer, Phys. Rev. D **104**, 053001 (2021).

[58] X. H. Cao, Q. Z. Li and H. Q. Zheng, Phys. Rev. D **105**, 094008 (2022).

[59] P. Choudhary, U. Raha, F. Myhrer, and D. Chakrabarti, Eur. Phys. J. A **60**, 69 (2024).

[60] R. Goswami, P. Talukdar, B. Das, U. Raha, and F. Myhrer, Phys. Rev. D **111**, 113009 (2025).

[61] F. Yang, PoS LATTICE2021, 607 (2022).

[62] Y. Fu, X. Feng, L.-C. Jin and C.-F. Lu, Phys. Rev. Lett. **128**, 172002 (2022).

[63] J. Gasser and H. Leutwyler, Phys. Rept. **87**, 77 (1982).

[64] E. Jenkins and A. V. Manohar, Phys. Lett. B **255**, 558 (1991).

[65] V. Bernard, N. Kaiser, and U.-G. Meißner, Nucl. Phys. B **338**, 315 (1992).

[66] G. Ecker, Phys. Lett. B **336**, 508 (1994).

[67] V. Bernard, N. Kaiser, and Ulf.-G. Meißner, Int. J. Mod. Phys. E **4**, 193 (1995).

[68] N. Fettes, Ulf.-G. Meißner and S. Steininger, Nucl. Phys. A **640**, 199 (1998). (Corrections to misprints can be found in N. Fettes, Ph.D. dissertation, Bonn University 2000, unpublished.)

[69] N. Fettes, Ph.D. Dissertation “*Pion nucleon physics in chiral perturbation theory*”, Bonn University, 2000.

[70] S. Scherer, In *Advances in Nuclear Physics*, Vol. 27, pp. 277-538 (Springer Publications, 2003).

[71] L. W. Mo and Yung-Su Tsai, Rev. Mod. Phys. **41**, 205 (1969).

[72] Y.-Su Tsai, Phys. Rev. **122**, 1898 (1961).

[73] W. A. McKinley and H. Feshbach, Phys. Rev. **74**, 1759 (1948).

[74] S. Scherer and M. R. Schindler, Lecture Notes in Physics, vol. 830, Springer-Verlag, Berlin, Heidelberg (2012).

[75] M. Mihovilović, *et al.*, [A1 Collaboration] Eur. Phys. J. A **57**, 107 (2021).

[76] A. Antognini, *et al.*, [CREMA Collaboration] Science **339**, 417 (2013).

[77] R. Pohl, R. Gilman, G. A. Miller, and K. Pachucki, Ann. Rev. Nucl. Part. Sci. **63**, 175 (2013).

[78] N. Fettes, U. G. Meißner, M. Mojžiš, and S. Steininger, Ann. Phys. **283**, 273 (2000).

[79] V. Bernard, H. W. Fearing, T. R. Hemmert, and Ulf.-G. Meißner, Nucl. Phys. A **635**, 121 (1998); Erratum: Nucl. Phys. A **642**, 563 (1998).

[80] B. Das, R. Goswami, P. Talukdar, U. Raha, and F. Myhrer, e-Print arXiv:2508.08104[hep-ph].

[81] G. Passarino and M. Veltman, Nucl. Phys. B **160**, 151 (1979).